

ȘTIINȚA ȘI INGINERIA MATERIALELOR

S U M A R		<u>Pag.</u>
ADRIAN ALEXANDRU și ROXANA GABRIELA ȘTEFĂNICĂ, Straturi Dure rezistente la uzură depuse pe oțelul 21MoMnCr12 pentru organe de mașini. Cercetări de microdurate (engl., rez. rom.)		7
ANCA ALUCULESEI, RĂZVAN LIȚOIU, IOANNIS ZERICHIOTIS, CONSTANTIN BACIU și MARICEL AGOP, Transferul termic în nanostructuri(I). Modelul matematic (engl., rez. rom.)		17
MIHAI AXINTE, CARMEN NEJNERU, MANUELA PERJU și ION HOPULELE Utilizarea triodei ionice într-o instalație pentru studiul transferului termic și de masă în plasmă, (engl., rez. rom.)		27
ROXANA-GABRIELA ȘTEFĂNICĂ și ADRIAN ALEXANDRU, Aspecte asupra unor aliaje de aluminiu îmbătrânite ciclic și clasic (engl., rez. rom.)		37
CIMPOEȘU NICANOR, AXINTE MIHAI, CIMPOEȘU HANU RAMONA, HOPULELE ION, ATUDOSIE IOAN și PARASCHIV PETRONELA, Simularea capacității de disipare a unor materiale metalice (engl., rez. rom.)		45
RAMONA CIMPOEȘU HANU, CONSTANTIN BACIU, SERGIU STANCIU, DELIA MARINELA AELENEI, NICANOR CIMPOEȘU și PETRONELA PARASCHIV, Studiul comportamentului la electrocoroziune a unui aliaj superelastice din Ni-Ti prin analize SEM și EDAX (engl., rez. rom.)		55
SANDA CRETU, Aspecte teoretice și experimentale privind modelarea fenomenelor ce se produc în asamblările nedemontabile (engl., rez. rom.)		67
ADRIAN GRECU, DAN-GELU GALUȘCĂ, CARMEN NEJNERU, ION HOPULELE și MIHAI AXINTE, Cercetări privind modificarea capacității de răcire a mediilor sintetice de călire tip poliachilenglicol (PAG) modificat (engl., rez. rom.)		73
ANCA ELENA LĂRGEANU, DAN-GELU GĂLUȘCĂ, CARMEN NEJNERU, MANUELA CRISTINA PERJU și ION HOPULELE, Impactul asupra coroziunii a straturilor superficiale obținute prin acoperire cu materiale de adaos prin metoda descărcării în impuls (engl., rez. rom.)		81

RĂZVAN LIȚOIU, IVANNIS ZERICHIORIS, ANCA ALUCULESEI, DAN GELU GĂLUȘCĂ și MARICEL AGOP (engl., rez. rom.)	89
.....	
NICOLETA MONICA LOHAN (MAHU) și IONUT LUCIAN BISTRICIANU, A supra proprietatilor mecanice a aliajelor dentare nenobile Co-Cr (engl., rez. rom.)	97
MANUELA CRISTINA PERJU, CARMEN NEJNERU, DAN-GELU GĂLUȘCĂ, PETRICĂ VIZUREANU și TUDOR RĂILEANU, Analiza grosimii stratului de wolfram depus prin metoda electrodului vibrator (engl., rez. rom.)	105
IRINA SURDU, CARMEN NEJNERU, ROXANA CARABET, DAN GELU GĂLUȘCĂ și MARCEL AGOP, Cercetări privind caracteristicile de răcire în pat fluidizat a mediilor pulverulente tip nisip, sare și șpan de fontă barbotate cu aer (engl., rez. rom).	113
IOANNIS ZERICHIOTIS, ANCA ALUCULESEI, RAZVAN LITOIU, DAN GELU GĂLUȘCĂ and MARICEL AGOP, Transferul termic in nanostructure(III). Comportamentul de tip convective (engl., rez. rom.)	121

MATERIALS SCIENCE AND ENGINEERING

CONTENTS		<u>Pp.</u>
ADRIAN ALEXANDRU and ROXANA GABRIELA ȘTEFĂNICĂ, Hard Layers with Wear Resistance Depose On 21MoMnCr12 Steel for Machine Parts. Microhardness Researches (English, Romanian summary)		7
ANCA ALUCULESEI, RĂZVAN LIȚOIU, IOANNIS ZERICHIOTIS, CONSTANTIN BACIU and MARICEL AGOP, On the Thermal Transfer in Nanostructures (I). Mathematical Model, (English, Romanian summary)		17
MIHAI AXINTE, CARMEN NEJNERU, MANUELA PERJU and ION HOPULELE, Using Ionic Triode in a Plasma Study Facility in Terms of Termic and Mass Transfer (English, Romanian summary)		27
ROXANA-GABRIELA ȘTEFĂNICĂ and ADRIAN ALEXANDRU, Aspects on Some Aluminum Alloys Cyclic and Classically Aged (English, Romanian summary)		37
CIMPOEȘU NICANOR, AXINTE MIHAI, CIMPOEȘU HANU RAMONA, HOPULELE ION, ATUDOSIE IOAN and PARASCHIV PETRONELA, Damping Capacity Simulation of Some Metallic Materials (English, Romanian summary)		45
RAMONA CIMPOEȘU HANU, CONSTANTIN BACIU, SERGIU STANCIU, DELIA MARINELA AELENEI, NICANOR CIMPOEȘU and PETRONELA PARASCHIV, Electro - Corrosion Behavior Study of a Superelastic Ni-Ti Alloy Through Sem and Edax Analysis (English, Romanian summary)		55
SANDA CRETU, Theoretical and Experimental Aspects Regarding Phenomenons That Are Produced in the Undismontable Assemblings (English, Romanian summary)		67
ADRIAN GRECU, DAN-GELU GALUȘCĂ, CARMEN NEJNERU, ION HOPULELE and MIHAI AXINTE, Research on Cooling Capacity Modification for Synthetic Quenching Environments Type as Modified Polyachilenglycol (PAG) (English, Romanian summary)		73
ANCA ELENA LĂRGEANU, DAN-GELU GĂLUȘCĂ, CARMEN NEJNERU, MANUELA CRISTINA PERJU and ION HOPULELE, Impact of corrosion on the surface layer pressed by material addition coating by impuls discharge method (English, romanian summary) . . .		

	81
RĂZVAN LIȚOIU, IVANNIS ZERICHIORIS, ANCA ALUCULESEI, DAN GELU GĂLUȘCĂ and MARICEL AGOP, On the Thermal Transfer in Anostrures (II) Conductive Type Behaviour (English, Romanian summary)	89
NICOLETA MONICA LOHAN (MAHU) and IONUȚ LUCIAN BISTRICIANU, On the Mechanical Characteristics of Commercial Non-Precious Co-Cr Dental Alloys (English, Romanian summary)	97
MANUELA CRISTINA PERJU, CARMEN NEJNERU, DAN-GELU GĂLUȘCĂ, PETRICĂ VIZUREANU and TUDOR RĂILEANU, Thickness Annalasis of Tungsten Coating Layer Deposited by Electrode Vibrator Method (English, Romanian summary)	105
IRINA SURDU, CARMEN NEJNERU, ROXANA CARABET, DAN GELU GĂLUȘCĂ and MARCEL AGOP, Researches Concerning the Cooling Characteristics of the Powder Backing in Fluidized Bed Tip Sand, Salt And Shavings Cast Iron Barbotaged with Air (English, Romanian summary)	113
IOANNIS ZERICHIOTIS, ANCA ALUCULESEI, RAZVAN LITOIU, DAN GELU GALUSCA and MARICEL AGOP, On the Thermal Transfer in Nanostructures(III). Convection Type Behavior (English, Romanian summary)	121

**HARD LAYERS WITH WEAR RESISTANCE DEPOSE ON
21MoMnCr12 STEEL FOR MACHINE PARTS.
MICROHARDENESS RESEARCHES**

BY

ADRIAN ALEXANDRU and ROXANA GABRIELA ȘTEFĂNICĂ

Abstract. The aim of this paper is to analyze the micro-hardness of hard layers deposed by electrical discharge in impulse on machine parts by 21MoMnCr12 steel.

In order to establish the influence of alloying deposition by electrical discharge in impulse on machine parts, were made researches on 21MoMnCr12 romanian steel which was thermal treated before alloying deposition by electrical discharge in impulse by two variants : quenching and quenching +tempering.

Key words: micro-hardness, layer, electrode.

1. Introduction

Alloying and deposition by electrical discharge in impulse method uses the inverse polarity – the part which is processed is the cathode and the electrode is the anode- and in this case the deposition takes place in air or other gas, with or without a rotation movement.

By comparing with other methods, alloying and deposition by electrical discharge in impulse presents a series of advantages as: the deposed metallic layer presents a resistant connection with the basis material; the method makes possible the deposition of pure metals (Ni, Cr, Mo, W, Ti) or metallic alloys; it is not necessary a preliminary preparation of the deposition surface, etc.

The demanded properties for the layer are different of those of the basic material and almost in contradiction with them. The efficient combination of alloying and deposition by electrical discharge in impulse with a superficial thermal treatment can make disappear many disadvantages of this method as:

large roughness of the alloyed surface, residual stress in layers which decrease the wear resistance.

2. Basis Material, Electrodes and Technologies

In order to determining the influence of alloying and deposition by electrical discharge in impulse of layers wear resistant on machine parts were made researches on 21MoMnCr12 steel used as support.

Chemical composition of 21MoMnCr12 steel is: 0,18-0,24 %C; 0,8-1,2 %Mn; 0,17-0,37 %Si; 0,02-0,04 %S; 0,035 %P; 1-1,4 %Cr; 0,2-0,3 %Mo. In table 2.1 are presented the mechanical properties and thermal treatment parameters for the 21MoMnCr12 steel.

The 21MoMnCr12 steel is recommended for machine parts thermal treated. This kind of steels are used only thermal or thermo chemical treated. The 21MoMnCr12 steel set in STAS 791 - 88, is a heat-treated steel for production of parts in machine building.

Alloy steels for machine building come in the form of rolled or forged products with thicknesses below 250 mm, capable of normalizing or annealing of (for softening, increased machinability and training structure for the final heat treatment).

Table 2.1

Mechanical Properties and Thermal Treatment Parameters

Steel	Mechanical properties					Thermal treatment parameters							
	R _{p0,2} , [N/mm ² , min]	R _m , [N/mm ² , min]	A ₅ , [%, min]	KCU, [J/cm ² , min]	HB, [daN/mm ²]	Annealing		Normalising		Quenching		Tempering	
						T, [°C]	Medium	T, [°C]	Medium	T, [°C]	Medium	T, [°C]	Medium
21MoMn Cr12	880	1080	8	68	R+217	680-700	c	-	-	810-830	u	170-230	a

It is used only for thermochemical or heat treated condition. The main characteristic of this steel is the depth of guaranteed hardening in bandwidth as hardening curves, which were drawn on Jominy specimens with austenitic grain score of at least 5. Finally, parts of this steel can be treated by thermochemical hardening, cyanide and carbonitration if they have under 0.25% C, by nitriding

if the steel has over than 0.3% and contains Mo, Cr or Al, through entered hardening, followed by a low or high return and with a superficial hardening followed by low return, if it contains more than 0.25% C.

The yield stress of these steel is 495...1275 N/mm², the breaking strength is 685...1620 N/mm², resilience between 50 and 88 J/cm², the elongation at break of 7...15%, hardness in annealed is 179...248 HB and fatigue of 278...564 N/mm².

Correlation between resilience and resistance for the case of hardening alloy steel and improvement is decreasing.

The tenacity of alloy steels depends mainly on the carbon content, decreasing with the increasing the carbon content in the alloy steels for hardening and to the improvement, also decreases with decreasing test temperatures.

Strength properties of this steel decrease with the increasing temperature for annealing, and properties of plasticity increases, as shown in the diagrams.

Special properties of this steel are provided by the alloying elements. Thus, Mn, increases hardening and wear resistance, but prints crude steel structures, insufficiently reduced by addition of Si or V. The steels which contains Mn and Si are more resistant to wear, but more difficult to process and have the trend of surface decarburizing. Cr increases hardening and plasticity, and together with Si and V improves over property after improvement. Mo greatly increases hardening and mechanical characteristics. Ni increases the tenacity of the steel and Al, Cr, Mo and V improve the properties of nitrated layers formed by nitrides.

Alloy steels weldableness is medium for machine building, it requires a pre-and after annealing with electric arc welding. Steels alloyed with Al, Cr, Mo and V, are not recommended for welding. The machinability of alloy steels is low, it is improved by annealing.

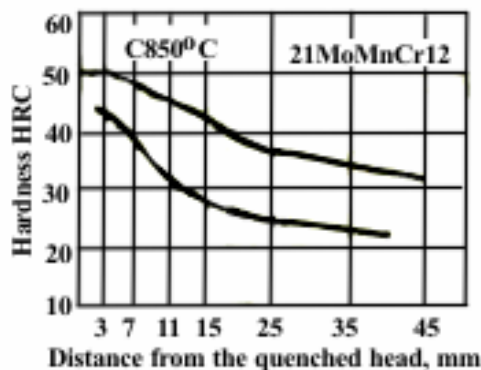


Fig. 2.1. – Hardening strips of 21MnMoCr12 steel.

As a specific use of 21MnMoCr12 steel, it is used as a substitute for steel chrome-nickel for machinery in the car industry: gearing, spare joint, shafts, axles, bolts, bushings, gears, wedges, etc.

2.1. Variants of Thermal Treatment Applied Before Alloying and Deposition by Electrical Discharge in Impulse

It was found that the filing and processing of metal surfaces by electrical discharge in impulse gives clear advantages such as: obtaining a layer and substrate with high adhesion to the basic material, get a higher hardness and wear resistance of the deposited layer obtaining special features of superficial layers decreases their fatigue, to obtain a high surface roughness, etc.

All the filing and alloying of the regions by electrical impulse filing can be totally or partially eliminated, combining effectively a thermochemical or thermal treatment with a processing of this kind.

Table 2.2.
Variants of the Applied Heat Treatment

Steel	Technological parameters
21MoMnCr12	a) Quenched at 820°C/oil; b) Quenched at 820°C/oil + tempered at 200 °C/air

In Fig 2.2 are presented the applied heat treatment.

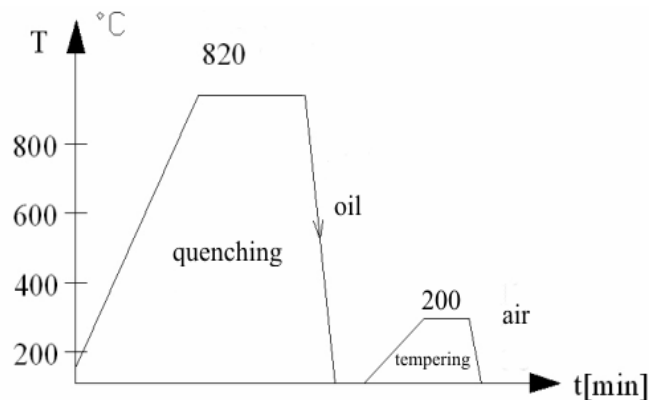


Fig. 2.2 - Applied heat treatment

2.2. Electrodes (Deposited Materials)

It was established that the electrode material has a large influence on the depth and hardness of hardened layer. The best electrodes for hardening the machine parts in terms of obtaining maximum hardness depths are chromium-based electrodes, made from ferrochromium chrome - manganese and pure chrome. The same materials ensure the highest wear resistance of hardened parts in comparison to other materials.

Based on the investigations and practical tests it was concluded that the deposit materials as electrodes with Ø4 x 25 mm dimensions are as shown in Table 2.3.

Table 2.3
Electrode Materials

No.	Electrode materials	
	Name	Chemical composition
1	Stelite	56%Co; 32%Cr; 21%W; 2,8%C; rest Fe
2	WCo8	92%W; 8%Co
3	Fe – Mo	67,9% Mo; 0,73% Si; 0,09% C; 0,35% Cu; rest Fe
4	Fe - Cr	60%Cr; 0,82% Si; 0,08% C; 0,31% Cu; rest Fe
5	Mo	Mo 100%
6	21MoMnCr12	0,21% C; 1,1% Mn; 0,3% Si; 0,9% Cr
7	40Cr10	0,43% C; 0,7% Mn; 0,3% Si; 0,9% Cr
8	OLC 55	0,56% C; 0,7506% Mn; 0,32% Si

2.3. Deposition Technologies

The samples submitted to the depositing and processing of alloy by electrical impulse discharge had the areas adjusted to Ra = 5 to 10 micrometers cleaned of oxides and other impurities.

To make deposits it was used ELITRON 52 for manual installation in the flat electrode with circular cross section diameter of 4 mm and 25 mm, is presented in Fig. 2.3.

Working conditions of ELITRON facility is chosen according to the electrode material, machinery material to be treated and the characteristics that are desired to obtain.

The form and gauge of the machine parts treated by deposit and alloy by electrical in pulse discharge can be any, the areas processed can be external

or internal. Power supply frequency is 50-60 Hz, and the roughness layer $2 \div 6$ microns.

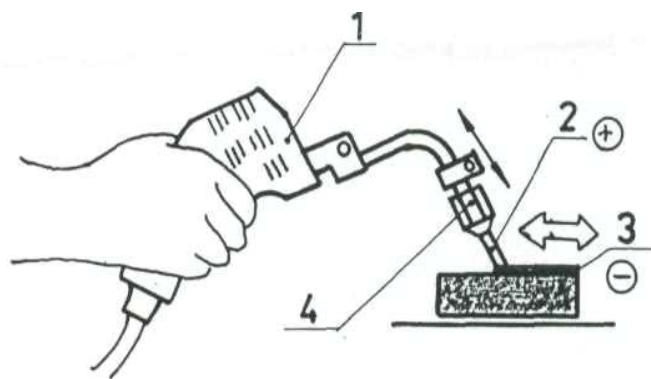


Fig. 2.3. Scheme of work for manual deposit and alloy by electrical in pulse discharge: 1-shaker; 2-electrode, 3-deposited layer on the piece, 4-chuck clamping the electrode.

Deposition parameters are given in Table 2.4

Table 2.4
Deposition Parameters

Power consumed	1,12 kVA
Productivity	2 cm ² / min
Voltage	220 V
Thickness of the deposited layer	0,05 ÷ 0,2 mm
Current Work	2,9 A
Surface roughness	1 ÷ 6 μm
Discharge energy	2,1 J

3. Experimental Research and Results

Rectangular samples (10x10x30 mm), on which were deposited layers by impulse electrical discharge on ELITRON 52 B installation, with electrodes from materials given from Table 2.3, were subjected micro-hardness measurements, thickness of the deposited layer, thickness of alloyed layer, roughness and microscopic investigations.

3.1. Mechanical Characteristics and Geometric Parameters of Layers

Measurements Results are Presented in Table 3.1.**Table 3.1**
Measurements Results

Sample	Steel	Electrode	Heat treatment	Micro-hardness, HV ₅₀			Thickness of the layers, [μm]		Roughness R _a , [μm]
				Deposited layer	Transition layer	core	deposited	transition	
1.a.1.	21MoMnCr12	Stelit	Q	1410	1110	407	61	46	4,72
1.a.2.		WCo8		1550	1231		67	39	5,20
1.a.3.		Fe-Mo		904	863		70	48	3,41
1.a.4.		Fe-Cr		880	791		72	45	3,14
1.a.5.		Mo		712	672		66	39	2,86
1.a.6.		21MoMnCr12		482	400		76	44	1,80
1.a.7.		40Cr10		588	411		75	41	1,92
1.b.1.	21MoMnCr12	Stelit	Q+T	1351	836	393	68	40	4,56
1.b.2.		WCo8		1402	912		76	36	4,02
1.b.3.		Fe-Mo		886	732		71	39	3,40
1.b.4.		Fe-Cr		813	728		71	45	3,16
1.b.5.		Mo		690	493		67	36	2,06
1.b.6.		21MoMnCr12		474	402		78	34	1,68
1.b.7.		40Cr10		568	412		74	38	1,52

Obs. Q - quenching, T- tempering.

Micro-hardness was measured on NAMICON 400DM/2006 microhardmeter with a force of 50 gf, a push time of 15 s and a thickness of 600:1. Roughness was measured on a SURTRONIC 3 + device.

Following implementation of experimental program is established that:

- High microhardness is obtained using for deposition stelite electrodes;
- Transition layer is alloy and very hard when it is used rich electrodes in alloying elements in descending order: WCo 8, stars, Fe - Mo - Fe - Cr - Mo;
- Filing of electrode layers of alloy steel and carbon (21MoMn Cr12, 40Cr12, OLC 55) allows obtaining denser layers than suport steel, the cause is a very fine structure (nanocrystalline) and high internal tensions in these layers;
- One and the same electrode gives different microhardness depending of the nature of support steel and heat treatment condition (Q or Q + T);
- Transition layers are diffusion layers at using the rich electrodes in alloying elements WCo8, stelite, Fe – Mo, Fe – Cr and Mo and return layers on quenched steels;
- On transition layers microdensity is a lot higher than core samples, while microhardness in return layers is smaller than hardened core;

- Thickness of white layers is between 61 and 70 microns, because it was used on ELITRON 52 B device current intensities and discharge energies in pulse greater (16 A și 2,1 J);

- The thickness of transition layer whether is diffusion or tempered is smaller than white layers $30 \div 60 \mu\text{m}$;

- Roughness Ra is higher when is using carbide electrodes (WCo8) and stelite (4,02...5,2 μm) and low when is using construction steel electrodes (1,12 \div 2,86 μm).

Micro-hardness values of the deposited layers on the three steels in hardened, toughened and tempered condition are given in Figure 3.1.

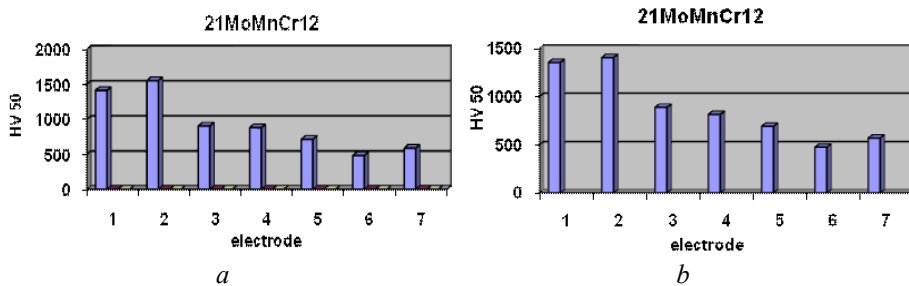


Fig. 3.1 – Micro-hardness values of the white layers (deposited) with different electrodes on steels 21MoMnCr12: *a* – quenched; *b* – quenched and tempered.

Transition micro-hardness values of this steel in hardened, toughened and tempered depending on the nature of the electrodes is given in Figure 3.2.

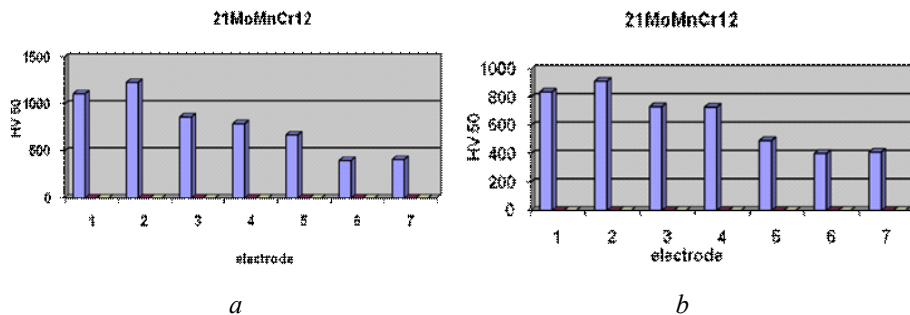


Fig. 3.2 – Micro-hardness values on transition values with different electrodes on 21MoMnCr12 steel: *a* – quenched; *b* – quenched and tempered.

Conclusions

- no matter of used electrode, the white layers are hard, even if the used electrode was from the same steel as the support;
- high micro-hardness values were obtained on the white layers deposited with WCo8 or stelite electrodes;
- on quenching steel, were obtained higher values of micro-hardness compared with quenched and tempering steel;
- Fe-Mo, Fe-Cr and Mo electrodes induced layers with high micro-hardness, and 21MoMnCr12 electrode induced smaller micro-hardness values, but higher than the case of the quenched or quenched + tempered steel.

Received: February 24, 2010

“Gheorghe Asachi” Technical University of Iași,
Department of Materials Science
e-mail: axa72us@yahoo.com

REFERENCES

1. Alexandru A., Strugaru S.I., *Alierea și depunerea superficială prin scânteie electrică-Influența tratamentelor termice asupra caracteristicilor straturilor*. Edit. Tehnopress, Iași, 2008.
2. Alexandru A., Pop F., *Metalic Materials with Hardened Deposit Created by Electric arc with Vibrating Electrode*. Euromat Junior-94, Lausanne, Elveția.
3. Alexandru I., Popovici R., Baciuc C., Călin M., Cojocaru V., Bulancea V., Carcea I., Alexandru A., Paloșanu G., *Alegerea și utilizarea materialelor metalice*. Edit. Did. și Ped., București, 1997.
4. Anderson A.W., *Physical Chemistry of Surfaces*. Wiley-Interscience, New-York, 1990.
5. Filip N., Abramciuc Alex., *Studii și cercetări experimentale privind formarea straturilor pe suprafețele pieselor de mașini cu ajutorul metodei de aliere cu descărcări electrice în impuls*. In vol. *Tehnologii avansate în secolul XXI*, Chișinău, 68-69 (2000).
6. Vermeșan G. et al., *Procedee speciale de tratamente termice*. Tipografia I.P. Cluj – Napoca, 1990.

STRATURI DURE REZISTENTE LA UZURĂ DEPUSE PE OȚELUL 21MoMnCr12 PENTRU ORGANE DE MAȘINI. CERCETĂRI DE MICRODURITATE

(Rezumat)

Scopul acestei lucrări este analiza microdurității straturilor dure depuse prin descărcare electrică în impuls pe organe de mașini din oțel marca 21MoMnCr12.

Pentru a stabili influența depunerii și alierii prin descărcare electrică în impuls asupra organelor de mașini, s-au făcut cercetări pe oțelul 21MoMnCr12, care a fost

tratat termic înainte de depunere și aliere prin descărcare electrică în impuls în două variante: călire și călire + revenire.

ON THE THERMAL TRANSFER IN NANOSTRUCTURES(I). MATHEMATICAL MODEL

BY

ANCA ALUCULESEI*, RĂZVAN LIȚOIU*, IOANNIS ZERICHIOTIS*,
CONSTANTIN BACIU* and MARICEL AGOP**

Abstract. Considering that the heat transfer in nanostructures takes place on fractal curves, a mathematical model which unites the microscopic-macroscopic scales of thermal transfer, the conductive-convective thermal type behaviours etc. is established.

Key words: nanostructures, thermal transfer.

1. Introduction

The Nottale's scale relativity (SR) model [1, 2] is based both on fractal space-time concept of Einstein's principle of relativity to scale transformations. In other words, the SR model is built by completing the standard laws of classical physics (motion in space-time) by new scale laws, the space-time resolution are used as intrinsic variables, playing for the scale transformation the same role as played by velocities for motion transformation [1, 2].

Three scales of interaction of SR were developed:

- i) A "Galilean" version corresponding to the standard fractals with constant fractal dimensions and which involves quantum mechanics;
- ii) A special scale-relativistic version which implies the high energy physics;
- iii) A „general scale-relativistic" version which implies the cosmology.

2. Consequences Extended of Non-Differentiability SR Model is Build According with the Unification of heat Transfer Phenomena in Nanostructures.

Let us suppose that the motion of particles take place on continuous but non-differentiable curves (fractal curves). The non-differentiability, according with Cresson's mathematical procedure [3, 4] and Nottale's physical principles [1, 2], implies the followings:

i) a continuous and non-differentiable curve (or almost nowhere differentiable) is explicitly scale dependent, and its length tends to infinity, when the scale interval tends to zero. In other words, a continuous and non-differentiable space is fractal, in the general meaning given by Mandelbrot to this concept [5];

ii) there is an infinity of fractal curves (geodesics) relating any couple of its points (or starting from any point), and this is valid for all scales;

iii) the breaking of local differential time reflection invariance. The time-derivative of a function F can be written two-fold:

$$(1) \quad \frac{dF}{dt} = \lim_{dt \rightarrow 0} \frac{F(t+dt) - F(t)}{dt} = \lim_{dt \rightarrow 0} \frac{F(t) - F(t-dt)}{dt}$$

Both definitions are equivalent in the differentiable case. In the non-differentiable situation these definitions fail, since the limits are no longer defined. „In the framework of scale relativity, the physics related to the behavior of the function during the „zoom” operation on the time resolution δt , here identified with the differential element dt („substitution principle”), which is considered as an independent variable. The standard function $F(t)$ is therefore replaced by a fractal function $F(t, dt)$ ([1, 4]) explicitly dependent on the time resolution interval, whose derivative is undefined only at the unobservable limits $\rightarrow 0$ ” [1, 2]. As a consequence, this leads us to define the two derivatives of the fractal function as explicit functions of the two variables t and dt ,

$$(2 \text{ a,b}) \quad \frac{d_+ F}{dt} = \lim_{dt \rightarrow 0_+} \frac{F(t+dt, dt) - F(t, dt)}{dt}$$

$$\frac{d_- F}{dt} = \lim_{dt \rightarrow 0_-} \frac{F(t, dt) - F(t-dt, dt)}{dt}$$

The sign, $+$, corresponds to the forward process and, $-$, to the backward process;

(iv) the differential of fractal function $F(t, dt)$ can be expressed as the sum of two differentials, one which is not scale-dependent, $dF(t)$, and the other dependent on it,

$dF''(t, dt)$, therefore [1,4]

$$(3) \quad dF(t, dt) = dF'(t) + dF''(t, dt)$$

Particularly, the differential of the generalised coordinates, $d_{\pm}X(t, dl)$, can be decomposed as follows:

$$(4a, b) \quad d_{\pm} \vec{X}(t, dt) = d_{\pm} \vec{x}(t) + d_{\pm} \vec{\xi}(t, dt)$$

where $d_{\pm}x(t)$ is the "classical part" and $d_{\pm}(t, dt)$ is the "fractal part". Starting from here, multiplying by dt^{-1} and using the substitutions

$$(5a -c) \quad \vec{V}_{\pm} = \frac{d_{\pm} \vec{X}}{dt}, \vec{v}_{\pm} = \frac{d_{\pm} \vec{x}}{dt}, \vec{u}_{\pm} = \frac{d_{\pm} \vec{\xi}}{dt}$$

we obtain the velocity field

$$(6a, b) \quad \vec{V}_{\pm} = \vec{v}_{\pm} + \vec{u}_{\pm};$$

(v) the fractal part of F , *i.e.* F'' , satisfies the relation [1-4]

$$(7) \quad |F''(t) - F''(t')| \approx |t - t'|^{\delta}$$

depends on the fractal dimension D_F ([1,2,5]).

Particularly, the differential of the "fractal part" of $d_{\pm}X$, becomes

$$(8a, b) \quad d_{\pm} \xi_i \approx dt^{\frac{1}{D_F}}$$

or more as an equality relation:

$$(9a, b) \quad \left(\frac{d_{\pm} \xi_i}{\lambda} \right) = \left(\frac{dt}{\tau} \right)^{\frac{1}{D_F}}$$

Written as

$$(10 \text{ a, b}) \quad d_{\pm} \xi_i = \frac{\lambda}{\tau} \left(\frac{dt}{\tau} \right)^{\left(\frac{1}{D_F} \right) - 1} dt$$

equations (9a,b) imply the temporal scales δt and τ , and the length scale λ , respectively. The significances of the time dt and τ result from the Random Walk (Brownian motion) or its generalization, Levy motion [1, 2]. The differential time dt is identified with the resolution time ("substitution principle" [1, 2]), $\delta t = dt$, while τ corresponds to the fractal -non-fractal transition time. The measure λ is a characteristic length, for example of Planck's or de Broglie's type ([1,2]) (vi) by the relation (10 a, b) the velocity field V_{\pm}^i becomes

$$(11 \text{ a, b}) \quad V_{\pm}^i = v_{\pm}^i + u_{\pm}^i = v_{\pm}^i + \frac{\lambda}{\tau} \left(\frac{\tau}{dt} \right)^{1 - \left(\frac{1}{D_F} \right)}$$

The transition scale τ yields two distinct behaviors of the speed, depending on the resolution at which it is considered, since $V_{\pm}^i \rightarrow v_{\pm}^i$ when $dt \gg \tau$, and $V_{\pm}^i = u_{\pm}^i$, when $dt \ll \tau$;

(vii) the local differential time reflection invariance is recovered by combining the two derivatives, d_+/dt and d_-/dt , in the complex operator ([1-4])

$$(12) \quad \frac{\hat{d}}{dt} = \frac{1}{2} \left(\frac{d_+ + d_-}{dt} \right) - \frac{i}{2} \left(\frac{d_+ - d_-}{dt} \right)$$

We call this procedure "an extension by differentiability" (Cresson's extension - for detail see [3, 4]). Applying this operator to the "position vector" yields a complex speed

$$(13) \quad \begin{aligned} \vec{v} &= \frac{\hat{d}\vec{X}}{dt} = \frac{1}{2} \left(\frac{d_+\vec{X} + d_-\vec{X}}{dt} \right) - \frac{i}{2} \left(\frac{d_+\vec{X} - d_-\vec{X}}{dt} \right) = \\ &= \frac{\vec{V}_+ + \vec{V}_-}{2} - i \frac{\vec{V}_+ - \vec{V}_-}{2} = \frac{1}{2} [(\vec{v}_+ + \vec{v}_-) + (\vec{u}_+ + \vec{u}_-)] - \frac{i}{2} [(\vec{v}_+ - \vec{v}_-) + (\vec{u}_+ - \vec{u}_-)] = \\ &\quad \vec{v} - i\vec{u} \end{aligned}$$

with

$$\vec{v} = \frac{\vec{V}_+ + \vec{V}_-}{2} = \frac{1}{2}[(\vec{v}_+ + \vec{v}_-) + (\vec{u}_+ + \vec{u}_-)]$$

(14 a, b)

$$\vec{u} = \frac{\vec{V}_+ - \vec{V}_-}{2} = \frac{1}{2}[(\vec{v}_+ - \vec{v}_-) + (\vec{u}_+ - \vec{u}_-)]$$

The real part, v , of the complex speed, V , represents the standard classical speed, which is differentiable and independent of resolution, while the imaginary part u is a new quantity arising from fractality, which is non-differentiable and resolution-dependent. In the usual classical limit, $dt \gg \tau$,

$$(15 \text{ a, b}) \quad \vec{v}_+ = \vec{v}_- = \vec{v}, \vec{u}_+ = \vec{u}_- = 0$$

so that

$$(16) \quad \vec{v} = \vec{V}, \vec{u} = 0$$

In the limit, $dt \ll \tau$;

$$(17) \quad \vec{v}_+ = \vec{v}_- = 0, \vec{u}_+ = \vec{u}_- = \vec{u}$$

and

$$\vec{v} = \vec{u}, \vec{u} = 0$$

$$(18) \quad \vec{v} = \vec{u}, \vec{u} = 0$$

(viii) "in order to account for the infinity of geodesies in the bundle, for their fractality and for the two valuedness of the derivative which all come from the non-differentiable geometry of the space-time continuum, one therefore adopts a generalized statistical fluid like description, where instead of a classical deterministic speed or of a classical fluid speed field, one uses a doublet of fractal functions of spaces coordinates and time which are also explicit functions of resolution time" [1, 2]. Thus, the average values of the quantities must be considered in the previously mentioned sense. Particularly, the average of $d_{\pm}X$ is

$$(19) \quad \langle d_{\pm}X \rangle = d_{\pm}\bar{x}$$

with

$$(20) \quad \langle d_{\pm} \bar{\xi} \rangle = 0$$

(ix) in such an interpretation, the "particles", are identified with the geodesies themselves. As a consequence, any measurement is interpreted as a sorting out (or selection) of the geodesies by the measuring device [1, 2].

3. A Equation for Thermal Transfer

Let us now assume that the movement curves (continuous but non-differentiable) are immersed in a 3-dimensional space, and that X of components x^i ($i = \overline{1,3}$) is the position vector of a point on the curve. Let us also consider the temperature $T(X, t)$ and the following Taylor series expansion, up to the second order:

$$(21a, b) \quad d_{\pm} T = \frac{\partial T}{\partial t} dt + \nabla f \cdot d_{\pm} \bar{X} + \frac{1}{2} \frac{\partial^2 T}{\partial X^i \partial X^j} d_{\pm} X^i d_{\pm} X^j$$

The relation (21) is valid in any point of the space-time manifold and also for the points

" X " on the fractal curve which we have selected in relation (21a, b).

From here, the forward and backward average values of this relation, take the form:

$$(22a, b) \quad \langle d_{\pm} T \rangle = \left\langle \frac{\partial T}{\partial t} dt \right\rangle + \langle \nabla T \cdot d_{\pm} \bar{X} \rangle + \frac{1}{2} \left\langle \frac{\partial^2 T}{\partial X^i \partial X^j} d_{\pm} X^i d_{\pm} X^j \right\rangle$$

We make the following stipulations: the mean values of the temperature / and its derivates coincide with themselves and the differentials $d_{\pm} X^i$ and dt are independent.

Therefore the averages of their products coincide with the product of average. Thus, Eqs. (22a, b) become:

$$(23a, b) \quad d_{\pm} T = \frac{\partial T}{\partial t} dt + \nabla T \cdot \langle d_{\pm} \bar{X} \rangle + \frac{1}{2} \frac{\partial^2 T}{\partial X^i \partial X^j} \langle d_{\pm} X^i d_{\pm} X^j \rangle$$

or more, using Eqs. (4a,b) with the properties (20 a,b),

$$(24a, b) \quad d_{\pm}T = \frac{\partial T}{\partial t} dt + \nabla T \cdot d_{\pm} \bar{X} + \frac{1}{2} \frac{\partial^2 T}{\partial X^i \partial X^j} (d_{\pm} X^i d_{\pm} X^j + \langle d\xi_{\pm}^i + d\xi_{\pm}^j \rangle)$$

Even the average value of the fractal coordinate, $d\xi_{\pm}^i$, is null (see (20 a,b)), for the higher order of the fractal coordinate average, the situation can be different. Let us focus on the mean $d\xi_{\pm}^i d\xi_{\pm}^j$. If $i \neq j$ this average is zero due the independence $d\xi^i$ of and $d\xi^j$. So, using (10a, b) we can write [1,2]

$$(25a, b) \quad \langle d\xi_{\pm}^i d\xi_{\pm}^j \rangle = \pm \delta^{ij} \frac{\lambda^2}{\tau} \left(\frac{dt}{\tau} \right)^{\left(\frac{2}{D_f} \right)^{-1}}$$

with

$$\delta^{ij} = \begin{cases} 1 & \text{if } i = j \\ 0 & \text{if } i \neq j \end{cases}$$

and we had considered that:

$$\begin{aligned} \langle d\xi_{\pm}^i d\xi_{\pm}^j \rangle &> 0 \quad \text{and} \quad dt > 0 \\ \langle d\xi_{\pm}^i d\xi_{\pm}^j \rangle &> 0 \quad \text{and} \quad dt < 0 \end{aligned}$$

Then Eqs. (24 a,b) may be written under the form:

$$(26 a, b) \quad \begin{aligned} d_{\pm}T &= \frac{\partial T}{\partial t} dt + \nabla T \cdot d_{\pm} \bar{X} + \frac{1}{2} \frac{\partial^2 T}{\partial X^i \partial X^j} d_{\pm} X^i d_{\pm} X^j \pm \\ &\pm \frac{\partial^2 T}{\partial X^i \partial X^j} \delta^{ij} \frac{\lambda^2}{2\tau} \left(\frac{dt}{\tau} \right)^{\left(\frac{2}{D_f} \right)^{-1}} dt \end{aligned}$$

If we divide by dt , and neglect the terms which contain differential factors (for details on the method see [23]), Eqs. (26 a,b) are reduced to:

$$(27a, b) \quad \frac{d_{\pm}T}{dt} = \frac{\partial T}{\partial t} dt + \bar{\nabla}_{\pm} T \pm \frac{\lambda^2}{2\tau} \left(\frac{dt}{\tau} \right)^{\left(\frac{2}{D_f} \right)^{-1}} \Delta T$$

with $\nabla^2 = \sum_i \frac{\partial^2}{\partial X_i^2}$.

These relations also allow us to define the operator,

$$(28 \text{ a, b}) \quad \frac{d_{\pm}}{dt} = \frac{\partial}{\partial t} + \bar{\mathbf{V}}_{\pm} \cdot \nabla \pm \frac{\lambda^2}{2\tau} \left(\frac{dt}{\tau} \right)^{\left(\frac{2}{D_F} \right)^{-1}} \Delta$$

Under these circumstances, let us calculate $\hat{d}f/dt$. Taking into account Eqs. (12), (13), and (28 a,b), we obtain:

$$(29) \quad \begin{aligned} \frac{\hat{d}T}{dt} &= \frac{1}{2} \left[\left(\frac{d_+ T}{dt} + \frac{d_- T}{dt} \right) - i \left(\frac{d_+ T}{dt} - \frac{d_- T}{dt} \right) \right] = \\ &= \frac{1}{2} \left[\left(\frac{\partial T}{\partial t} + \bar{\mathbf{V}}_+ \cdot \nabla T + \frac{\lambda^2}{2\tau} \left(\frac{dt}{\tau} \right)^{\left(\frac{2}{D_F} \right)^{-1}} \Delta T \right) - \left(\frac{\partial T}{\partial t} + \bar{\mathbf{V}}_- \cdot \nabla T - \frac{\lambda^2}{2\tau} \left(\frac{dt}{\tau} \right)^{\left(\frac{2}{D_F} \right)^{-1}} \Delta T \right) \right] - \\ &- \frac{i}{2} \left[\left(\frac{\partial T}{\partial t} + \bar{\mathbf{V}}_+ \cdot \nabla T + \frac{\lambda^2}{2\tau} \left(\frac{dt}{\tau} \right)^{\left(\frac{2}{D_F} \right)^{-1}} \Delta T \right) - \left(\frac{\partial T}{\partial t} + \bar{\mathbf{V}}_- \cdot \nabla T - \frac{\lambda^2}{2\tau} \left(\frac{dt}{\tau} \right)^{\left(\frac{2}{D_F} \right)^{-1}} \Delta T \right) \right] = \\ &= \frac{\partial T}{\partial t} + \left(\frac{\bar{\mathbf{V}}_+ + \bar{\mathbf{V}}_-}{2} - i \frac{\bar{\mathbf{V}}_+ - \bar{\mathbf{V}}_-}{2} \right) \cdot \nabla T - i \frac{\lambda^2}{2\tau} \left(\frac{dt}{\tau} \right)^{\left(\frac{2}{D_F} \right)^{-1}} \\ &\Delta T = \frac{\partial T}{\partial t} + \bar{\mathbf{v}} \cdot \nabla T - i \frac{\lambda^2}{2\tau} \left(\frac{dt}{\tau} \right)^{\left(\frac{2}{D_F} \right)^{-1}} \Delta T \end{aligned}$$

This relation also allows us to define the fractal operator

$$(30) \quad \frac{\hat{d}}{dt} = \frac{\partial}{\partial t} + \bar{\mathbf{v}} \cdot \nabla f - i \frac{\lambda^2}{2\tau} \left(\frac{dt}{\tau} \right)^{\left(\frac{2}{D_F} \right)^{-1}} \Delta$$

We now apply the principle of scale covariance and postulate that the passage from classical (differentiable) mechanics to the "fractal" mechanics, which is considered here, can be implemented by replacing the standard time-derivative, d/dt , by the complex operator (\hat{d}/dt) (this result is the principle of scale covariance given by Nottale [1], [2]). "This operator (\hat{d}/dt) plays the role of a covariant derivative operator', namely, it is used to write the fundamental equation

of dynamics under the same form as in the classical and differentiable case.

Under its above form, the covariant derivative operator is not itself fully covariant since it involves second order derivative terms, while it is a first order time derivative. These second order terms imply that the Leibniz rule for a product is no longer the first order Leibniz rule, but a linear combination of the first and second order rules.

The strong covariance can be fully implemented by introducing new tools allowing us to keep the form of the first order Leibniz rule, despite the presence of the second order derivatives [1, 2]. In this purpose, one defines the complex speed operator:

$$(31) \quad \hat{\mathbf{v}} = \bar{\mathbf{v}} - i \frac{\lambda^2}{2\tau} \left(\frac{dt}{\tau} \right)^{\left(\frac{2}{D_F} \right)^{-1}} \nabla$$

Particularly, for movements on fractal curves of the Peano type, *i.e.* in the fractal dimension $D_F = 2$, the complex speed operator (31) takes the form

$$(32) \quad \hat{\mathbf{v}}_{D_F=2} = \bar{\mathbf{v}} - i \frac{\lambda^2}{2\tau} \nabla$$

Thus, the covariant derivative recovers the standard first order form of a total derivative in terms of partial derivatives, namely, the strong covariance Nottale's principle [1, 2]

$$(33) \quad \frac{\hat{d}}{dt} = \frac{\partial}{\partial t} + \hat{\mathbf{v}} \cdot \Delta$$

In this condition the equation of heat transfer take the form:

$$(34) \quad \frac{\hat{d}T}{dt} = \frac{\partial T}{\partial t} + \bar{\mathbf{v}} \cdot \nabla T = \frac{\partial T}{\partial t} + \bar{\mathbf{v}} \cdot \nabla T - i \frac{\lambda^2}{2\tau} \left(\frac{dt}{\tau} \right)^{\left(\frac{2}{D_F} \right)^{-1}} \Delta T = 0$$

or more, by separating the real and imaginary parts:

$$(35 \text{ a,b}) \quad \frac{\partial T}{\partial t} + \bar{\mathbf{v}} \cdot \Delta T = 0, \quad -\bar{\mathbf{U}} \cdot \nabla T = \frac{\lambda^2}{2\tau} \left(\frac{dt}{\tau} \right)^{\left(\frac{2}{D_F} \right)^{-1}} \Delta T$$

By addition of equations(35 a,b), the equation of the heat transfer becomes:

$$(36) \quad \frac{\partial T}{\partial t} + (\bar{v} - \bar{u}) \cdot \Delta T = \frac{\lambda^2}{2\tau} \left(\frac{dt}{\tau} \right)^{\left(\frac{2}{D_F} \right) - 1} \Delta T$$

4. Conclusions

The main conclusions of the present paper are the followings:

i) considering that the movements of the particles take place on fractal curves, a fractal operator is build. This operator replaces the derivative d/dt from the classical mechanics:

ii) in such context the equations of the heat transfer for different scales are obtained;

iii) if $\mathbf{v}=\mathbf{u}$ the equation (36) becomes a equation of diffusion (convective) type.

Received: February 24, 2010

“Gheorghe Asachi” Technical University of Iași,

* Faculty of Materials Science and Engineering

e-mail: constantin_baciu@yahoo.com

** Department of Physics

e-mail: m.agop@yahoo.com

REFERENCES

1. Maxwell J.C., *A Treatise on Electricity and Magnetism*. (Dover, New York, 1954), 3rd ed., Vol. 1, p. 435
2. El Naschie M.S., Rosier O. E., Prigogine I. (Eds.), *Quantum Mechanics, Diffusion and Chaotic Fractals*, Elsevier, Oxford 1995
3. Cresson J., *Int. J. of Geometric Meth. In Mod. Phys.*, 3, 1395 (2006).
4. Cresson J., *J. Math. Anal. Appl.*, 307, 48 (2005).
5. Mandelbrot B.B., *The Fractal Geometry of Nature*, W.H. Freeman, San Francisco 1983.

TRANSFERUL TERMIC ÎN NANOSTRUCTURI(I). MODELUL MATEMATIC

(Rezumat)

Considerând că transferul termic în nanostructuri are loc pe curbe fractale, în prezenta lucrare se construiește un model matematic ce unește scările microscopice – macroscopice de transfer termic, comportamentele de tip termal conductiv - convectiv etc.

USING IONIC TRIODE IN A PLASMA STUDY FACILITY IN TERMS OF THERMIC AND MASS TRANSFER

BY

**MIHAI AXINTE, CARMEN NEJNERU, MANUELA PERJU
and ION HOPULELE**

Abstract. Discharging process can produce an undesirable phenomena such as arc discharge or the double cathode effect. Active screen plasma nitriding (ASPN) is an emerging surface engineering technology. By placing the ionic triode is amended both polarized electric field distribution between electrodes and the characteristic volt-ampere curve configuration of electrical discharge. We can change a classical plasma nitriding facility very easy into ionic triode terms by placing a screen between anode and cathode with a power source to the active screen. A simplified scheme for a fizico-mathematical model for stability study of electrical discharge inside the thermo-chemical treatment is presented. Analysis of the test facility has resulted in a better stability in terms of discharge for polarization of the screen and possibly an increase in heating efficiency

Key words: active screen plasma nitriding, ionic triode.

1. Introduction

Heating installations currently operating in the heat treatments sectors have a low thermal efficiency, both due to constructive solutions, and inefficient methods of chemical energy or electrical energy transformation required in heating premises by thermo-chemical treatment. Using modern heating fluidized layer in the flow of electrons in vacuum, plasma and laser are effective methods to increase yield and quality of plants and treated parts.

A classical plasma nitridings should create necessary conditions for achieving an electrical luminescence in an atmosphere of nitrogen and hydrogen at a pressure as low as (2-12) mBa. where the nitriding parts should be the discharging cathode, voltage electrical 400 - 1000V.

Physically, the ionic nitriding facility form ionic diode cathode where the cathode is the nitrided part subject and the discharge atmosphere is formed from a mixture of nitrogen and hydrogen at low pressure.

Physical discharging process produce an undesirable phenomena such as arc discharge or the double cathode effect, also part of the accumulated heat in the piece is lost in the environment by radiation.

To avoid these 2 phenomena several measures are taken to prevent, so to prevent arc discharge there are used specialized electronic circuits and to avoid double cathode is amended in convenient way pressure and supply voltage. Reduced heat loss is achieved through the use of thermal screens.

In case of ionic triode the screen between anode and cathode is electrically polarized, so it changes the configuration of electric field between anode and cathode.

Changing the electrical field between anode and cathode changes both degeneration conditions of the discharge in electric arc and the double cathode forming by adjusting electric potential of the screen. Due to changing electric field that surround the part in the thermo-chemical treatment process the forming difused layer parameters will change.

For the analysis of nitriding process in ionic triode conditions was manufactured a laboratory facility that allows to track the nitriding technology and physical parameters of discharge in the tenuous gas environment.

2. Facility for Nitriding Process Analysis in Conditions of Using an Ionic Triode System Type

The physical principle of a triode ion consists in introducing a polarized screen in the electric field between anode and cathode. This screen is intended to change the configuration of electric field between anode and cathode, so that the discharge to change in a convenient way. Polarized screen conditions are good for both of discharge starting and the discharge stability.

A classical plasma nitridings facility is very easy to adjust in the ionic triode conditions by an electrical power source to the active screen.

In order to establish the electric discharge operation conditions in the heating process and the diffused layer effects we designed a laboratory facility that allows the ionic triode presence parameters measurement.

Operational scheme plant is shown in Fig. 1.

After chamber washing and a vacuum of 10^{-1} Torr connects anodic current and regulates the discharging current. After a while the power is connected to the screen and adjust the desired value. It shall then reduce the degree of vacuum by introducing the gas then adjust anodic current to the

desired value. Due to changing discharge conditions the screen current is changing, which requires appropriate correction.

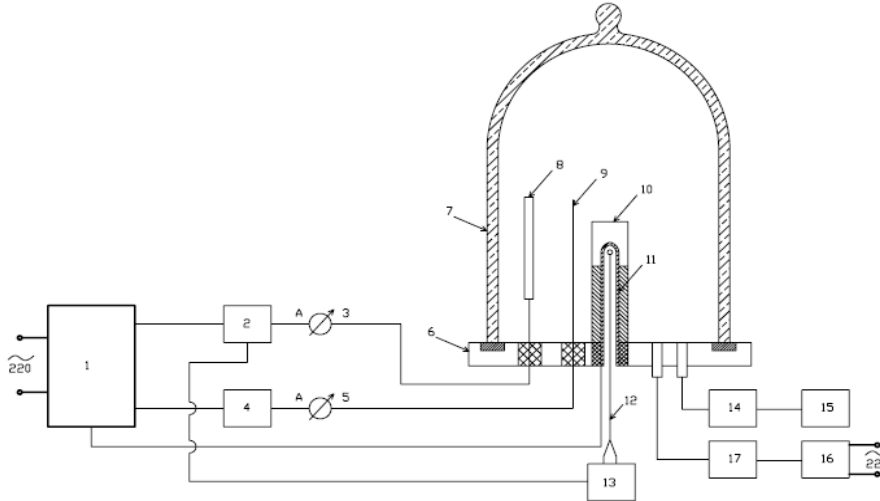


Fig.1. – Block scheme of the discharge in the tenuous gas in terms of ionic triode: 1 - Transformer - rectifier, 2 - Anodic current regulator, 3 - Device for measuring the anodic current, 4 - Current regulator for polarization display, 5 - Device for measuring the current screen, 6 – The installation support, 7 -Vacuum chamber, 8 - Metal anode, 9 - Polarized screen, 10 - Under heating tubes, 11 - Insulated sheath metal, 12 –Thermocouple, 13 - Temperature measuring and controlling installation, 14 - Regulating gas flow system , 15 - Gas tank , 16 - Vacuum pump, 17 - Vacuum regulating system.

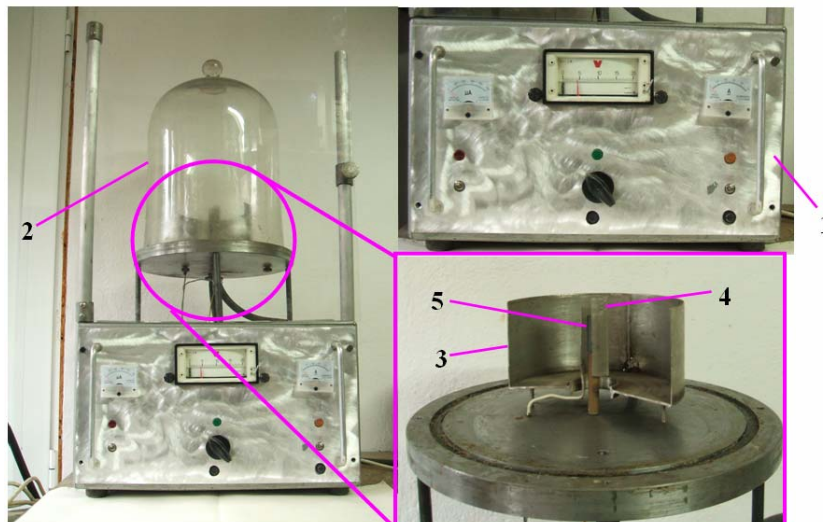


Fig.2. – Photo- installation in terms of ionic triode: 1 - desk power adjustment and control, 2 - Vacuum bell, 3 - Anode, 4 - Polarized screen, 5-Under heating tubes.

When the temperature reaches near the prescribed temperature the anodic current discharge is automatically reduced.

A photo of the plant is shown in Fig. 2 where is observed both power supply, adjustment and measurement desk and the precinct work.

Analysis of the test facility has resulted in a better stability in terms of discharge for polarization of the screen and possibly an increase in heating efficiency.

3. Electric Discharge Stability Analysis in Tenuous Gas

In the technological aspects (for the thermo-chemical treatment), the discharge in the tenuous gas must be stable and efficient in terms of heat and mass transfer in the superficial layer. In electrical discharge between two electrodes in a tenuous gas there are a range of physical phenomena that lead to a distribution of electric field (Fig.3).

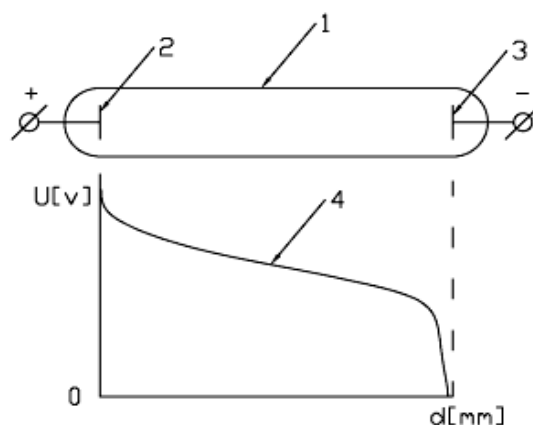


Fig. 3. – Distribution of electric field in the discharge: 1 - Tenuous gas space, 2 - Anode, 3 - Cathode, 4 - Distribution of electric field, U-voltage power between anode and cathode, d-distance between anode and cathode.

From electric field distribution analysis, it follows that the voltage drop occurs near the cathode, leading to a process of heating it. This phenomenon is even more intense as the current is higher and the vacuum is lower (1-10 Torr).

To have a picture of the phenomenon must be analyzed the characteristic curve volt-amps of discharge into the environment of tenuous gas, an example is provided in Fig. 4.

To achieve thermo-chemical treatment is used the discharge conditions of FG part, which gives both a good stability of discharge and a power strong enough to ensure that the process of heating the cathode.

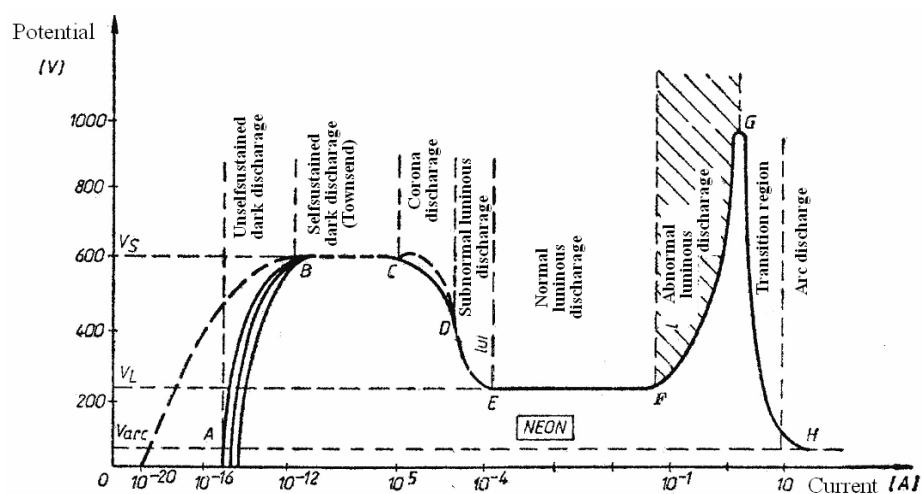


Fig. 4. – Characteristic volt-amperes curve for neon at a pressure of 1 Torr in a tube length of 50 cm and electrodes section of 10 cm^2

An objective analysis of the technological process of thermo-chemical treatment by discharge into the environment of tenuous gas can be achieved by using a physico-mathematical model so as to reveal the stability of the process taking into account characteristic diagram volt-amperes.

To ensure stability of the process must take into account both the source of electric power and consumer characteristics (the discharge gas in tenuous gas).

A simplified scheme for a fizico-mathematical model for stability study of electrical discharge inside the thermo-chemical treatment is presented in Fig. 5.

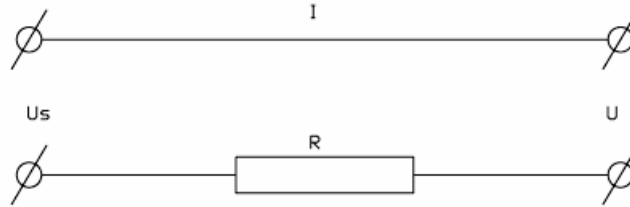


Fig. 5 - The source-consumer circuit for discharge into the environment of tenuous gas. U_s -voltage power source, U -voltage discharge between electrodes, R -resistance on the circuit power, I -current intensity.

Under the scheme of figure 5 can be written following equation (physico-mathematical model):

$$(1) \quad U_s = U + IxR$$

Product $I \times R$ represents the drop of resistance voltage circuit. Electrical voltage U (of the discharge process) is in accordance with characteristic curve volt-amperes (presented in Figure 4) the portion is F-G:

$$(2) \quad U = \Phi(I)$$

If in the download process appears a disturbance, meaning a variation of current (an instability), then the voltage will change according to changes in current.

$$(3) \quad \Delta U = \frac{dU}{dI} \Delta I$$

Power supply will respond with a power of selfinduction, knowing that the power network is currently via a high voltage transformer. Changing supply voltage U_s will value:

$$(4) \quad \Delta U_s = L \frac{d(\Delta I)}{dt}$$

L inductance value depends on the electrical transformer and network features. As a result of these disruptions, relationship 1 acquires the following form:

$$(5) \quad U_s + \Delta U_s = U + \Delta U + R(I + \Delta I)$$

Introducing the 3,4 values in the relationship 5 resulting:

$$(6) \quad U_s - L \frac{d(\Delta I)}{dt} = U + \frac{dU}{dI} \Delta I + R(I + \Delta I)$$

Using 1 and simplifying the relationship bearing in mind that the $U_s - U - IR = 0$ resulting:

$$(7) \quad -L \frac{d(\Delta I)}{dt} = \Delta I \left(R + \frac{dU}{dI} \right)$$

This relationship can be written as:

$$(8) \quad \frac{d(\Delta I)}{\Delta I} = -\frac{1}{L} \left(R + \frac{dU}{dI} \right) dt$$

By integrating resulting:

$$(9) \quad \ln(\Delta I) = -\frac{1}{L} \left(R + \frac{dU}{dI} \right) t + c$$

Conditions for the constant (C) are subject to the disturbance triggering:

For $t = 0$ corresponds:

$$(10) \quad \Delta I = \Delta I_0$$

Thus the relationship (9) can be written as:

$$(11) \quad \Delta I = \Delta I_0 e^{-\frac{1}{L} \left(R + \frac{dU}{dI} \right) t}$$

For the perturbation (ΔI) to be reduced as quickly as possible it needs to have an electrical resistance (R) on electrical supply circuit of the discharge as high and a slope of the curve characteristic volt-amperes more pronounced (F-G portion).

Increasing resistance from the electrical supply leads to lower efficiency plant which requires the minimum possible limiting value of this resistance.

Regarding discharge characteristic curve inclination may be altered by adjusting gas pressure in the chamber and by changing the work current.

By placing the thermal screen is amended both polarized electric field distribution between electrodes and the characteristic volt-amperes curve configuration of electrical discharge in the environment of tenuous gas.

For this purpose facility can be used to analyze the thermo-chemical technological treatment process stability.

4. Conclusions:

1. Ionic triode has positive effect to the nitrated item surface quality, ionic sputtering do not affect the item roughness.

2. From the approached mathematical model we observe that facility energetic efficiency grows.

3. Ionic triode gets all the unwanted discharges avoiding the arc and the double cathode.

Received: February 14, 2008

"Gheorghe Asachi" Technical University of Iași,
Department of Materials Science
e-mail: mihai.axinte@gmail.com

REFERENCES

1. Gălușcă D.G., *Plasma nitriding*. Sedcom Publishing House, Iași, 1997.
2. Popa, Gh., *Technological Applications of Plasma*. Al. I. Cuza University publishing house, Iași, 1998.
3. Ștefan. M., *Considerations About the Thermal and Thermochemical Treatment. Equipments Utilisation using Vacuum Atmosphere*. 15th Heat Treatment National Conference Dunaujvaros, Hungaria, 19-21 oct. 1993.
4. Vermesan G., *Plasma nitriding technological bases*. Sibiu University Publishing House, Sibiu, 1992.
5. Axinte M., Carmen Nejneru, Hopulele I., Ștefan M., *Facility for Study Heating and Diffusion Processes in Terms of Ionic Triode Plasma*. Suceava, The 15-th International Conference Tehnomus, 2009 pag. 223.

UTILIZAREA TRIODEI IONICE ÎNTR-O INSTALAȚIE PENTRU STUDIUL TRANSFERULUI TERMIC ȘI DE MASĂ ÎN PLASMĂ

(Rezumat)

Nitrurarea în plasma cu ecran activ (ASPN) este o tehnologie în curs de dezvoltare în domeniul ingineriei suprafațelor. În procesul fizic de descărcare se produc

și fenomene nedorite cum ar fi: descărcarea în arc sau efectul de catod dublu. Prin introducerea ecranului termic polarizat se modifică atât distribuția câmpului electric dintre electrozi cât și configurația curbei caracteristice volt-amper a descărcării electrice în mediu de gaz rarefiat. O instalație clasică de nitrurare în plasmă este foarte ușor de reglat în condiții de triodă ionică printr-o sursă de energie legată la ecranul activ. Este prezentată de asemenea o schemă simplificată pentru realizarea unui model fizico-matematic de studiu a stabilității descărcării electrice în incinta de tratament termochimic. Din analiza procesului de testare a instalației a rezultat o stabilitate mai bună a descărcării în condiții de polarizare a ecranului și posibil o creștere a randamentului de încălzire.

ASPECTS ON SOME ALUMINUM ALLOYS CYCLIC AND CLASSICALLY AGED

BY

ROXANA-GABRIELA ȘTEFĂNICĂ and ADRIAN ALEXANDRU

Abstract. The paper presents some aspects on some aluminum alloys taken into consideration with respect to tensile strength and micro-hardness. These aluminum alloys takes part of 7xxx series, more precisely A7075 T651. The results shown in the paper present a comparison between two different kinds of artificial ageing like classical versus cyclic heat treatment.

Key words: cyclic artificial ageing, mechanical response, A7075 T651.

1. Introduction

One of the most significant metallic materials discovered is aluminum. Yet, it is relatively new discovered although it is well known the fact it particularly forms the third part of Earth's crust. Hence, is considered as the metal of the twenty's century. Its particularly unique properties make it one of the most versatile, economic and attractive metallic material for a broad range of uses such as for aviation, navy, transportation etc.

Yet, aluminum is a soft metallic material with a density of only 2.73g/cm^3 and it uses as plating material because it is a good anticorrosive. It also uses for electric cables, cookers, viewing mirrors of the telescopes etc.

Unalloyed aluminum is soft and ductile and in commercial shape, it needs a higher strength that aluminum cannot afford. This strength achieves by adding different elements such as copper, magnesium, zinc, silicon, iron etc. In addition, there is almost no branch of the modern industry where aluminum alloys does not develop such as castings, forgings, rods, wires, profiles etc.

Aluminum alloys fall under different points of view such as density, number of electrons, processing method etc. Yet, aluminum alloys divide in

heat treatment and non-heat treatment aluminum alloys. More precise one can say that aluminum alloys divide in wrought and cast aluminum alloys.

The figure bellow presents the existent aluminum alloys:

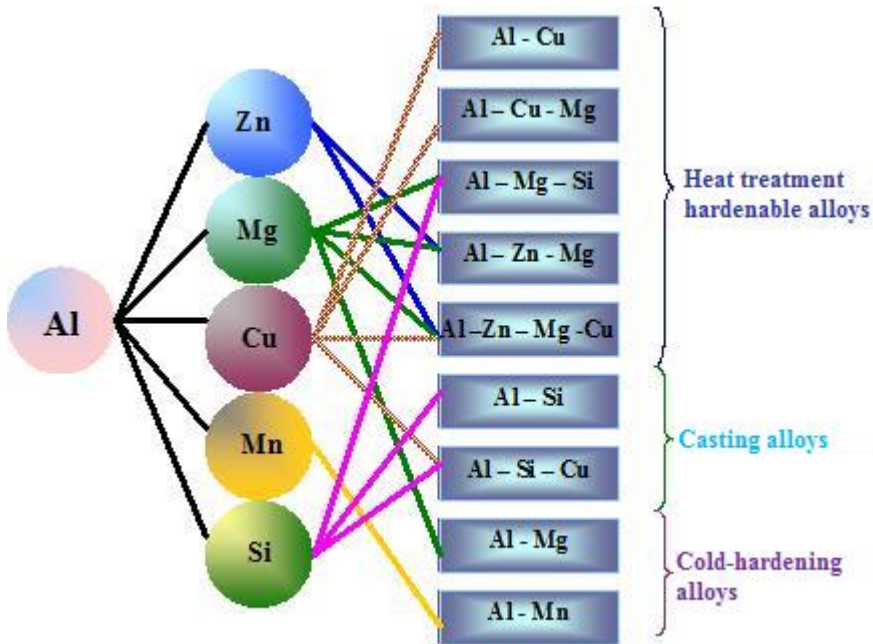


Fig. 1. – Aluminum and its alloys.

In this paper, we discuss wrought aluminum alloys from 7xxx series, A 7075 T651, that support heat treatment in order to get strength.

2. Discussion

In engineering applications, strength is, without any doubt, an important parameter. Yet, it is by no means the only important parameter and usually a material must provide a certain combination of properties.

Wrought aluminum alloys discussed in the paper are heat treatable alloys. The basic strength of these alloys intensifies by addition of alloying elements such as copper, magnesium, zinc, and silicon. Once these elements in different combinations show a solubility increase in aluminum with temperature increase, we can make them support some heat treatments. These heat treatments will give them a pronounced hardness and tensile strength.

The heat treatments an alloy support consist in annealing, solution treatment, quenching, and precipitation hardening (artificial ageing).

In the wake of a suitable heat treatment, the atoms of the solute

accumulate progressively to form smaller particles, which separate the proper grains of the matrix – this process is called precipitation. It should be well-known from the beginning the fact that precipitation is a metallurgical process (a phase transformation) that responds to the fact that alloy is initially in out of equilibrium state and giving him a sufficient time at a certain temperature, it take place progressively atoms diffusion. This transforms metallurgical structure (microstructure) to equilibrium. After rapid quenching in water or oil, under certain conditions of heat treatment, through precipitation, particles of precipitate create. They form a real impediment in dislocations path. The precipitation process goes on and the number and size of the precipitates increases so that aluminum alloy gets harder. Another name, frequently used for precipitation hardening is ageing hardening.

The aluminum alloy taken into discussion belongs to Al-Zn-Mg-Cu quaternary diagram.

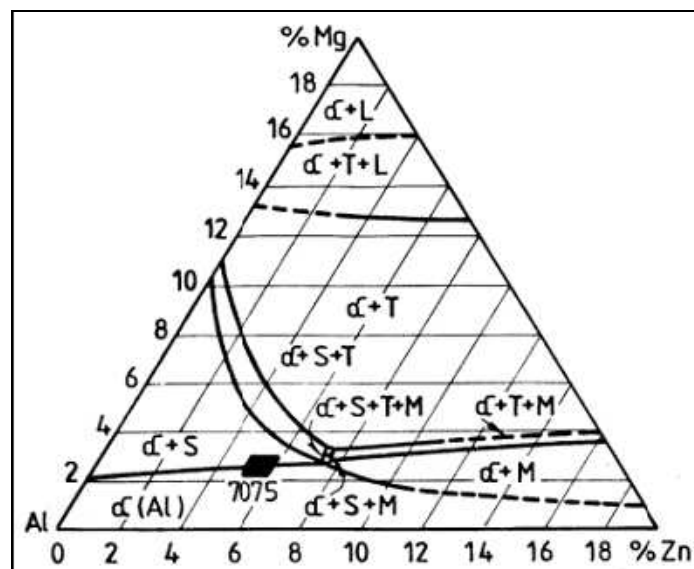


Fig. 2. – Isotherm section at 460°C of the aluminum rich angle from Al-Zn-Mg-Cu diagram for a constant copper content of 1.5%.

Although in this paper, 7xxx series discusses, aluminum-copper equilibrium diagram can be used to exemplify the structures achieve after a complete heat treatment.

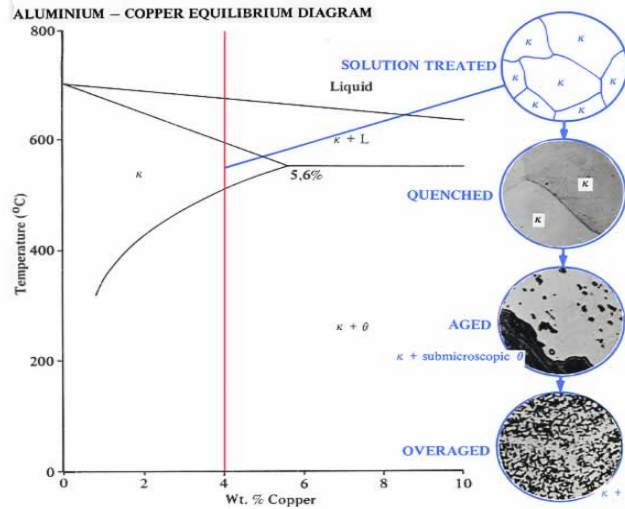


Fig. 3. – Al-Cu equilibrium diagram.

3. Results

The aluminum alloys taken into consideration take part from the remarkable 7xxx series. They use especially for structures, stressed parts etc. In addition, they must have a significant strength in order to bear different loads.

The chemical composition of the material influences its plasticity and deformation resistance both by nature and by distribution of the alloying elements and by phase transformations they produce. Along with increase of alloying degree plasticity decreases and deformation resistance increases.

Copper and chromium is added to improve corrosion resistance and crack strength. The content of iron (max. 0,2%Fe) and silicon (max. 0,1%Si) as impurities is very important because they diminish plasticity, and manganese additions (almost 1%Mn) neutralize the damaging influence of iron and increases corrosion resistance and hardening.

A7075 alloy has the chemical composition given in the table bellow:

Table 1.
Chemical Composition of A7075 Alloy

Si %	Fe %	Cu %	Mn %	Mg %	Cr %	Zn %	Ti %
0.09	0.25	1,2	0.05	2,253	0.209	5,53	0.034

The proper heat treatment consisted in:

- annealing at 413°C for two hours and cooling rate in air;

- solution heat treatment, which consisted in heating to 480°C, maintaining for two hours and quenching in cold water.

Solution quenching is an intermediary heat treatment, which aims to achieve two goals:

- the achievement of the control values for plasticity, in order to be cold-processed;

- the achievement of starting structure for ageing.

- Artificial ageing in two different ways, which consisted in heating the alloy to 121°C, maintain at this temperature for 8 hours and air cooling and the second way was to heat the aluminum alloy to 121°C, maintaining it for 20 minutes, water cooled and maintained for 5 minute, heated again to 121°C maintained for 20 minutes, water-cooled. This heat treatment consisted in 3 complete cycles as described above.

By artificial ageing understands a subcritical heat treatment realized for getting the materials in thermodynamic equilibrium. The material gets harder if the precipitates are coherently connected with the matrix. Once the coherency is broken, hardness starts to decrease.

The samples were heat treated and analyzed for microhardness and tensile strength.

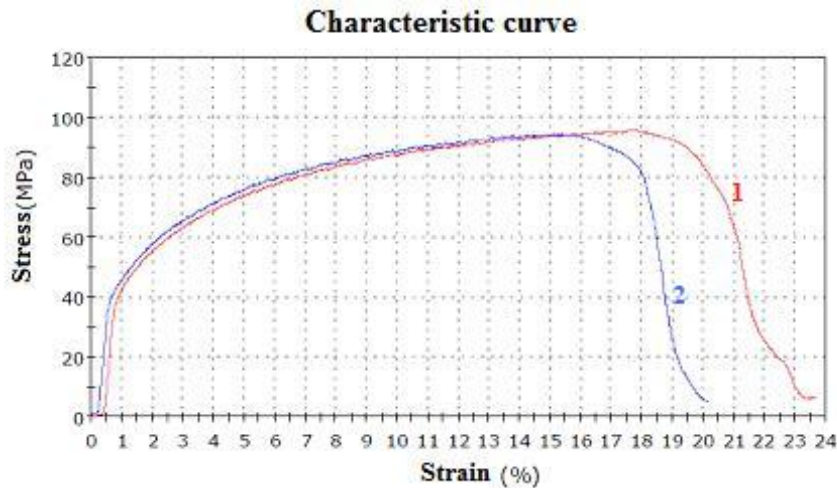


Fig. 4. – Characteristic curve for a cyclic artificially aged sample (1) and a classic artificially sample (2).

In Table 2 presents the values for tensile stress and tensile strain at break for the samples that were cyclic and classically heat treated.

Table 2.

Values for Tensile Stress at Tensile Strength and at Break for A7075 Cyclic and Classic Aged

Sample	Tensile stress at Tensile Strength MPa	Tensile strain at Break %
1	94.86	23.69
2	93.99	20.17

Table 3.

Variation of Micro-Hardness HV for a Cyclic Aged sample and a Classical One

Sample	HV
1 cyclic aged	46.9
2 classic aged	59.8

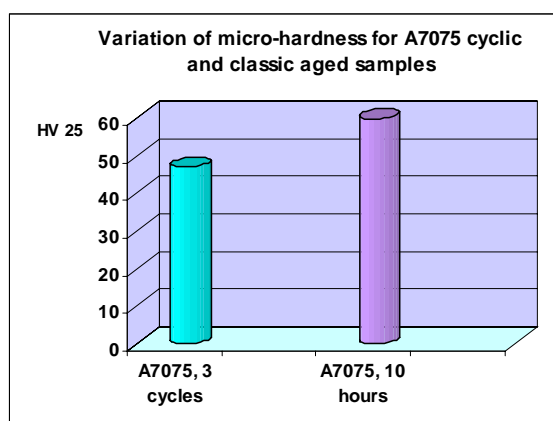


Fig. 5. – Variation of micro-hardness of A7075 cyclic and classical aged samples.

4. Conclusions

- Both samples were annealed, solution quenched and artificially aged. Yet, one of the samples was classically aged for 10 hours and the other one suffered a cyclic artificial age. From the values above of the tensile stress at Tensile Strength and tensile strain at Break, they clearly have a similar characteristic curve although the time for the artificial ageing was very different 200 minutes instead of 10 hours;

- From the variation diagram of the micro-hardness values, we see that the samples aged for 10 hours is a little bit harder than the other one cyclic aged, and yet it can be used for different commercial purposes.

Received: February, 2010

“Gheorghe Asachi” Technical University of Iași,
Department of Materials Science

e-mail: r_carabet@yahoo.com

R E F E R E N C E S

1. Aluminum and Aluminum Alloys, in *Metals Handbook Desk Edition*, 2nd ed., J.R. Davis, Ed., ASM International, 417–505 (1998).
2. Gibson, J. (n.d.) Equilibrium diagrams and common metal alloy systems. Sydney: Clarendon.
3. http://hsc.csu.edu.au/engineering_studies/aero_eng/2580/aluminium_age2.jpg
4. Shwe Wut Hmon Aye-The effect of ageing treatment of aluminium for fuselage structure light aircraft.Proceedings of world Academy of Science, Engineering and technology, **36**, 2008.

ASPECTE ASUPRA UNOR ALIAJE DE ALUMINIU ÎMBĂTRÂNITE
CICLIC ȘI CLASIC

(Rezumat)

Lucrarea prezintă unele aspecte ale aliajelor de aluminiu luate în studiu cu privire la rezistența la tracțiune și microduritate. Aceste aliaje de aluminiu fac parte din seria 7xxx, mai exact A7075 T651. Rezultatele prezentate în lucrare sunt o comparație dintre două tipuri diferite de îmbătrânire artificială și anume îmbătrânire artificială clasică față de îmbătrânire artificială ciclică.

DAMPING CAPACITY SIMULATION OF SOME METALLIC MATERIALS

BY

**CIMPOEȘU NICANOR, AXINTE MIHAI, CIMPOEȘU HANU RAMONA,
HOPULELE ION, ATUDOSIE IOAN* and PARASCHIV PETRONELA**

Abstract. A shape memory alloy was analyzed about his dissipation capacity by simulation using Catia specialize software. The data's used in this study was obtained with a dynamic mechanical analyzer concerning the variation of internal friction end elasticity modulus of the material with temperature.

Key words: damping capacity, shape memory alloy, dissipation simulation.

1. Introduction

The vibration problem is a serious one in the modern practical applications this relaxation type IF (internal friction) is more world *e.g.* in the aerospace, transportation, and manufacturing. Among many damping mechanisms, the one utilizing the rapidly when the temperature is held at a constant martensitic/displace transformation in shape memory as Delorme's theory [1] predicts.

Internal friction at metals appear because of a big number of phenomena's which take place at microscopic scale and one or on other interfere more or less function of material nature.

Paying attention to the internal friction causes is impose to give up to internal friction name and replace with amortization like in English or German languages (damping, respectively *dampfung*). By historical reasons this term keeps not only in Romanian language but also in French or Russian languages (*frotte-ment*, respectively *trenie*). Even in English language the old terms like friction are still used in different applications context.

Internal friction causes can be grouped after different criteria's like type of amortization produce: relaxation, resonance or hysteresis. Now we will use a succession claim by the caused nature itself showing each time the type of internal friction that appear from that cause, also we resume the most important and frequent causes giving up a quantitative handling of phenomena's. Some of the internal friction causes can be systematize as:

- a) Thermo elasticity;
- b) conduction electrons;
- c) magnetic phenomena's;
- d) structural defects of crystalline network.

An important source of internal friction in metals is the tensions relaxation during grains boundaries, Ke being first that demonstrate the existing of some big peaks of internal friction because of grain boundaries relaxation by experiments done on high purity aluminum wires as monocrystal or polycrystal material [2],..., [5]. Also was observe different values of elasticity modulus (which is proportional with the frequency square) at different temperatures with a big and sudden decrease in polycrystal material case and decrease that can't be seen in monocrystal case, this behavior correspond to hypothesis that grains limits behave in certain limits, at high temperatures similar to viscous materials.

During the past century physicians reach to establish equations from what to result the real behavior of metallic bodies at variable sollicitations in time and especially about the relaxation phenomena's [2].

For deviation explication from perfect elasticity at the beginning was considered that some aspects of internal friction mechanism are analog to liquids viscosity. By these reasons we appeal to Newton formula for viscous force express under equation 1 form:

$$(1) \quad \sigma = \eta \dot{\varepsilon}$$

One of the simplest interpretations phenomenological of internal friction owes to J.C. Maxwell which refers to tension relaxation phenomena. The studied metallic body can be considered as being compound by "Maxwell" elements comparable as behavior with a system form by an elastic resort and a damper connected in series, the resort behave under Hooke law and the damper under Newton law. In consequence the deformation suppose to be a sum $\varepsilon = \varepsilon_{el} + \varepsilon_{vasc}$ where

$$(2) \quad \varepsilon_{el} = \frac{\sigma}{M}, \quad \dot{\varepsilon}_{vasc} = \frac{\sigma}{\eta}$$

by derivation we obtain the relation: $\dot{\varepsilon} = \frac{\dot{\sigma}}{M} + \frac{\sigma}{\eta}$, we suppose that starting with

moment $t = 0$ deformation remain constant meaning $\dot{\varepsilon} = 0$, in this case the derive equation became $\sigma + \frac{\eta}{M}\dot{\sigma} = 0$ marking $\tau_\varepsilon = \frac{\eta}{M}$ equation take form $\sigma = \sigma_0 \exp(-t/\tau_\varepsilon)$ from where result the relaxation time interpretation at constant deformation like being time that σ value decrease by e times by the moment that ε became constant. Let's calculate the internal friction of a body which behaves as equation $\dot{\varepsilon} = \frac{\dot{\sigma}}{M} + \frac{\sigma}{\eta}$. If the processes are quasi-periodical meaning: $\sigma = \sigma_0 e^{i\omega t}$ and $\varepsilon = \varepsilon_0 e^{i\omega t}$ we will find by derivation $\dot{\sigma} = i\omega\sigma$ and $\dot{\varepsilon} = i\omega\varepsilon$ which replaced in $\dot{\varepsilon} = \frac{\dot{\sigma}}{M} + \frac{\sigma}{\eta}$ take to:

$$(3) \quad i\omega\varepsilon = \frac{i\omega\sigma}{M} + \frac{\sigma}{\eta}$$

and the complex elasticity modulus is: $\mathcal{K} = \frac{\sigma}{\varepsilon} = \frac{i\omega}{\frac{i\omega}{M} + \frac{1}{\eta}}$ (a) and internal friction

will be given by relation 4.

$$(4) \quad Q^{-1} = \frac{M}{\omega\eta} = \frac{1}{\omega\tau}$$

At a Maxwell type body internal friction vary inverse proportionally with the frequency. The equation propose by Maxwell explain that behavior of some metals, that reaction as liquids when are stressed by slow variable forces (small ω) and as solids at fast variable forces (big ω), indeed for a very small ω (a) became $\mathcal{K} = i\omega\eta$ and the tension became as in relation 5.

$$(5) \quad \sigma = \mathcal{K}\varepsilon = \eta i\omega\varepsilon = \eta\dot{\varepsilon}$$

that is Newton equation for liquids. For a ω bigger $\mathcal{K} = M$ and $\sigma = M\varepsilon$ that mean Hooke's law for solids.

Maxwell elements has disadvantage of not presenting the relaxation phenomena of deformation at constant tension. If $\sigma = \text{const}$ so $\dot{\varepsilon} = \text{constant}$, than we have a constant rate smelting which is not a relaxation. More Q^{-1} doesn't represent a peak function of ω like the experiment proves. For these reasons the Maxwell elements can be replace with Voight-Kelvin elements, were the elastic element and the viscous one are in parallel connected, so we will totaled the tensions like in relation 6.

$$(6) \quad \sigma = M\varepsilon + \eta \dot{\varepsilon}$$

for the case when σ drop to zero in moment $t=0$, from relation 6 we obtain

$$\dot{\varepsilon} + \frac{M}{\eta} \varepsilon = 0 \text{ or if we note with } \tau_{\sigma} = \eta/M \text{ we have:}$$

$$(7) \quad \dot{\varepsilon} + \varepsilon / \tau_{\sigma} = 0$$

Solution of this equation is: $\varepsilon = \varepsilon_0 \exp(-t/\tau_{\sigma})$ so the interpretation of τ_{σ} like being time after the deformation decrease by e times from the moment that σ became zero. For internal friction calculation we precede the same obtaining relation 8.

$$(8) \quad \mathcal{K} = M + i\omega\eta \quad \text{și} \quad Q^{-1} = \omega\eta/M = \omega \tau_{\sigma}$$

In this case the observation is that IF is directly proportional with frequency. For the experimental part we will use the link between internal friction and elasticity modulus. The phase angle δ is the phase difference between the dynamic stress and the dynamic strain in a viscoelastic material subjected to a sinusoidal oscillation. The phase angle is expressed in radians (rad). The loss factor $\tan \delta$ is the ratio of loss modulus to storage modulus. It is a measure of the energy lost, expressed in terms of the recoverable energy, and represents mechanical damping or internal friction in a viscoelastic system. The loss factor $\tan \delta$ is expressed as a dimensionless number. A high $\tan \delta$ value is indicative of a material that has a high, nonelastic strain component, while a low value indicates one that is more elastic [6-10].

According to ISO 6721-1 [11], the storage modulus E' represents the stiffness of a viscoelastic material and is proportional to the energy stored during a loading cycle. It is roughly equal to the elastic modulus for a single, rapid stress at low load and reversible deformation, and is thus largely equivalent to the tabulated figures quoted in DIN 53457. In the same ISO standard, the loss modulus E'' is defined as being proportional to the energy dissipated during one loading cycle. It represents, for example, energy lost as heat, and is a measure of vibration energy that has been converted during vibration and that cannot be recovered. According to [12], modulus values are expressed in MPa, but N/mm^2 is sometimes used. The real part of the modulus may be used for assessing the elastic properties, and the imaginary part for the viscous properties [12]. E'' "loss modulus" represent an amortization term describing the energy dissipation capacity in heat when a material is deform and appear named imaginary modulus as a part of complex elasticity modulus, $E = E' + iE''$. Discovering metallic materials with damping properties improve all the resistance properties of the materials all ready in use like polymers. High damping capacity has been one of the most important properties of materials

used in engineering structures where undesirable noise and vibration are to be passively attenuated. Among the prevalent high damping metallic materials, shape memory alloys (SMAs) could be one of the most promising candidates due to their high damping capacity arising from the reversible martensitic phase transition (MT) and the stress induced reorientation of martensite variants [13].

2. Experimental

Using results from a dynamic mechanical analyzer test, presented in Fig. 2, we simulate the behavior of a shape memory alloy body part. As material we use a copper-zinc-aluminum alloy, known as material with damping capacity.

For simulation we use Catia drawing and analysis software used in automotive industry or other complex applications. Finite elements method (FEM – Finite Element Method) represents one of the best existent methods for different calculations realization and simulations in engineering domain. This method and, of course the programs that are incorporate became base components of modern systems for projection assisted by computer.

The analysis made through FEM are, today, indispensable in all engineering activities of high performance, assisted projection being a creative activity with many implications in other disciplines. To solve complex problems of samples and assemblies analysis the project engineer must have all information's which have to permit him wording the problem numerical way.

Must be remark that in order CAD – FEM – CAM exist a iterative process for projection - calculus – execution. In this process are realized successively synthesis operations and analysis of prototype and o the model for finite elements calculus (Fig. 1) [14].

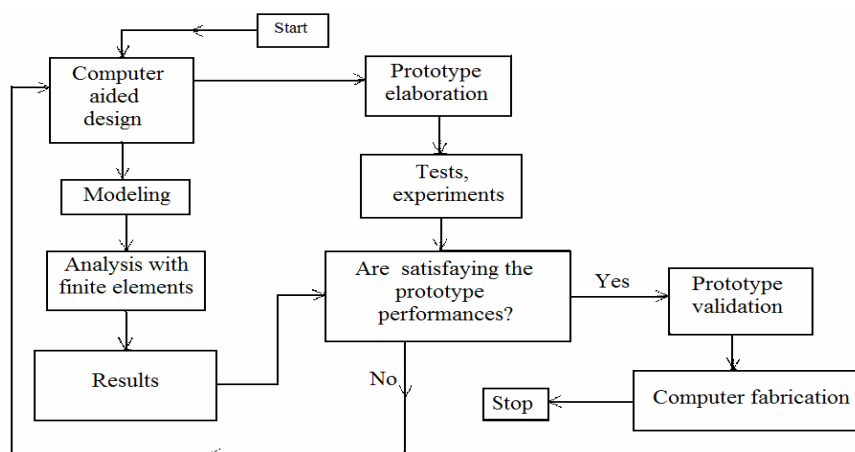


Fig. 1 – Main components of an integrate system CAD-CAM.

The investigated alloy is a shape memory alloy based on copper with chemical composition, determined with a spark spectrometer type Foundry Master, presented in Table 1. The small amounts of other elements are elementally for good damping properties.

Table 1.
Chemical Composition of the Shape Memory Alloy

Cu %	Zn %	Al %	Pb %	Fe %	Sn %	Co %	Ni %
68,6	13,2	4,85	2,36	4,05	1,57	1,22	1,12

Dynamic mechanical analyzer register the internal friction and elasticity modulus variation with temperature, all data's – 700 registered values being stoked in a text file under table form or graphical expose like in Fig. 2.

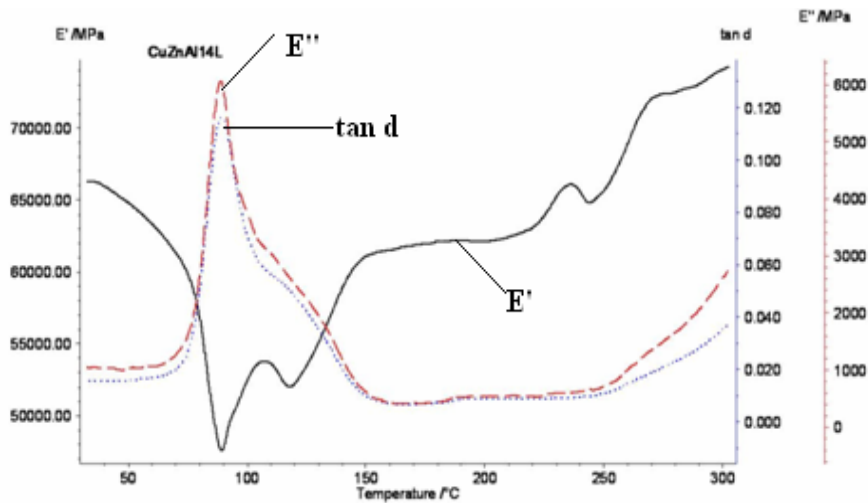


Fig. 2 – Dynamic behavior of a copper based alloy with form memory [15].

From Fig. 2 we observe a peak of internal friction in martensitic-austenitic field around 90°C temperature. Simulations of material behavior will pay respect for these experimental values and for plate shape as well. After this temperature range doesn't appear other peaks of internal friction or significant decreases of elasticity modulus.

For the begin we analyze a plate form material having sizes 100x10x5 mm with restrains at the edges, presented in Fig. 3, and applying a 5000 N force on the center of the plate.

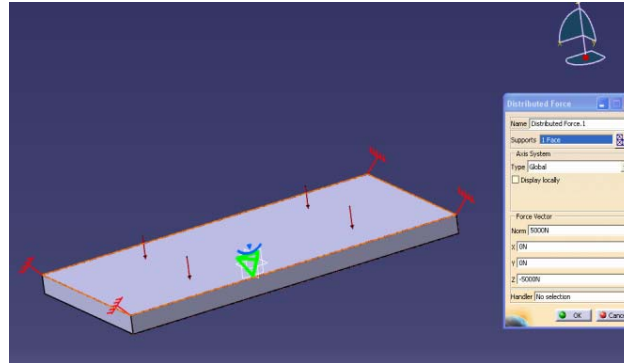


Fig. 3 – Plate form with edges restrains and force applied.

Using the software we can chose any part to restrain or any area to apply the forces depending on the investigated case. The simulation program give the chance for user to change the material, choosing one from a list already loaded in the software programs or to create one with his proper properties. In this case using as material steel and ordinary brass are evident differences between the maxim tensions results in the end with Von Mises model. In this order we analyze two brasses, one normal and one with memory effect and possible damping properties [15]. The entire model, from the shape to simulation must be correctly proposed to clear off all the inadequacies that might appear. On the material properties we can change the elasticity modulus, so we can use values from the DMA test to follow the material behavior.

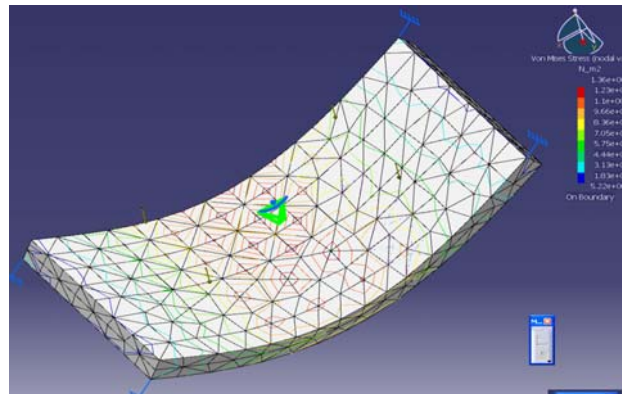


Fig. 4 – Tensions Von Mises in nodal points for an ordinary brass for a 5000 N load.

For the first material we obtain a maximum tension of $1,36e+008$ N/m² in the middle area, with red color, having smaller values at the borders, changing the material with a shape memory alloy, we obtain different values, presented in Fig. 5.

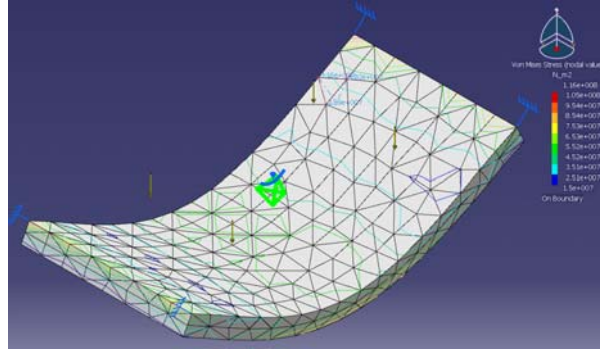


Fig. 5 – Tensions Von Mises in nodal points for a shape memory alloy from copper – zinc – aluminum system with chemical composition presented in Table 1.

In the second material case we have a maximum tension $1,05e+008$ N/m^2 , a value smaller than first, fact that presents the improvement obtained with this alloy paying respect for the fact that the value used in this simulation is at room temperature, were conforming to diagram 2 the elasticity modulus is not decreased in the same time with an internal friction peak. After the tests made with computer, simulations of under force behavior of internal tensions in material we try to find methods to improve the material response, same work conditions, same material conditions but different geometrical dimensions. Thinking about the practical applications of this damper material, we test the same plate but with four connection holes for clamps. In this purpose, the plate, presented in figure 6, after simulation exhibit smaller von Mises tensions about $6,29e+007$ N/m^2 more than a half as an ordinary brass.

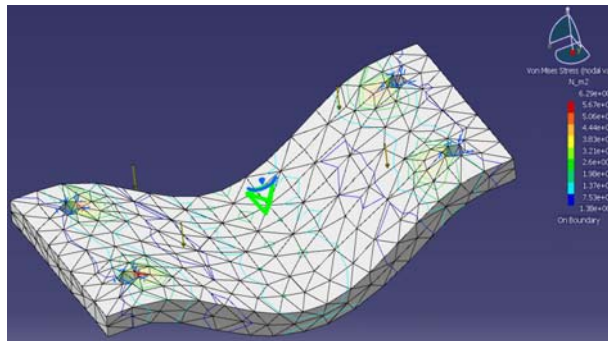


Fig. 6 – Tensions Von Mises in nodal points for a shape memory alloy from Cu-Zn-Al with holes on the edges.

Improving, with computer help by software, products for practical application represent an important gain in manufacturing area because of some

very important issues that we deal in our day's time and of course money.

3. Conclusions

- Damping metallic materials in the last decades won some new and very interesting partners in shape memory alloys.
- Using simulation software, Catia we can investigate the material behavior under extern stress by nodal tensions point of view.
- A shape memory alloy behave, in temperature martensitic transformation domain, 15 times better than a usually steel or brass at extern tension.

Received: February 14, 2010

"Gheorghe Asachi" Technical University of Iași,
*University "Al.I.Cuza", Iași,
e-mail: nicanornick@yahoo.com

REFERENCES

1. Delorme J.F., Schmid R., Robin M., Gobin P., J. Phys. 32 (1971) (in press).
2. Otsuka K., Wayman C.M. (Eds.), *Shape Memory Materials*. Cambridge University Press, Cambridge, 1998.
3. Wasilewski G.W., Trans. AIME 233 (1965) 169. Suzuki, Jpn. J. Appl. Phys. 33 (1994) 2897.
4. Hasiguti R.R., Iwasaki K., J. Appl. Phys. 39 (1968) 2182.
5. Postnikov V.S., Lebedinskiy V.S., Yevsykov V.A., Sharhakov I.M., Spring Meeting of Jpn. Inst. Metals, Narashino, Japan, Collected March 2002, 237.
6. Mercier O., Melton K.N., Y. de Preville, Acta Metall. 27 (1979).
7. Sugimoto K., Kamei K., Sugimoto T., Soeda T., in: Proc. Int. Conf.
8. Coluzzi B., Biscarini A., Campanella R., Trotta L., Mazzolai G., Watanabe A.Y., Saburi T., Nakagawa Y., Nenno S., J. Jpn. Inst. Metals Tuissi, F.M. Mazzolai, Acta Mater, 47 (1999) 1965, 54 (1990) 861 (in Japanese).
9. Yoshida I., Ono T., Asai M., J. Alloys Comp. 310 (2000) 339.
10. Yoshida I., Yoshida S., *Solid State Phenomena 89* (2003) 315. Sci. Eng. A, a Special Issue for ICIFUAS-13, Bilbao.
11. http://files.hanser.de/hanser/docs/20041012_2411215439-82_3-446-22673-7.pdf
12. Humbeek J.V., J. Alloys Comp. 355, 58 (2003).
13. San Juan J., J.M.L. N6, J. Alloys Comp. 355, 65(2003).
14. Ghionea I., *Proiectare asistată în Catia V5, Elemente teoretice și aplicații*. Edit. Bren, București, 2007.
15. Cimpoesu N., Stanciu S., *A Shape Memory Alloy Characterization Through Thermal Analysis*. Bul. Inst. Polit. Iași, **LV (LIX)**, 4, s. Știința și Ingineria Materialelor, 83, 90 (2009).

SIMULAREA CAPACITĂȚII DE DISIPARE A UNOR MATERIALE METALICE

(Rezumat)

Un aliaj cu memoria formei a fost analizat cu privire la capacitatea lui de disipare prin simulare folosind soft-ul specializat Catia. Rezultatele folosite în acest studiu au fost obținute pe un analizor mecanic-dinamic realizându-se variația frecării interne și a modulului de elasticitate cu varierea temperaturii.

BULETINUL INSTITUTULUI POLITEHNIC DIN IAȘI

Publicat de

Universitatea Tehnică „Gheorghe Asachi” din Iași

Tomul LVI (LX), Fasc. 1, 2010

Secția

ȘTIINȚA ȘI INGINERIA MATERIALELOR

ELECTRO - CORROSION BEHAVIOR STUDY OF A SUPERELASTIC Ni-Ti ALLOY THROUGH SEM AND EDAX ANALYSIS

BY

**RAMONA CIMPOEȘU HANU, CONSTANTIN BACIU, SERGIU STANCIU,
DELIA MARINELA AELENEI, NICANOR CIMPOEȘU
and PETRONELA PARASCHIV**

Abstract. A Ni-Ti superelastic alloy was studied by electrochemical polarization method, SEM and EDX analysis, analyzing the effects of corrosion test on material surface. These studies reveal that in natural aerated Fusayama saliva this alloy behaves as a corrosion resistant material. In linear and cyclic polarization studies the alloy showed a passive behavior with a large potential independent region up to a potential of about 500 mV (SCE), followed by a region with significant increase in current density. At over-potentials greater than 500 mV (SCE) in Fusayama saliva this alloy exhibits a pitting corrosion; EDX studies evidences that the corrosion take place especially by nickel dissolution.

Key words: corrosion, superelastic alloy.

1. Introduction

NiTi SMA is a new kind of functional material used in many fields, such as atomic energy, ocean development, instruments and medical device, aviation and space-flight etc., due to its special shape memory effect (SME) and superelasticity as well as excellent erosion resistance and outstanding biocompatibility [1],..., [3]. However, successful applications of any novel material not only hinge on its inherent characteristics, but also depend on solving problems of processing technologies (joining, machining, etc.). As a result, the uses of this material will be greatly limited unless problems of joining the material itself and to other materials are solved. Since 1980, the

joining of TiNi SMA has become the hot spot and front edge in the joining research field. NiTi shape memory alloy has been widely employed in various medical fields because of its special mechanical properties, good corrosion resistance and excellent biocompatibility [4]. In this work we analyze the effects of electro-corrosion tests on Ni-Ti wire using qualitative and quantitative EDS (Energy-dispersive X-ray spectroscopy) microanalysis by EDX detector. The shape memory metal Nitinol has increased in use and popularity since its discovery in 1959. Today we see Nitinol-based stents, guide wires, surgical instruments, coliosis rods, embolic protection filters and a whole host of other medical applications. Nitinol has become a valuable part of the medical device designer's armamentarium. Much of the early technical development of Nitinol alloys focused on refining the melting processes and understanding the basic metallurgical mechanisms. Nitinol melting is especially challenging, as Nitinol alloys must be melted under vacuum to minimize impurities.

The last decade has seen significant improvement in the understanding of manufacturing process technologies for producing Nitinol devices, especially advances in laser-cutting technology and surface finishing. Nitinol manufacturing has moved beyond the realm of blacksmithing, and most medical device manufacturing operations have implemented six sigma methodologies, including sophisticated manufacturing and test method validations, statistical process control and lean manufacturing tools. Another significant change over the last ten years has been greater knowledge and understanding of Nitinol among medical device engineers, both from a processing technology and a device development standpoint. This is due in part to a concerted effort on the part of the Nitinol producers to educate the industry on how to design, test and manufacture Nitinol medical devices. A key element of this educational process was the formation of the Shape Memory and Superelastic Technologies Society (SMST), and the launching of its conference series starting in 1994 [5].

A further development during the last decade has been improved understanding of Nitinol fatigue and corrosion behavior. Nitinol contains about 50% nickel, so its corrosion performance has been closely scrutinized. Like stainless steel, Nitinol is protected from corrosion by a protective surface layer, which is composed of titanium dioxide. When properly processed, the biocompatibility and corrosion resistance of Nitinol is excellent, with a performance close to that of titanium alloys. Finally, the last ten years have seen development of a number of ASTM standards that apply to both the Nitinol raw material itself and various test methods used to characterize the material. The F2063 wrought material standard now gives medical device engineers assurance that the starting material meets the basic requirements for use in a medical device.

However, Nitinol's final properties are mostly determined by the

processing it undergoes during the rest of device manufacturing. The various testing standards, the F2129 corrosion testing standard in particular, describe the currently acceptable test methods for verifying many of the critical outputs of the Nitinol medical device manufacturing process, including the effects of heat treatments and surface finishing.

In the past decade, the Nitinol medical device marketplace has been dominated by peripheral vascular products, such as stents and guidewires. The Nitinol self-expanding stent market took off with the 1998 market release of the Cordis SMART Stent®. Total worldwide sales of the SMART Stent are estimated to be about \$1bn, making it arguably the Nitinol medical device industry's first true blockbuster product. In recent years, endovascular aneurysm repair devices, inferior vena cava filters and embolic protection devices have also developed into significant commercially successful products. In 2006, Nitinol-based devices accounted for over \$750m of the US peripheral vascular device market. The extended worldwide market for these devices is currently estimated at \$1.1–1.5bn [5].

2. Experimental Details

Corrosion behavior was realized by rapid electrochemical tests, particularly by dynamic potentiometry. The measurements of open potential circuit and potentiodynamic polarizations were performed on a VoltaLab 21 Electrochemical System (PGP201 - Radiometer Copenhagen) equipped with the acquisition and processing data software VoltaMaster 4. A three-electrode electrochemical cell was used. From commercial materials, the working electrodes were performed in cylindrical form and mounted in a Teflon support to enable the connection to rotating port-electrode of the electrochemical cell. The free area was precisely measured before embedding in the Teflon support. A saturated calomel electrode (SCE) was used as a reference and platinum as auxiliary electrode.

After the electrochemical treatments, a study of the modifications of the alloys surface was performed on a VEGA-TESCAN Scanning Electron Microscope equipped with QUANTAX Bruker AXS Microanalysis system, find on the SIM Faculty laboratories Iasi. The microscopy's was realized using a Secondary Electrons detector at different scales to present the corrosion effects at 30 kV power supply of the tungsten filament. The images were taken from a 10 mm distance of samples, for SEM results and by 16 mm distance between samples and AXS detector for chemical analysis, producer best performance recommendations. The alloy used in this study is a manufactured by Saes Getters Group, USA, and is a superelastic material at room temperature with characteristics presented in Table 1, under round wire type shape.

Table 1
Properties of Ni-Ti Superelastic wire [6]

As (Fully annealed)	-15
Nominal Loading plateau stress@3% strain, in Austenite	500 MPa, 72,500 psi
Nominal Ultimate Tensile Strength in Austenite	1250 MPa, 181,000 psi
Max. Residual elongation after 8% strain in Austenite [%]	0.5
Min. elongation to failure in Austenite [%]	10
Main Applications	Guidewires, Stents, Archwires, Implantable devices, Embolic Protection
Diameter:	0.001" (0.025mm) to 0.040" (1mm) ± 0.0003" (0.075mm) 0.040" (1mm) to 0.100" (2.5mm) ± 0.0005" (0.00127mm) 0.100" (2.5mm) to 0.175" (4.4mm) ± 0.001" (0.025mm)
Mechanical treatments:	- Cold drawn, Superelastic, Trained
Surface finish:	- Hard dark oxide, Dark oxide, Drawn Bright, Pickled, Mechanically or electro-polished
Typical impurity content in wt:	- O < 250 ppm: C < 250 ppm: Total all others < 1000 ppm
Standard Cut-length:	± 0.007" (0.18mm) for L < 12" (0.3m)
Tolerances:	± 0.2% of specified cut-length for L > 12" (0.3m)
Formats:	Round, Square ¹ , Rectangular ¹ , Shaped Wires ¹

3. Results and Discussions

Because in this study we intend to analyze the electro-corrosion effects on a nitinol wire in artificial saliva using SEM and EDX equipments it is necessary to present the wire surface before and after the test.

The surface wire, having a 700 µm diameter, is presented in Fig. 1 in an image of 950 µm view field presenting a smooth surface and a composition, presented in Table 2, with equal percents of nickel and titan and

a small percent of oxygen from titan oxide (the protector layer from the alloy surface).

In Table 2 are presented belong atomic number (AN), the series (in this scanning electrons microscope case K-series), weight percents (wt.%), (norm. wt%) and also norm at.% with the equipment error in % supported.

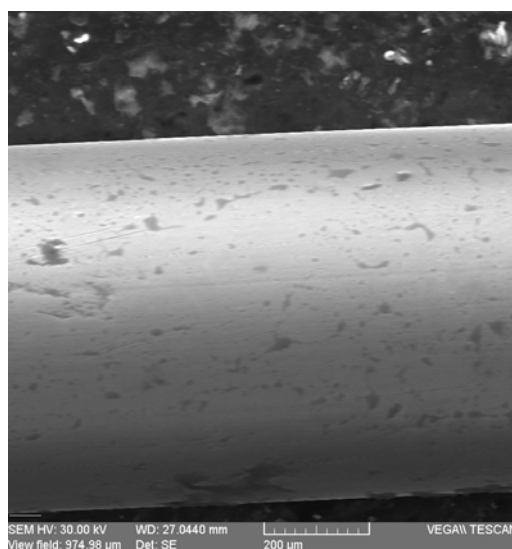


Fig. 1 – Ni-Ti wire surface at 500x magnify power, obtain with a SEM equipment.

Table 2

Chemical Composition of Ni-Ti wire Before Electro-Corrosion Test

Element	AN	series	Net	wt. %	norm. wt. %	norm. at. %	Error in %
Nickel	28	K-series	60223	52,78445	49,94344	44,63196	1,3475
Titanium	22	K-series	90626	51,96307	49,16628	53,86044	1,460073
Oxygen	8	K-series	1259	0,940916	0,890273	1,5076	0,076463
Sum:				105,6884	100	100	

As corrosion medium an aerated solution of Fusayama Meyer artificial saliva (Normalization 591-141) [7] was used, having the composition presented in table 3 and pH = 8.

Table 3
Electrolytic Solution of Artificial Saliva for Electro-Corrosion Test

Artificial saliva/ Compounds	NaCl g/l	KCl g/l	Na ₂ HPO ₄ / 2 H ₂ O g/L	NaHCO ₃ g/L	KSCN g/L	Urea g/L	CaCl ₂ g/L	NaH ₂ PO ₄ H ₂ O g/L	Na ₂ S g/L
FUSAYAMA	0.4	0.4	-	0.69	-	1	0.65	0.69	0.05

Urea or carbamide is an organic compound with the chemical formula (NH₂)₂CO. The molecule has two amine (-NH₂) residues joined by a carbonyl (-CO-) functional group [8]. Paying respect for the alloy component elements, nickel and titan and for artificial saliva compounds we will do the chemical analysis looking for all these elements. In Fig. 2 is presented the material surface after the corrosion test, at two different scales, 1 mm which present almost the entire wire surface and 200 μm for detail of the pitting points that characterize the behavior of this material in the Fusayama type of artificial saliva. For better observations we increase the magnify power to 5000 and focus on a pitting hole, as dimensions determination we can say that is 100 μm long, 70 μm large and 10 to 15 μm deep.

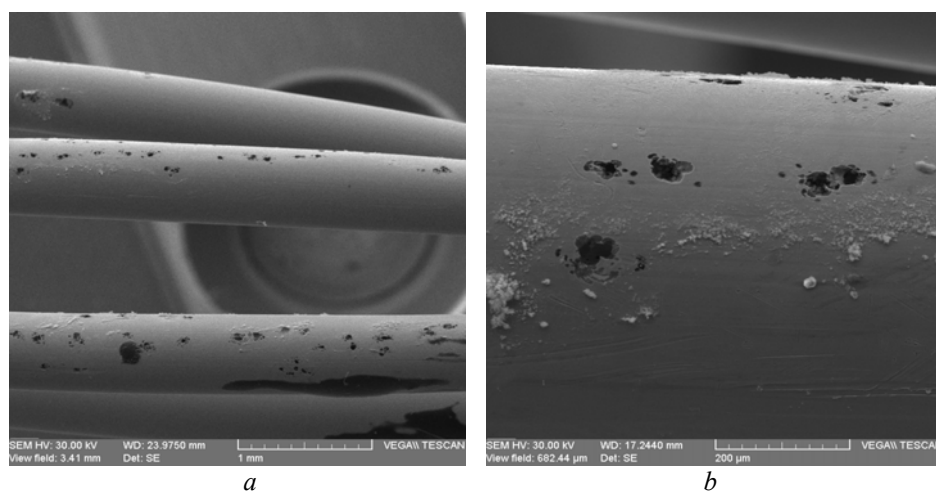


Fig. 2 – Ni-Ti wire surface after electro-corrosion test:
a – 100x magnify; *b* – 500x magnify.

Appreciating by holes distribution on the surface, for a 7000 μm² area by hole with five by an average surface of 490000 μm² we can appreciate that 1/14 from the surface is corroded value that confirm reduce of material weight during the process.

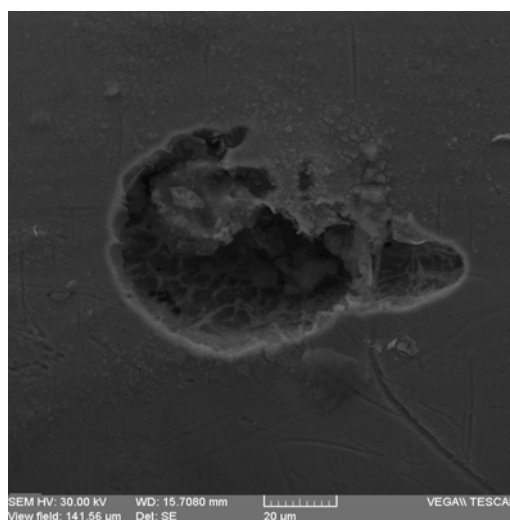


Fig. 3 - Detail of a pitting hole from the Ni-Ti alloy surface at 5000x magnify and a 20 μm scale

On the surface, near to pitting hole are observed some compounds formed after corrosion based on elements from artificial saliva solution. In table 4 is presented the chemical composition of the Ni-Ti alloy after the corrosion test with elements like phosphorus, sodium or nitrogen which are all from the artificial saliva and a quite high amount of oxygen 31.84605 wt % that appear from the protective titan oxide that form on the surface. Increasing of this element, oxygen decrease the titan percentage, values presented in Table 4, so from this reason appear to be smaller than nickel percent.

Table 4
Chemical Composition of Surface Alloy After the Corrosion Test

Element	AN	series	Net	wt. %	norm. wt. %	norm. at. %	Error in %
Nickel	28	K-series	59737	40,37506	35,28934	17,89257	1,036719
Oxygen	8	K-series	3176	36,43555	31,84605	59,23392	59,24764
Titanium	22	K-series	91023	34,80742	30,42301	18,90891	0,986241
Phosphorus	15	K-series	2350	1,433917	1,253298	1,204145	0,095073
Sodium	6	K-series	1360	0,764059	0,667816	1,654613	0,184293
Nitrogen	7	K-series	233	0,595499	0,520489	1,105845	1,049779
Sum:				114,4115	100	100	

To analyze the pitting hole area we can use the Line Mode Analysis, result presented in Fig. 4, to observe the elements from the surface variation with length, in our case on 100 μm . Analyzed elements are those obtain by chemical quantitative test presented in Table 4. The Ti variation, qualitative and quantitative present a big decrease of percentage on the hole zone, which is normal for a signal loss.

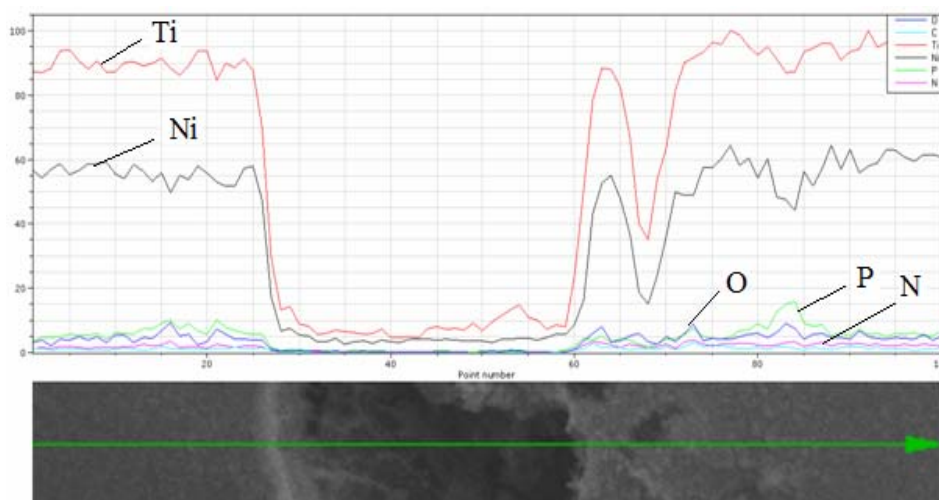


Fig. 4 – Elements variation on a line of 100 μm length on the Ni-Ti wire after the corrosion test.

We observe a variation of Ti near to pitting area as well given by the elements from the compounds formed, like oxygen, phosphorous or nitrogen that increase as percentage in those areas. All this elements appear from the electrolytic solution, nitrogen from the urea compound, in reaction with alloy surface. The compounds forms on the surface are not well bond with the material disappearing at a oxygenated water wash. From this variation diagram we observe that Ni percent is smaller than titan, which is a normal fact considering the electrodynamic activity scales [9] that gives the weaker element nickel and which theoretically got to corroded more.

Continuing with this analyze we investigate the interior of a pitting hole trying to determine the amounts of elements loss. By this point of view we realize a chemical analyze in a selected point having the results presented in the lower part of the Fig. 5. In the corroded area the element that loss more weight is nickel with 0.5 % more than titan, thinking that some non - homogeneities of the material are weaker and favorites the corrosion.

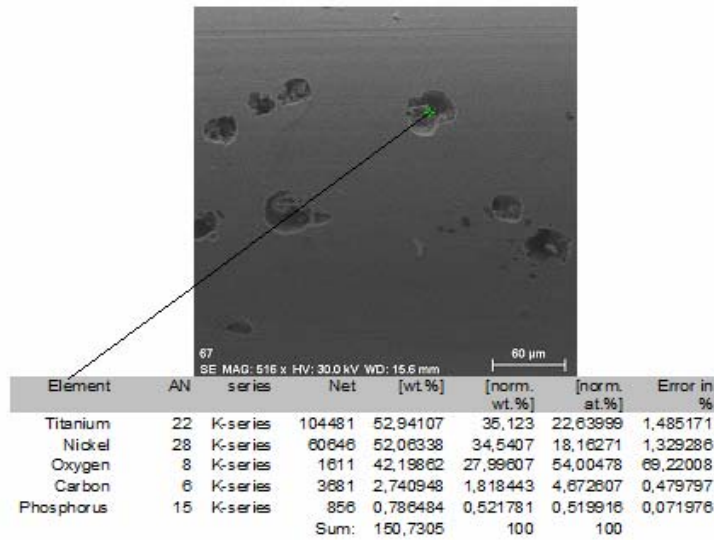


Fig. 5 – Point EDAX chemical analyze in corroded area.

Using mapping mode analysis to track the elements distribution we investigate the same area observing from Fig. 6 the phosphorus compounds, titan and nickel distribution and some reduce areas with nitrogen.

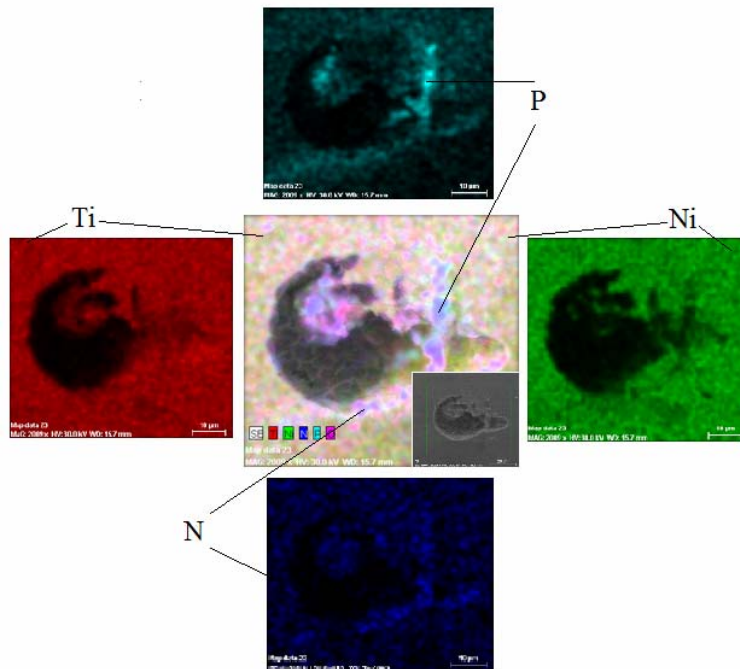


Fig. 6 - All elements distribution in center, investigated area in ingot and Ti distribution, Ni distribution, N distribution and P distribution.

The lack of signal is represented in mapping analysis type by black color, showing the pitting corrosion hole. In the detail, is represented the selected area for analysis.

4. Conclusions

- A fabricated Nitinol wire, with superelastic behavior, was investigated concerning surface electro-corrosion behavior by SEM and EDX point of view;
- The material behave very good in artificial saliva solution but under current exhibit pitting corrosion, a very dangerous type of corrosion;
- Sem and EDX analysis after the corrosion test reveal the pitting points and the loss of material during this process;
- The loss of superelastic alloy is around nanometers of material with reducing quantities of titan and nickel, a little more for the second one;
- Phosphorous, nitrogen and sodium compounds appear on the surface near to pitting holes.

Received: February 14, 2010

“Gheorghe Asachi” Technical University of Iași,
e-mail: ramonahanu@yahoo.com

REFERENCES

1. Qiu X.M., Li M.G., Sun D.Q., Liu W.H., Study on Brazing of TiNi Shape Memory Alloy with Stainless Steels; *Key Laboratory of Automobile Materials, School of Materials Science and Engineering, Jilin University, Changchun 130025, China*. J. of Materials Processing Technology 176 (2006) 8–12 Received 12 June 2003.
2. Nam T.H., Saburi T., Kawamura Y., et al., *Shape Memory Characteristics Associated with the B2→B19 and B19→B19₂ Transformations in a Ti–40Ni–10Cu (at.%) Alloy*. Mater. Trans. JIM 31, 262–269, (1990).
3. Dilibal Savas, Murat Tabanlı R., Dikicioglu Adnan, *Development of Shape Memory Actuated ITU Robot Hand and its Mine Clearance Compatibility*. J. Mater. Process. Technol. 105/106, 1390–1394, (2004).
4. Saburi T., in: Otsuka K., Wayman C.M. (Eds.), *Ti–Ni Shape Memory Alloys. Shape Memory Materials*. Cambridge University Press, London, 1998.
5. <http://www.medicaldevice-network.com/features/feature1338/>
6. <http://www.memry.com/products/wire.php>
7. http://ljs.academicdirect.org/A11/033_040.htm
8. <http://en.wikipedia.org/wiki/Urea>
9. Cimpoesu Hanu R., Baciuc C., Nejneru C., Cimpoesu N., Aelenei D.M., *Corrosion Resistance of a Shape Memory Alloy Based on Copper in Artificial Saliva*. Bul. Inst. Polit. din Iași, LV (LIX), 2, s. Știința și Ingineria Materialelor 2009.

STUDIUL COMPORTAMENTULUI LA ELECTRO-COROZIUNE A UNUI ALIAJ
SUPERELASTIC DIN Ni-Ti PRIN ANALIZE SEM ȘI EDAX

(Rezumat)

Un aliaj superelastice Ni-Ti a fost investigat prin polarizare electrochimică, analize SEM și EDX urmărind efectele testului de coroziune asupra suprafeței materialului. Aceste studii prezintă că în saliva Fusayama aerată natural aliajul se manifestă prin rezistență la coroziune. În studiile de polarizare liniară și ciclică aliajul prezintă un comportament pasiv cu o regiune de potențial independent până la un potențial de aproximativ 500 mV (SCE), urmată de o regiune cu o creștere semnificativă a densității curentului. Pentru un supra potențial mai mare de 500 mV (SCE) în salivă Fusayama acest aliaj prezintă o coroziune de tip pitting, studiile prin EDX evidențiind o pierdere în special de nichel.

THEORETICAL AND EXPERIMENTAL ASPECTS REGARDING PHENOMENONS THAT ARE PRODUCED IN THE UNDISMONTABLE ASSEMBLINGS

BY

SANDA CRETU

Abstract: The paper presents a computer modeling of the phenomenons that are produced in the undismontable assemblings such as different types of materials tree-pad, constant length and different thickness.

Key words: undismontable assemblings, phenomenons modeling.

1. Introduction

For the phenomenon optimization that are produced on the tree-pad undismontable assemblings interface surface level and to give a good corrosion resistance these systems, it is considered that we have different materials of the joint elements, different thickness dimensions and constant length.

For relieved joints obtained we will use as a material: steel OLC 45 for the tree, standardized STAT 880-80, and for the steel pad 16MnCr5, standardized according to STAS 7131 DIN.

OLC 45 has the following chemical composition

Chemical elements	C	Si max.	Mn	P max.	S max.
%	0,42-0,50	0,20-0,42	0,50-0,80	0,035	0,045
The allowed deviation	± 0,02	+ 0,02	± 0,05	0,003	0,005

Technical Features

STAS	Material mark	Quality class (heat treatment)	Traction resistance R_m [MPa]	Flowing limit $R_{p0,2}$ [MPa]	Break elongation A_5 [%] min.	Brinell HB hardness informative
880-82	OLC45	CR	700 ... 840	480	14	-

Observation: C- hardening; R- high return.

Steel mark	Heat treatment	With tension concentrators				Without tension concentrators			
		Traction on R	Bending on R	Twisting on R	Shear on R	Request			
		$\sigma_{at}=\sigma_{ac}$ MPa	σ_{ai} MPa	τ_{at} MPa	τ_{af} MPa	Traction $\sigma_{at}=\sigma_{ac}$ MPa	Bending σ_{ai} MPa	Twisting τ_{at} MPa	Shear τ_{af} MPa
OLC 45	N	65	72...78	39...42	52	180	207	117	144

Observation: N =normalization; R= rezistance.

Otel 16MnCr5 (EC80) has the Following Chemical Composition

Chemical elements	C	Si max.	Mn	P max.	S	Cr
%	0,14-0,19	0,40	1,00-1,30	0.035	≤ 0035	0,80 - 1,10
Allowed deviation	± 0,02	+ 0,03	± 0,05	+ 0,005	+ 0,005	± 0,05

According to STAS 7131 DIN the steel presents the following peculiarities:

- Deliver tyoughness <207 HRC;
- After cementing:

Diameter DD mm	Flowing limit $R_{p0,2}$ N/mm ²	Traction rezistance R_m N/mm ²	Elongation A_5 < %	Strangulati on Z < %	Breacking energy (resilience) KCU
< 11	> 635	880÷1180	9	35	>41
< 30	>590	780÷1080	10	40	>41
< 63	>440	640÷930	11	40	>41

- Forging temperature: 1100 ÷ 850 °C;
- Rebaking for the softening: 750 ÷ 700 °C;
- The normalisation can be done in 2 ways:
 - 850 ÷ 900 °C;
 - 900 ÷ 1000 °C;

- Cementary temperature: $900 \div 950$ °C;
- After the cementaring it is aply direct hardening (simple) which is the most adequate, or duble hardening (very rarely). The cementary can be done in an solid invironment or controoled atmosphere;
 - The cooling it is done in 2 ways: in oil ($160 \div 210$ °C) or in nitrogen bath ($580 \div 650$ °C);
 - The recomended hardness after the return is: $170 \div 210$ HRC.

2. Tensions and Moments Modeling That Are Submissive Undismontable Assemblings

Phenomenons modeling that are produced on the interface surface level it is done after hardening from which results a large amount of rezidual austenit in the mechanical induced martensit, which confers the assambling an high hardness, high mechanical resistance.

Pursuant to, for obtaining good peculiarities after treatments that are submissived the assemblings, we will heat up the pad at 180°C temperature and we cool the tree at -20°C , the tree that initial was hardened. This way we have an improved material and another one cemented. Tension distribution in cemented and hardened level is very important because thats why is depending directly the resistance on the assamblly tiredness.

On the computer modeling in the undismontable assembling such as tree-pad from the material that were presented higher and the moments that are exposed, we considered the contact lenght of an such an assembly being 70 mm, but with different thicknesses of the fretaj (of the joining area).

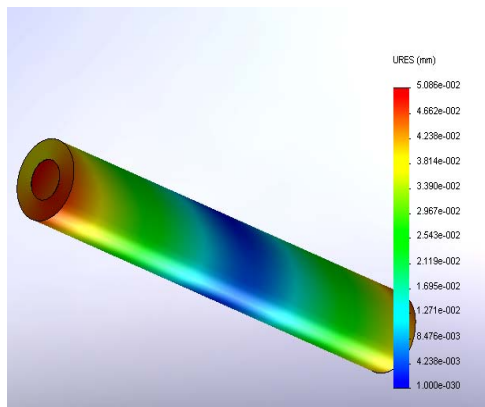


Fig. 1 – The phenomenons distribution in assembling by 70mm lenght and 5,013 fretaj- the tree diameter 5,013, interior pad 5mm and exterior 10 mm.

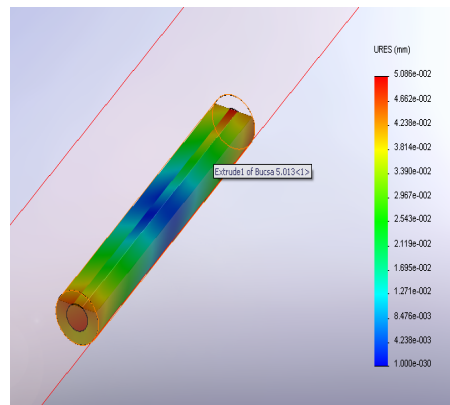


Fig. 2 – The phenomenons distribution in assembling by 70mm lenght and 5,013 fretaj- the tree diameter 5,013, interior pad 5mm and exterior 10 mm, in section.

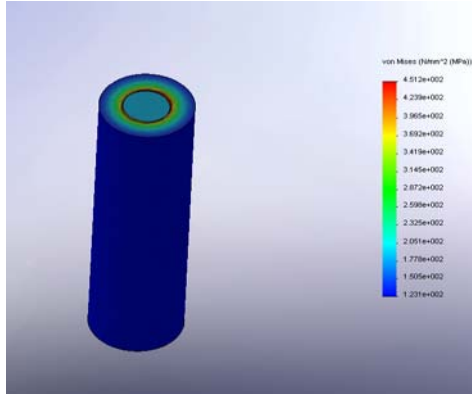


Fig. 3 – The phenomenons distribution in assembling by 70mm lenght and 10,025mm-the tree diameter 10,025mm, the interior pad 10mm and exterior 20mm.

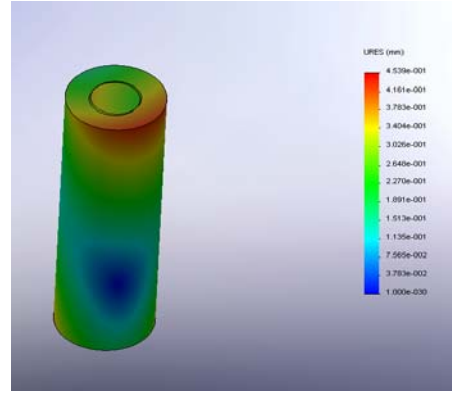


Fig. 4 – The phenomenons distribution in assembling by 70mm lenght and 10,025mm-the tree diameter 10,025mm, the interior pad 10mm and exterior 20mm.

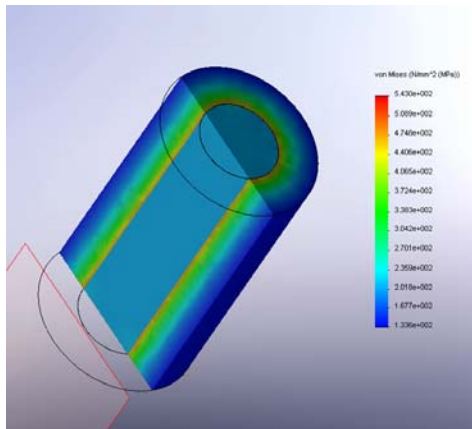


Fig. 5 – The phenomenons distribution in assembling by 70mm lenght and 20,055mm-the tree diameter 20,055mm, the interior pad 20mm and exterior 40mm, in section.

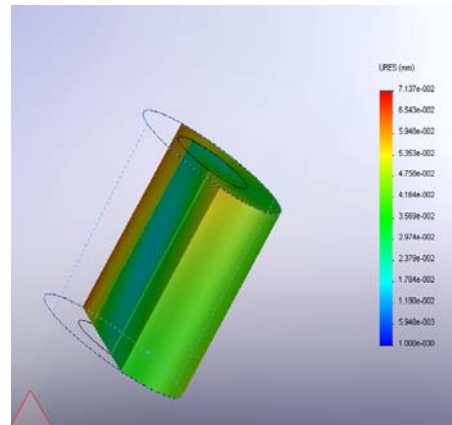


Fig. 6 – The phenomenons distribution in assembling by 70mm lenght and 30,085mm-the tree diameter 30,085mm, the interior pad 30mm and exterior 60mm, in section.

3. Conclusions

Following this simulation of tensions and moments request of an undismontable assembling, with different dimensions of the fretaj, of the contact area, we can concluded:

- in assembling ends appear powerfull sources of tensions concentration;

- pressure contact growing at the assembling ends leads to the tensions normal growth and the shear ones;
- the tensions shear growth caused by twisting in the passing area from the hub to the pad;
- tensions shearing appearance on the contact surface;
- tensions distribution in the cemented and hardened level limits is very important because that's why depends directly the resistance of the assembling fatigue;
- compression of the stretching area is directly related to the level's thickness.

Received: August 12, 2009

"Gheorghe Asachi" Technical University of Iași,
email: cretu.sanda@yahoo.com.

REFERENCES

1. Chișiu AL., Matieșan D., Pop D., *Organe de mașini*. Edit. Did. și Pedag., București, 1991
2. Minkevici A. N., *Tratamente termochimice ale metalelor și aliajelor*. Edit. Tehnică, București, 1968.
3. Sucală F., *Organe de mașini, I*, Casa de Editură "Transilvania PRESS", Cluj-Napoca, 1981.
4. Soporan V., Vermeșan H., *Considerații privind modelarea proceselor care au loc în cadrul ingineriei suprafețelor*. Capitolul XVI, apărut în volumul *Procedee avansate în ingineria suprafețelor*, Edit. UTPRES Cluj-Napoca 1998.
5. Teodorescu C., Mocanu D., Buga M., *Îmbinări sudate*. Edit. Tehnică, București, 1972.
6. Tudor I., Rîpeanu R.G., *Ingineria coroziunii. I și II*, Ed. Universității din Ploiești, 2002.
7. Vermeșan G., et al. – *Introducere în ingineria suprafeței*, Editura Dacia, Cluj-Napoca, 1999

ASPECTE TEORETICE ȘI EXPERIMENTALE PRIVIND MODELAREA FENOMENELOR CE SE PRODUC ÎN ASAMBLĂRILE NEDEMONTABILE

(Rezumat)

Lucrarea prezintă o modelare pe calculator a fenomenelor ce se produc în asamblările nedemontabile de tipul bușă-arbore din materiale diferite, lungime constantă și grosimi diferite.

**RESEARCH ON COOLING CAPACITY MODIFICATION FOR
SYNTHETIC QUENCHING ENVIRONMENTS TYPE AS
MODIFIED POLYACHILENGLYCOL (PAG)**

BY

**ADRIAN GRECU, DAN-GELU GALUȘCĂ, CARMEN NEJNERU,
ION HOPULELE and MIHAI AXINTE**

Abstract. Were studied and compared cooling environment like oil TT50, polyachilenglycol solution (PAG) 5% in water, 5% PAG solution in water with Na +: silicate: 0, 8, 16% and Calcium carbonate: 0, 5, 10% in water; have been traced cooling curves of a standardized Ag test-piece in above mentioned environments, with and without stirring. Based on cooling curves were calculated and plotted variation curves for cooling speeds versus temperature and variation curves of heat transfer coefficient part-environment. For each case was calculated cooling intensity also.

Key word: heat transfer coefficient, polyachilenglycol, cooling medium, cooling curves, cooling intensity.

1. Introduction

Cooling as the final operation of thermal treatment is of particular importance because it determines the structure and hence properties of heat-treated parts.

For a correct chose of a cooling environment must be analyze the kinetic cooling curve of alloy (T.R.C. diagram) and it compares to environments cooling curves.

The normal conduit of the cooling process has an important role for operation success with purpose of obtaining some structures in sample section (martensitic water quenching type structures) without producing quenching defects as cracks, deformations or big remanent tensions.

The oil has a has a very appreciate curve at cooling because of fast

passes through minimal stability domain of subcooled austenite (**A**) and have a reduce rate of cooling in martensitic transformation domain (**B**) when tension from structural transformations are very big. ($v_{specific \underline{M}} > v_{specific \underline{A}}$) and thermal tensions induce by cooling rate are smaller.

But the oil have disadvantage that present a high ignition danger, is a nonecological environment (because of gas emanations which appears during hardening), for this was searched replacement of mineral oil for thermal treatment there was possible with cooling alternatives with reduce or nonstart ignition danger which can be synthetic environments.

Due this reasons in large quenching baths in the industry is currently used carbodimetil cellulose. Quenching bath during operation modifies its properties, therefore the presence of additives is required to give both constant properties and good cooling capacity depending on the type of steel and the type of each piece.

Another very important factor is represented by the environment agitation degrees which modify substantially the cooling curve, implicit instantaneous cooling rates and thermal transfer on different periods.

2. Experimental Results

Cooling curves were drawn for these quenching media:

1. OIL TT50
2. Solution 5% PAG in water
3. Solution 5% PAG + silicate Na 8% in water
4. Solution 5% PAG + silicate Na 16% in water
5. Solution 5% PAG + silicate Na 0% + 5% Ca carbonate in water
6. Solution 5% PAG + silicate Na 0% + 10% Ca carbonate in water
7. Solution 5% PAG + silicate Na 8% + 10% Ca carbonate in water

To do a proper comparison between environments cooling characteristics mentioned above, all were heated up to 40°C.



Fig. 1 - Installation for cooling characteristics determination.



Fig. - 2. Silver samples with the following sizes and features: $\varnothing = 12,5$ [mm], $h = 25$ [mm], $S = 1408$ [mm²], $m = 39.9$ [g], $\rho_{Ag} = 10.5$ g/cm³, $\lambda_{Ag} = 418.5$ W/m·

Facility as a whole is shown in the picture above and consists of the following main elements:

- a) Test tube of silver
- b) Cooling precinct
- c) Furnance
- d) Electric power supply
- e) Cromel – Alumel thermocouple
- f) Milivoltmeter for indication
- g) Recorder OH 816/H

Test tube was heated in the oven to 800°C temperature then was introduced into researched environment, the cooling curve was recorded on „y-t recorder”.

For each of the cooling medium were calculated:

- i) Cooling rate on intervals [°C/s]
- ii) Thermal transfer ceficient on intervals.

$$\alpha_i = \frac{3600 \cdot m \cdot c}{\Delta t_i \cdot S} \ln \frac{T_i - T_o}{T_f - T_o} \text{ [w/m}^2\text{k]}$$

where: $m = 0.0399$ [kg] sample mass; $c = 0.056$ [kcal/kg·grd] specific heat of silver; $S = 0.001408$ [m²] sample surface; Δt [s] time interval; T_i T_f [°C] final and initial temperature on interval; T_o environment temperature.

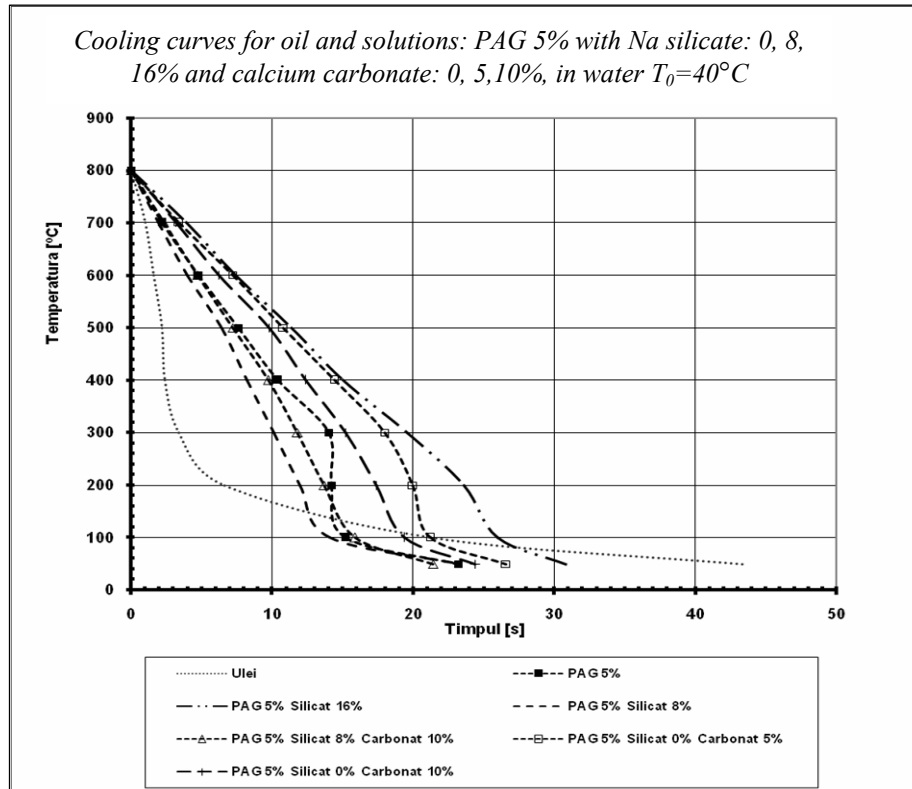
The obtained results were put in a table and based on them were made:

- a) Cooling curves $T = f(t)$ (table 1)
- b) Cooling rate variation depending on temperature $v_r = f(T)$
- c) Heat transfer coefficient variation depending on the temperature

$\alpha_i = f(T)$.

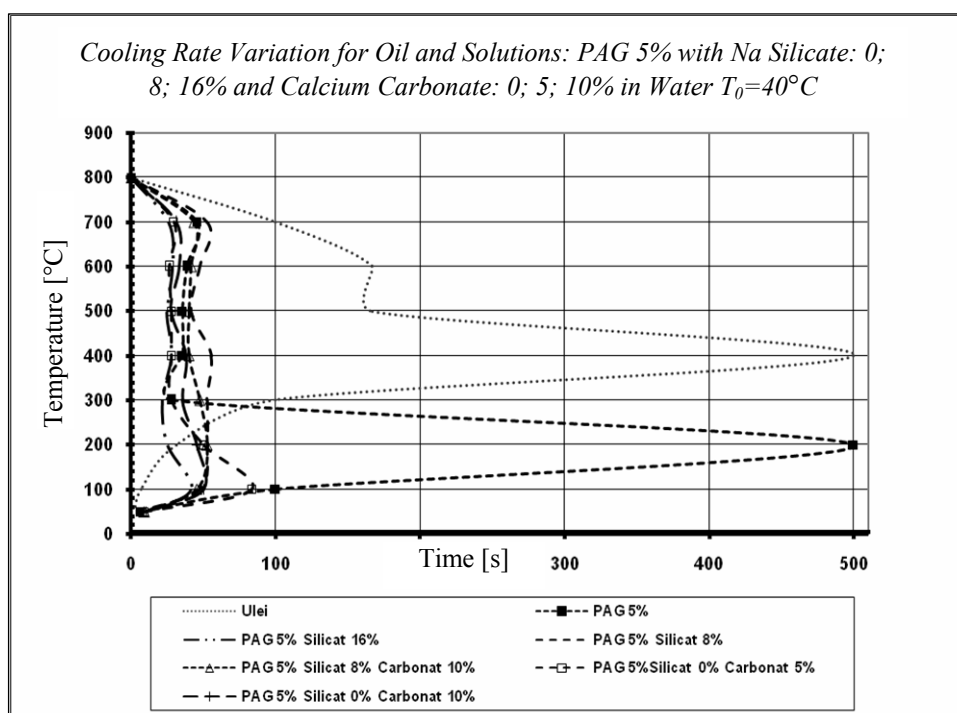
Cooling Curves for Oil and Solutions: PAG 5% with Na Silicate: 0, 8, 16% and Calcium Carbonate: 0, 5,10%, in Water $T_0=40^\circ\text{C}$

T[°C]	Oil t [s]	PAG 5% t [s]	PAG 5% Silicate 16% t [s]	PAG 5% Silicate 8% Carbonate 10% t [s]	PAG 5% Silicate 0% Carbonate 10% t [s]	PAG 5% Silicate 8% t [s]	PAG 5% Silicate 0% Carbonate 5% t [s]
800	0	0	0	0	0	0	0
700	1	2.2	3.9	2.3	3.2	1.9	3.4
600	1.6	4.8	7.4	4.7	6.2	4	7.2
500	2.2	7.6	11.4	7.2	9.8	6.4	10.8
400	2.4	10.4	15	9.7	12.4	8.2	14.4
300	3.4	14	19.6	11.8	15.2	10.1	18
200	6.6	14.2	23.6	13.7	17.4	12	20
100	21.2	15.2	26	15.9	19.4	14.1	21.2
50	43.4	23.2	30.8	21.4	24.4	23.4	26.6



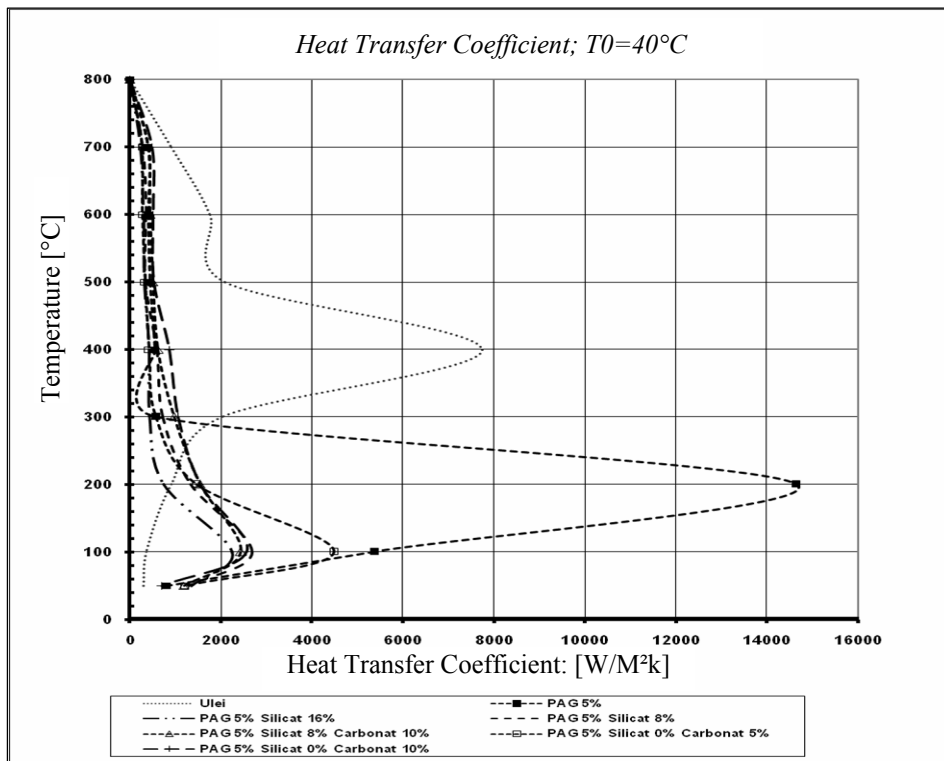
Cooling Rate Variation for Oil and Solutions: PAG 5% with Na Silicate: 0; 8; 16% and Calcium Carbonate: 0; 5; 10% in Water $T_0=40^\circ\text{C}$

T[°C]	Oil V [°C/s]	PAG 5% V [°C/s]	PAG 5% Silicate 16% V [°C/s]	PAG 5% Silicate 8% Carbonate 10% V [°C/s]	PAG 5% Silicate 8% V [°C/s]	PAG 5% Silicate 0% Carbonate 10% V [°C/s]	PAG 5% Silicate 0% Carbonate 5% V [°C/s]
800	0	0	0	0	0	0	0
700	100	45.5	25.64	43.38	52.63	31.25	29.41
600	166.7	38.5	28.57	41.67	47.62	33.33	26.32
500	166.7	35.7	25	40	41.67	27.78	27.78
400	500	35.7	27.78	40	55.56	38.46	27.78
300	100	27.8	21.74	47.62	52.63	35.71	27.78
200	31.2	500	25	52.63	52.63	45.45	50.00
100	6.8	100	41.67	45.45	47.62	50.00	83.33
50	2.3	6.3	10.42	9.09	5.38	10.00	9.26



Heat Transfer Coefficient; $T_0=40^\circ\text{C}$, $\text{W}/\text{M}^2\text{k}$

	Oil V [$^\circ\text{C}/\text{s}$]	PAG 5% V [$^\circ\text{C}/\text{s}$]	PAG 5% Silicate 16% V [$^\circ\text{C}/\text{s}$]	PAG 5% Silicate 8% Carbonate 10% V [$^\circ\text{C}/\text{s}$]	PAG 5% Silicate 8% V [$^\circ\text{C}/\text{s}$]	PAG 5% Silicate 0% Carbonate 10% V [$^\circ\text{C}/\text{s}$]	PAG 5% Silicate 0% Carbonate 5% V [$^\circ\text{C}/\text{s}$]
800	0	0	0	0	0	0	0
700	909,2356	413,2889	233,1373	395,3198	284,1361	478,545	267,4222
600	1756,877	405,4331	301,1789	439,2192	351,3754	501,9648	277,4016
500	2090,186	447,8971	313,528	501,6448	348,3644	522,5466	348,3644
400	7740,86	552,9186	430,0478	619,2688	595,4508	860,0956	430,0478
300	2023,773	562,159	439,9505	963,7012	722,7759	1065,143	562,159
200	915,0118	14640,19	732,0094	1541,072	1330,926	1541,072	1464,019
100	368,0861	5374,057	2239,19	2442,753	2687,028	2559,075	4478,381
50	292,792	812,4978	1354,163	1181,815	1299,996	698,9228	1203,7



Alfa global	497,50	930,67	701,02	1008,95	884,90	922,71	811,71
H	0,59	1,11	0,84	1,21	1,06	1,10	0,97

3. Conclusions

1. PAG 5% with 16% Na₂SiO₄ and PAG 5% with 5% CaCO₃ curves presents in the high temperature (800 ÷ 350°C) cooling rates too low (danger do not appear martensite in the structure) and excessive speed cooling below 350°C leading to the emergence of tensions.

2. Was observed that PAG 5% with 8% Na₂SiO₄ and 10% CaCO₃ has a high speed between 150°C and 100°C when the martensitic transformation was already primed which shows that the effect of carbonate in the presence of silicate is to generate a more accurate curvature of the cooling rate in the second cooling interval.

Received: August 11, 2009

“Gheorghe Asachi” Technical University of Iași,
Department of Technologies and Equipment for Materials Processing
email: greuceanu24@yahoo.com

REFERENCES

1. Nejnaru C., Galusca D.G., Grecu A., Carabet R., *Researches Looking the Modification Cooling Capacity of Hardening Compounds in Magnetic Field*, Technical University Galati, Romania, October 2007, **II**, Advanced Technologies and Materials, 161-165.
2. Nejnaru C., Grecu A., Carabet R., Hopulele I., *Researches concerning the reconditioning of hardening bathes in synthetic medium based on carbodimethyl cellulose*. Technical University Galati, Romania, October 2007, **II**, Advanced Technologies and Materials, 318-324.

CERCETĂRI PRIVIND MODIFICAREA CAPACITĂȚII DE RĂCIRE A MEDIILOR SINTETICE DE CĂLIRE TIP POLIACHILENGLICOL (PAG) MODIFICAT

(Rezumat)

S-au studiat comparativ mediile de răcire precum uleiul TT50, soluție de poliachilenglicol (PAG) 5% în apă, soluție de PAG 5% în apă + cu Silicat de Na: 0; 8; 16% și Carbonat de Ca: 0; 5; 10% în apă; s-au trasat curbele de răcire a unei epruvete standardizate de Ag în mediile mai sus menționate, cu și fără agitare. Pe baza curbelor de răcire s-au calculat și trasat și curbele de variație a vitezelor de răcire cu temperatură precum și curbele de variație a coeficientului de transfer termic piesă-mediu. S-a calculat în fiecare din cazuri și intensitatea de răcire.

**IMPACT OF CORROSION ON THE SURFACE LAYER
PROCESSED BY MATERIAL ADDITION COATING BY
IMPULS DISCHARGE METHOD**

BY

**ANCA ELENA LĂRGEANU, DAN-GELU GĂLUȘCĂ, CARMEN NEJNERU,
MANUELA CRISTINA PERJU and ION HOPULELE**

Abstract. The paper presents results from corrosion tests on cast-iron with phosphorous eutectic coated with nickel using the vibrator electrode technique. Corrosion tests were made using Volta lab 21 machine, and the aggressive environment used was sea water. Electronic scanning microscope investigations were made before coating to show the coating quality and after the corrosion to show the effect on the coated layer.

Key words: impulse discharge, coating layer, corrosion, saline environment, electrode.

1. Introduction

Corrosion is the main factor involved in a product's lifetime. This is the deterioration factor of the most important material properties, because of the chemical reactions with the surrounding environment. Environment etching leads to material properties aggravation and subsequent destruction.

Corrosion is not only metallic material destruction, it affects also plastic, ceramic materials, concrete and even the surrounding environment.

Everything is corrodible and any environment can be corrosive to a certain material. For example:

- a) darkening of glass under bacterial action;
- b) PVC is damaged under the influence of UV beams;
- c) cars and their structural architectural fittings are affected by corrosion;
- d) copper electric contacts are affected by oxidation;
- e) super-alloys from warm gas turbines are affected by corrosion;

- f) brass cracks in hydrogen nitride presence;
- g) steel is becoming brittle in hydrogen, etc.

Corrosion process, is the chemical spontaneously modification of metals or alloys composition, after a chemical, electrochemical or biochemical reaction during environment interaction. Corrosion leads to changes of physical proprieties in metallic materials: crystalline structure, hardness, strength, thermal and electrical conductivity etc., as well as changes in chemical proprieties transforming a percent from the material in chemical compounds. Protection against corrosion consists in all measures taken to protect technical materials from the aggressive action of corrosive environments.

Anticorrosion methods are very varied and numerous; grouped in some categories:

- i) corrosion prevention methods;
- ii) using stainless metals and alloys;
- iii) action methods on corrosive environment;
- iv) metal coating methods.



Fig. 1 – Ornamental parts damage exposed to atmospheric corrosion.

One of the metal coating methods is the vibrator electrode.

2. Methodology

Hardening with electric sparks of metallic parts consists of , polar transport of the electrode material (anode) under the action of pulsating recovered current sparks discharge on the surface of the part (cathode).

The process starts by approaching the anode to the cathode. After penetrating the space between the electrodes and beginning of discharge flow development (plasmatic stage of discharge), vaporization and liquid stage discharge starts from the electrodes surfaces. In the time between two sparks, the small quantity of melted metal solidifies developing a protection layer. This coating layer must have a very good adherence on part surface and a large chemical and thermal compatibility with the substrate, as well as high ware and

oxidation proprieties.

Electrochemical corrosion studies were made in sea water, collected from Romanian seaside (Constanta), and with composition in terms of g L⁻¹: Cl⁻ - 8.26; HCO₃⁻ - 0,183; CO₃⁻ - 0.022; SO₄⁻ - 1.137; Na⁺ - 4.47; K⁺ - 0.158; Ca²⁺ - 0,203; Mg²⁺ - 0,557. This composition has a salinity of 15.0 g L⁻¹.

Potential measurement in open circuit and potentiodynamic polarizations were made with Volta Lab 21 equipment. Data processing was done with Volta Master 4 software. A three electrodes cell was used, equipped with agitation system.

Cylindrical electrodes were mounted on teflon support that allows connection to the electrochemical system spinning electrode. As auxiliary a platinum electrode is used and a calomel saturated electrode as reference. The measurements were made at 25°C, with natural airing.

Linear polarization curves were registered at the electrode scanning potential of 1 mV/s, in a potential domain of ± 150 mV, around potential in open circuit. Cylindrical polarization curves were registered with a speed of 10 mV/s between (-700 ...+1500 mV).

Corrosion potential for zero corrosion currents $E_0 \equiv E(I=0)$, Tafel grades (ba and bc) Polarization resistance (Rp), corrosion current density (Jcox) and corrosion speed (Vcox) were processed with Volta Master 4 software.

3. Discutions and Results

For studies, a phosphorous cast-iron was used, witch composition was determinated by spectrometry- using Foundry-Master (emission spectrometer).

Table 1
Phosphorous Eutectic Cast-Iron Chemical Composition, %

Material	Fe	C	Si	Mn	P	S	Cr	Ni	Cu
Phosphorous cast-iron	91.8	4.50	1.54	1.03	0.620	0.140	0.097	0.0572	0.148

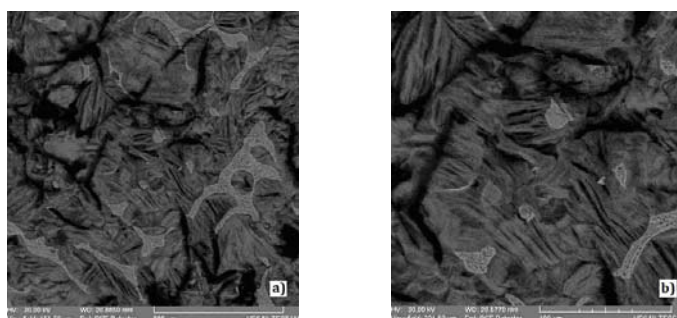


Fig. 2 – Pictures using electronic scanning on corroded phosphorous

cast-iron without coating; *a* – scale X500; *b* – scale X1000.

For impulse discharge coating method Elitron 22A machine was used, and the electrode for the coating layer is nickel electrode (Ni).

Nickel was used for coating because it shows the following characteristics from chemical point of view:

- a) thermodynamic unstable in acid environment;
- b) can not be corroded in pH=9-12 environments;
- c) nickels corrosion speed in acid environment ill low because of the high ionization supratension of the metal and the passivation tendence in aerated solutions;
- d) it is punctiform corroded by carbonated and chlorides water;
- e) organic acids have a low impact on nickel;
- f) very stable to basic and atmospheric corrosion action.

Complex investigation of the test parts was made on a electronic scanning microscope (SEM).

Nickel is used by electro erosion coating method because it improves ware proprieties and it adheres well on the part obtaining high thickness coating layers.

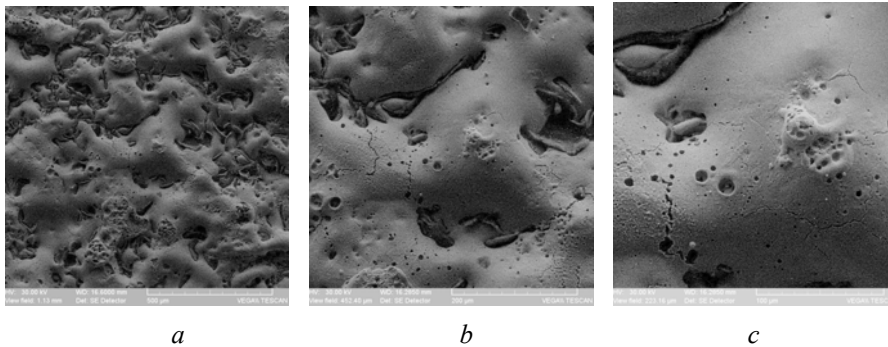


Fig. 3– Picture of nickel coating on phosphorous cast-iron substrate, using electronic scanning: *a* – scale X200; *b* – scale X500; *c* – scale X1000.

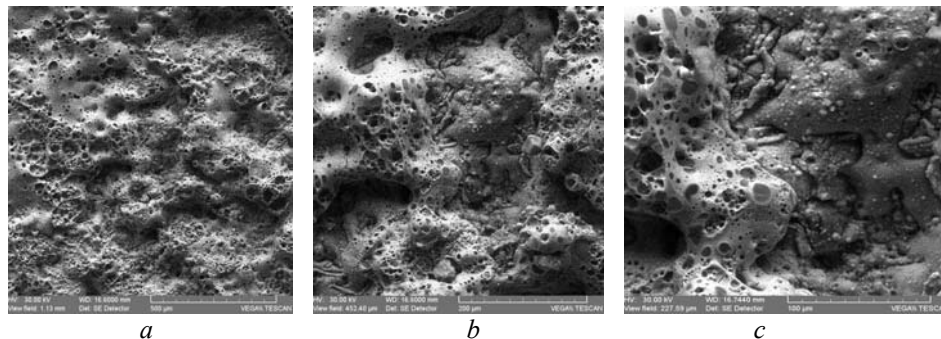


Fig. 4 – Pictures using electronic scanning on nickel double layer coating on phosphorous cast-iron; *a* – scale X200; *b* – scale X500; *c* – scale X1000.

Nickel is used mainly for obtaining corrosion resistant coating layers. Nickel's corrosion speed in acid environment is low because of high ionization supratension and pasivation tendency in aerated solutions. The metal is stable at no chloride water and very stable to basics and atmospheric action.

Nickel's atomic number is 28 very close to iron (26), witch means that their atomic radius difference is very low an so nickel can be transferred easily from the surface into the substrate creating a high thickness transition area, with beneficial impute on the coating layer adherence.

Corrosion behavior was achieved by fast electrochemical tests (dynamic potentiometer) Under quantity aspect, in Table 2 are presented corrosion process parameters in sea water on the sparked test part for nickel one layer coating as weal as for double layer coating, comparing with witness test part – eutectic phosphorous cast-iron material.

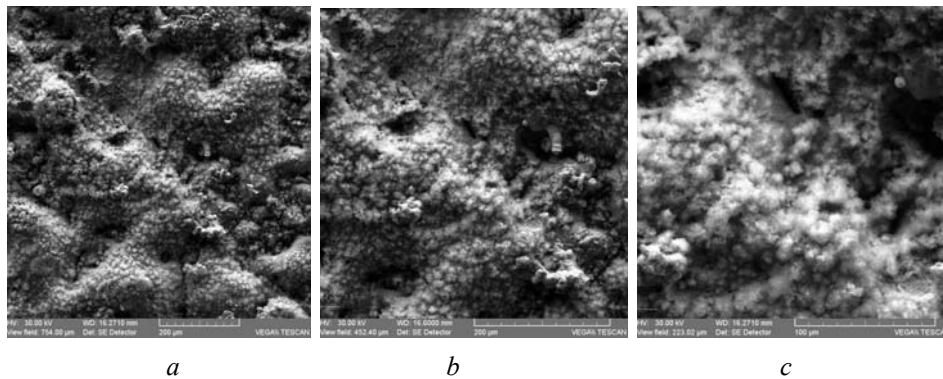


Fig. 5 – Pictures using electronic scanning on one layer nickel coating of phosphorous cast-iron support - sea water corrosion; *a* – scale X200; *b* – scale X500; *c* – scale X1000.

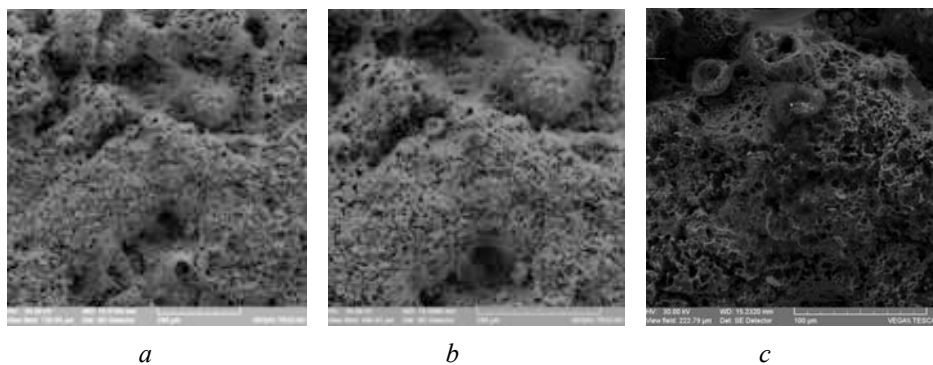


Fig. 6 – Pictures using electronic scanning on double nickel coating of phosphorous cast-iron – sea water corrosion; *a* – scale X200; *b* – scale X500; *c* – scale X1000.

Table 2

Corrosion Process Parameters in Sea Water for the Coated Test Parts

Test part	In line polarization						Cyclic polarization		
	E_0 (mV)	b_a (mV)	b_c (mV)	R_p (Ohm.cm ²)	J_{cor} (mA/cm ²)	v_{cor} (μm/an)	E_{cor} (mV)	E_{tr} (mV)	J_{1500} (mA/cm ²)
Ni 1 s	-732	52	-508	685	0.0332	388	-700	-698	318
Ni 2 s	-633	64	-225	587	0.0306	357	-661	-649	274
Witness	-760	51	-503	1210	0.0195	229	-724	-671	293

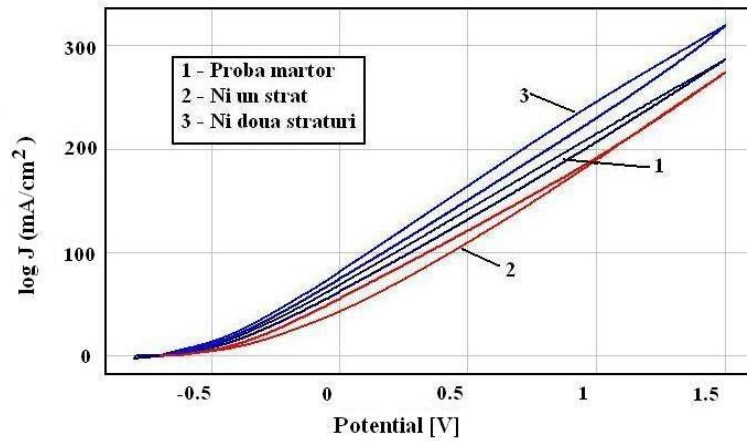


Fig. 7 – Linear polarization curve.

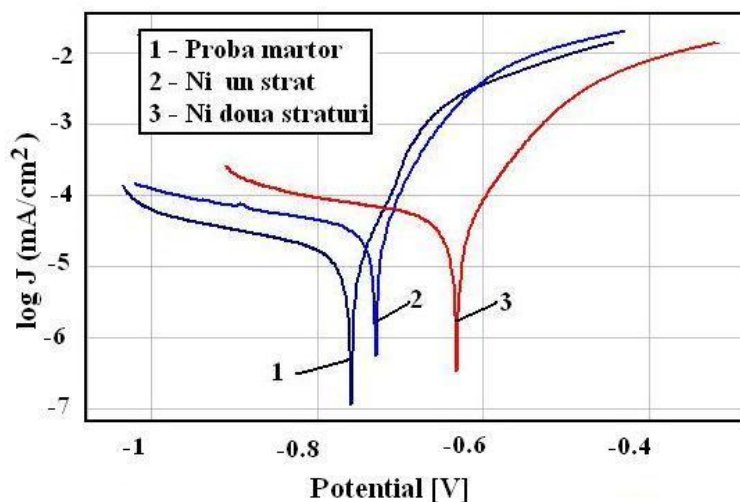


Fig. 8 – Cyclic polarization curve.

4. Conclusion

- 1) We can see at vibrator electrode nickel coating a corrosion resistance improvement for multiple layer coating.
- 2) When the coating degree raises and micro cracks from the first deposition are covered, electric rasps that sustain corrosion are formed.
- 3) The method ensures, beside corrosion resistance improvement, for acid rains an esthetic quality improvement of decorative objects.
- 4) Corrosion starts harder for electrode vibrator method nickel coating because is not pitting type, but on entire surface corrosion.

Received: February 18, 2010

“Gheorghe Asachi” Technical University of Iași,
e-mail: pufankapuf@yahoo.com

REFERENCES

1. Nejnaru, C., Perju M., Sandu A.V., Axinte M., Ungureanu G., *Improvement on Cast-Irons Corrosion Properties for Decorations Through Metallic Coatings*. ARTCAST, Galați, Mai 2008, 98,
2. Alexandru A., *Contribuții privind alierea și depunerea superficială prin scântiere electrică și influența tratamentelor termice asupra caracteristicilor straturilor obținute ale materialelor metalice*. PH. D. DISS., Iași, 2002.
3. Vermeșan E., Mureșan, I., *Coroziune și protecție anticorozivă*. UTC-N 1995.
4. www.yachtblogromania.blogspot.com/2007/10/coroziune
5. www.xtreme.hawaii.edu/corrosion/
6. www.paxcam.com/images/metal_corrosion_71.htm

7. www.commonswikimedia.org/wiki/file:corrosion

IMPACTUL ASUPRA COROZIUNII A STRATURILOR SUPERFICIALE
OBȚINUTE PRIN ACOPERIRE CU MATERIALE DE ADAOS PRIN METODA
DESCĂRCĂRII ÎN IMPULS

(Rezumat)

Lucrarea prezintă rezultatele obținute la încercări de coroziune pe material de fontă cu eutectic fosforos pe care au fost depuse straturi de nichel folosind metoda electrozudului vibrator. Încercările de coroziune s-au realizat folosind un aparat tip Voltalab 21, iar mediul agresiv ales pentru testare a fost apa de mare. S-au făcut investigații cu microscopul cu scanare electronică, înainte de depunere pentru evidențierea calității depunerii și după coroziune pentru evidențierea efectului acesteia asupra stratului depus.

ON THE THERMAL TRANSFER IN NOSTRUCTURES (II) CONDUCTIVE TYPE BEHAVIOUR.

BY

RĂZVAN LIȚOIU*, IVANNIS ZERICHORIS*, ANCA ALUCULESEI*,
DAN GELU GĂLUȘCĂ* and MARICEL AGOP**

Abstract. Considering that the “movements” of the heat take place in fractal curves, the conductive type behavior of the nanostructures is analysed. It result that the enhancement in thermal conductivity is given through “self structuring” type mechanism.

Key words: nanostructures, conductive type behaviour, heat transfer

1. Introduction

In a recent paper we established a mathematical model on the “movements” of the particles on continuous equations non-differentiable curves, *i.e.* on fractals [1, 2]. In the present paper we shall use this model to study the conductivity type selftransfer in nanostructures.

2. Mathematical Model

Let us consider the fractal operator [1] :

$$\begin{aligned} \hat{d} &= \frac{\delta}{\delta t} + \bar{V} \nabla - iD \nabla \\ D &= \frac{\lambda^2}{2\tau} \left(\frac{dt}{\tau} \right)^{\left(\frac{2}{D_f} \right) - 1} \end{aligned} \quad (1a, b)$$

In relations (1a,b) \mathbf{v} is the complex speed field.

$$\bar{\mathbf{V}} = \bar{\mathbf{v}} - i\bar{\mathbf{u}}$$

With $\bar{\mathbf{v}}$ the standard classical speed, differentiable and independent of resolution and $\bar{\mathbf{u}}$ the fractal speed, non-differentiable and resolution dependent, λ is a length scale, $d\mathbf{t}$ and τ are temporal scales.

As a consequence, we are now able to write the conservation law of a fractal function ϵ in a fractal space-time under its strong covariant form:

$$(2) \quad \frac{\bar{\square}\epsilon}{dt} = \frac{\delta\epsilon}{\delta t} + \bar{\mathbf{V}}\square\nabla\epsilon - i\frac{\lambda^2}{2\tau}\left(\frac{dt}{\tau}\right)^{\left(\frac{2}{D_f}\right)-1} \Delta\epsilon = 0$$

or more, by separating the real and imaginary parts:

$$(3a, b) \quad \frac{\delta\epsilon}{\delta t} + \bar{\mathbf{v}}\square\nabla\epsilon = 0,$$

$$-\bar{\mathbf{u}}\square\nabla\epsilon = \frac{\lambda^2}{2\tau}\left(\frac{dt}{\tau}\right)^{\left(\frac{2}{D_f}\right)-1} \Delta\epsilon$$

Consequently, at the differentiable scale the local temporal variation $\frac{\delta\epsilon}{\delta t}$ and the term, $\bar{\mathbf{v}}\square\nabla\epsilon$, are equal, while at the non-differentiable scale, the term, $\bar{\mathbf{u}}\square\nabla\epsilon$, and $\Delta\epsilon$, compensate each other.

Particularly, for $\bar{\mathbf{v}} = \bar{\mathbf{u}}$ (*i.e.* "synchronal" movements at different scales), from (3a,b) we get the diffusion type equation,

$$(4) \quad \frac{\delta\epsilon}{\delta t} = \frac{\lambda^2}{2\tau}\left(\frac{dt}{\tau}\right)^{\left(\frac{2}{D_f}\right)-1} \Delta\epsilon$$

Such an equation is implied by the Fourier type law

$$(5) \quad \bar{j}(\varepsilon) = -\frac{\lambda^2}{2\tau} \left(\frac{dt}{\tau} \right)^{\left(\frac{2}{D_F}\right)-1} \Delta\varepsilon$$

with a current density \bar{j} . Therefore, eqs. (4) and (5) describe a fractal fluid of conductive type behavior.

Particularly, for movements on fractal curves of the Peano's type [2,3], *i.e.* in the fractal dimension [3], $D_F = 2$, the equation (4) and (5) take the standard forms:

$$(6) \quad \frac{\delta\varepsilon}{\delta t} = \frac{\lambda^2}{2\tau} \Delta\varepsilon$$

and respectively:

$$(7) \quad \bar{j}(\varepsilon) = \frac{\lambda^2}{2\tau} \Delta\varepsilon$$

Let us now apply the previous considerations in the numerical simulations of thermal transport in a nanostructure.

The thermal expansion in a fractal fluid is solved in the planar normalized coordinative system.

$$(8) \quad \bar{T} = \frac{T}{T_0}, \tau = \omega t, kx = \zeta, ky = \eta$$

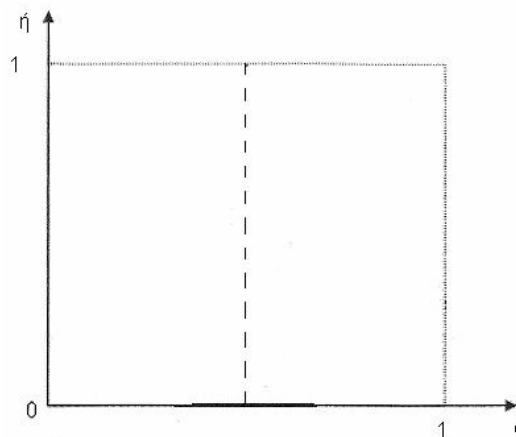


Fig. 1 – Integration domain used for the numerical simulation of thermal “expansion”.

The thermal evolution is described with the following assumptions:

- i) the fractal fluid is in the state of local thermo-dynamical equilibrium;
- ii) the "mouvements" of the heat take place on Peano's type curves of fractal dimension $D_F = 2$ [2]. Than, we can choose:

$$(9) \quad D \frac{k^2}{\omega} = \frac{\lambda}{c\rho} \frac{k^2}{\omega} \equiv 1$$

where λ , c and ρ are the standard coefficients [4];

- iii) the thermal expansion is described in the approximation of a diffusion type equation;
- iv) the thermal source term is introduced through the boundary condition.

In such circumstances, the two-dimensional heat dynamics is described by the equation:

$$(10) \quad \frac{\delta \bar{T}}{\delta \tau} = D \Delta \bar{T}$$

For the numerical integration, the following initial and boundary conditions are taken:

- i) the box integration domain is initially "filled" with undisturbed fractal fluid

$$\bar{T} = 1 \quad \text{for} \quad \tau=0, \quad 0 \leq (\zeta \times \eta) \leq (1 \times 1)$$

that is preserved on the boundaries,

$$\bar{T}(\tau, \zeta, 1) = \bar{T}(\tau, 1/2, \eta) = \bar{T}(\tau, 1/2, \eta) = 1$$

- ii) the thermal source is located as in Figure 1 and is assumed to have a Gaussian space-time profile,

$$\bar{T} = \exp \left[-\frac{(\tau-1)^2}{(1/2)} \right] \exp \left[-\frac{\zeta^2}{(1/2)^2} \right],$$

The diffusion equation of concentration with initial and boundary condition is numerically solved using finite differences [5]. Moreover, if the diffusion takes place in the presence of a wall, the previous condition is replaced by $\bar{T}/\eta(\tau, \zeta, 1) = 0$

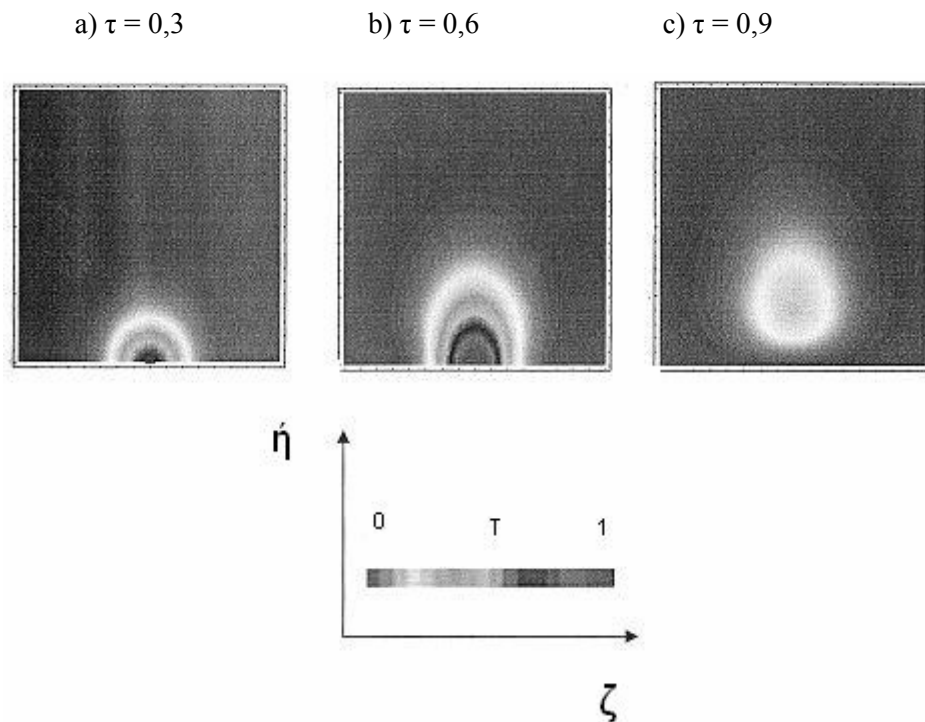


Fig. 2 – The contour curves of normalized temperature for various normalized time moments as resulted from the numerical simulation of the diffusion equation.

In Figs. 2 and 3 the two dimensional contour curves of the normalized temperature at the normalized time moments $\tau = 0,3$ (a),

$\tau = 0,6$ (b) and $\tau = 0,9$ (c) are given as obtained from the numerical simulations (Fig. 2 in the absence of wall, Fig. 3 in the presence of wall).

The following considerations results:

- i) the "temperature plume" "disappears" by diffusion;
- ii) near the wall the "temperature plume" is 'regenerating'.

We noted that previous proceedings may be transferred to explain the growth of nanofluid thermal conductivity.

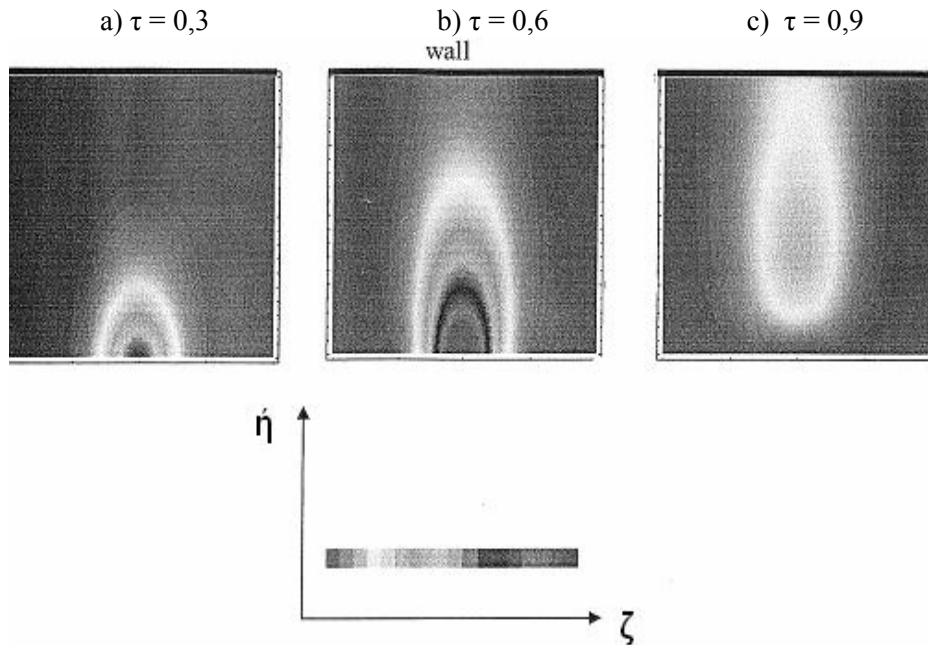


Fig. 3 – The contour curves of normalized temperature for various normalized time moments as resulted from the numerical simulation of the diffusion equation in the presence of a wall.

3. Conclusions

The main conclusions of the present paper are the followings:

- i) considering that the "movements" of the heat take place on fractal curves, the conductivity type transfer in nanostructures is analyzed;
- ii) numerical solutions in the absence of a wall and in presence of a wall are given. It result that the "temperature plume" is regenerating near the wall.

In such context the enhancement in thermal conductivity in nanostructures is given through "selfstructuring" type mechanism.

Received: February 18, 2010

"Gheorghe Asachi" Technical University of Iași,

* Faculty of Materials Science and Engineering
e-mail: dangalusca@yahoo.com

** Department of Physics

e-mail: m.agop@yahoo.com

REFERENCES

1. Aluculesei A., Lițoiu R., Zerichioris I., Gălușcă D.G., Agop M., *On the Thermal Transfer in Nanostructures (I). Mathematical Model*, Bul. Inst. Polit., Iași, **LVI (LX)**, 1, s. de Știința Materialelor (2010 in press).
2. L. Nottale *Fractal Space-Time and Microphysics: Towards a Theory of Scale Relativity*, World Scientific, Singapore 1993.
3. Mandelbrot B.B., *The Fractal Geometry of Nature*. W.H. Freeman, San Francisco 1977.
4. Kurz W., Fischer D.J., *Fundamentals of Solidifications Trans. Tech. Publ.*, 82-92 (1989).
5. Avzamasov B., *Material Science*. Mir Publisher, Moscow, 90-95 (1989).
6. Zienkiewicz O.C., Taylor R.L., *The Finite Element Methods*. McGraw-Hill, 132-136 (1991).

ASUPRA TRANSFERULUI TERMIC IN NANOSTRUCTURI (II) COMPORTAREA DE TIP CONDUCTIV

(Rezumat)

Considerând că "mișcările" căldurii au loc pe curbe fractale, în prezenta lucrare este analizat comportamentul conductiv al nanostructurilor. Rezultă că creșterea conductivității termice se datorează unui mecanism de autoorganizare.

BULETINUL INSTITUTULUI POLITEHNIC DIN IAȘI
Publicat de
Universitatea Tehnică „Gheorghe Asachi” din Iași
Tomul LVI (LX), Fasc. 1, 2010
Secția
ȘTIINȚA ȘI INGINERIA MATERIALELOR

ON THE MECHANICAL CHARACTERISTICS OF COMMERCIAL NON-PRECIOUS CO-CR DENTAL ALLOYS

BY

NICOLETA MONICA LOHAN (MAHU) and
IONUT LUCIAN BISTRICIANU*

Abstract. A large variety of dental alloys are available now on the market and a fair selection of them is a difficult task. Although the mechanical properties of the dental materials do not represent necessarily their clinical performance, they can be used as a selection guide. Generally, dental alloy are placed in the mouth of the patients for a long time and they have to resist the mechanical load and corrosive action. Therefore, they must be extremely strong so that the small, delicate tooth restorations and appliances will not be broken or bent by the forces exerted during chewing. It is important to know the physical and mechanical properties of these materials because the material election for a prosthetic work manufacture those properties are very important, with biocompatibility and cost. The paper represents a references synthesis of the most important published works and mechanical properties of the non-precious dental alloys based on cobalt.

Key words: non-precious dental alloy, Co-Cr alloy, mechanical properties of Co-Cr dental alloys.

1. Introduction

The materials employed in the mouth must be completely tarnish-resistant, they must not react with the many alkaline and acid foods that are taken into the mouth, and they cannot be affected by mouth fluids. Non-precious dental alloys have been used in the dental practice over 70 years. From the benefits they offers, are mentioned a good corrosion resistance, superior mechanical properties (high hardness, high elastic modulus), low density, good compatibility and a low cost [2], [4], [5], [1], [8]. From the point of view of dental technique, Co–Cr alloys have been used for the fabrication of removable partial dentures, but also for metal ceramic prostheses, where fine framework

constructions are needed. In Fig. 1 are shown non-precious alloys used for removable partial denture, fixed partial denture and surgical implant.

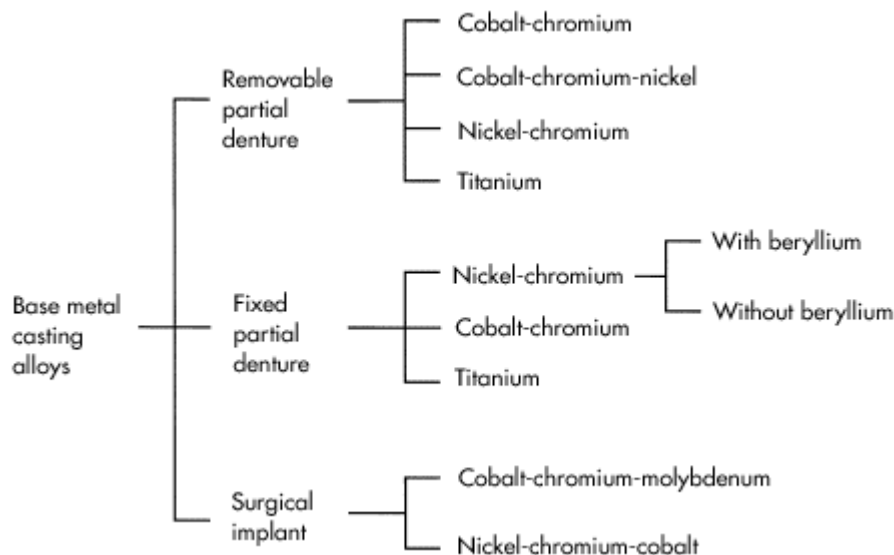


Fig. 1 – A classification of base metal casting alloys [2, 3].

For the casting of partial prosthesis, the most important parts of dental non-precious alloys are Co and Cr, which totalize almost 90% from the most used dental materials. Co-Cr alloys include almost 65% Co, 30% Cr and others elements (Mo, Si, C) with a percentage of 5%. The cobalt provides stiffness and hardness, while chrome increases strength and corrosion resistance. Although cobalt and chromium are major components of these casting alloys and constitute more than 90% of their mass, other components such as molybdenum, carbon, manganese, iron, silicon, beryllium, tungsten, boron and titanium have a great influence on the mechanical and physical properties of these alloys [3].

2. Mechanical Properties of Dental Alloys

The dental product market has developed very much in the last years and the studies on features evaluation are many also. The technicians are busy with the importance of the clinical tests before using the materials. Mechanical properties are therefore important in understanding and predicting a material's behavior under load. Knowing mechanical properties is essential for some dental works achievement to be performant for a long time [6]. In oral cavity, the restorations are submissive to the forces that born in the mastication process.

These forces act on the teeth/the materials producing a different reactions, that can lead to their distortion, which causes the reduction of the durability in time [3], [6]. The information regarding the base properties are available through national and international standards, from manuals and specialized journals of some types. The forces that have to submit most of the restoration materials appear during fabrication process or in mastication process. Therefore, mechanical properties are very important for understanding and anticipate the behavior on material request. Because the real quality measure is not given by one mechanical property, the introduction and knowing the principles involved in different behaviors of the tested materials in some conditions is very important [3], [6]. Dental materials are under the influence of two types of forces, some who are bound to the structure, and some that are related to the request on biomaterial [7]. The requests on the biomaterial results from the combining these internal and external forces, requests that can be simple through axial force application, through traction force, compression force, friction forces with cutting effect. Depending on these forces, there are many tests that are submitted the dental material samples. Depending on the loading features and the applied force, the materials can react in a different way. The exterior force applied can lead to the modified structure and initial dimensions. The rate between these is defined strain. This rate is important for determination of the mechanical properties. For each material there is a stress-strain curve – Fig. 2.

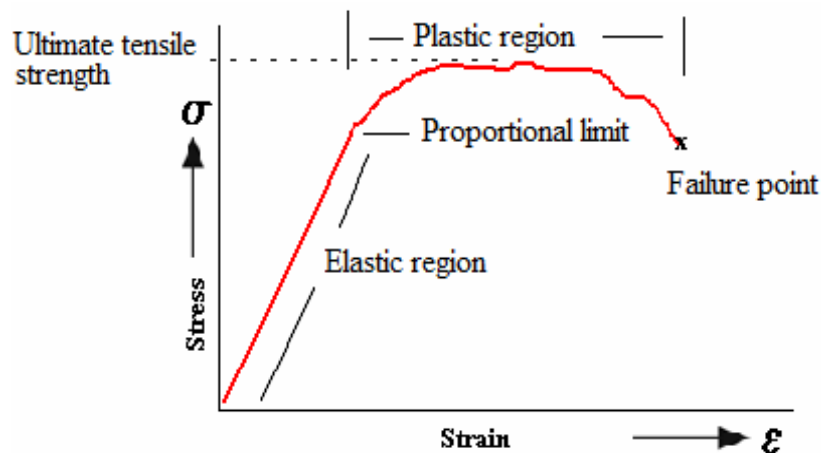


Fig. 2 – Stress-strain curve.

If under forces action the body does not modify his dimensions, the material elasticity is demonstrated (elastic region); the value that tension needs to produce permanent distortions in material represents the

proportionality limit; after this limit takes place the plastic distortion of the material (plastic region); material elasticity is been calculated through tension and distortion ratio and represents the elasticity modulus or Young's modulus; each material presents a resistance to deformation, but if the applied force goes after ultimate strength, the breaking will happen. All these concepts are applied in clinic situations [3], [6]. The elasticity modulus values, yield strength, tensile strength and elongation are given in Table 1.

The elasticity modulus - a material elasticity degree is appreciated through elasticity modulus or Young's modulus. This is a relatively material stiffness size. The higher the elastic modulus, the more rigid a structure can be expected, provided the dimensions of the casting are the same in both instances. With a greater elastic modulus, one can design the restoration with slightly reduced dimensions. The elasticity modulus value for the basis cobalt alloys it is twice then gold type IV, as it is seen in Table 1.

Yield strength – indicates the moment when it is going to be made a permanent deformation of a work or some parts of it, being one of the most important properties of the alloys destined removable partial denture. From the table it can be seen that the values for yield strength specific for the cobalt basis alloys, are up to 650 MPa and comparative with other dental alloys, are superior (with exception of the Cr-Ni alloy).

Tensile strength – this property it is used in dentistry to indicate dimension or transversal section necessary for a specific restoration. It is important to note that the alloy that was required till almost extreme value will remain deformed permanent and if the work will receive a supplementary request during use time, will became non-functional. From the table is seen that tensile strength of cobalt basis alloys has values higher than 800 MPa.

Elongation - alloy percent elongation it is important as an indicator of relative brittleness or ductility a restoration will exhibit. Therefore, elongation is an important property for comparison of alloys for removable partial-denture appliances. Because of their toughness, partial denture clasps cast of alloys with a high elongation and tensile strength do not fracture in service as often as do those with low elongation

Dental material surface properties represent a determinant factor in cases when these are placed in mouth cavity. These ones give information about scratches appearance and exterior loads application. Surface hardness is a parameter frequently used to evaluate material surface resistance to plastic deformation by penetration. Knowing materials hardness values in dentistry use is very important because on mouth cavity level are developed forces that demands dental work mechanical. These can lead to dental work deformation and even their breaking. That is why the hardness tests have an extreme important application in dentistry.

Table 1
Mechanical Properties of Dental Alloys [2], [3], [7], [9]

Alloys	Elastic modulus GPa	Yield strength MPa	Tensile strength MPa	Elongation %
Co-Cr alloys	210	300-650	870-900	1.5-4
Type IV gold alloys	100	480-510	480-510	6-10
Cr-Ni alloys	190	690	690-800	2-4
Ti	117	170-480	240-550	18-31

There are four standard methods of hardness testing: Brinell, Vickers, Knoop and Rockwell. Brinell method consists in force indenting of a steel ball penetrator with settled diameter, perpendicular on analyzed sample surface. The resulting hardness value, known as the Brinell hardness number (BHN), is computed as a ratio of the load applied to the area of the indentation produced. The Vickers hardness test, or 136-degree diamond pyramid, is also suitable for testing the surface hardness of materials. The indenter diagonals length is used in determination of trade size left by this one in material. Knoop test uses a load is applied to a carefully prepared diamond indenting tool with a pyramid shape, and the lengths of the diagonals of the resulting indentation in the material are measured. The Knoop hardness number (KHN) is the ratio of the load applied to the area of the indentation calculated from the following:

$$\text{KHN} = \frac{L}{l^2 \cdot C_p}$$

where L is the load applied, l is the length of the long diagonal of the indentation and Cp constant relating l to the projected area of the indentation.

Rockwell test consists in indentation of the studied material surface with a diamond or steel ball. The main advantage of this hardness test method is its achieving time, which is 10 or 15 seconds until obtaining the results that are read on quadrant. In this case it is measured the trade depth with a sensitive comparator micrometer. In Table 2 are presented Brinell Vickers and Knoop harnesses for the three non-precious alloys and one gold alloy. It is observed that specific values of the Co-Cr alloy have superior values to the Au alloy.

Table 2
Dental alloys Hardness [2], [3], [7], [8], [9]

Alloys	Hardness, (Kg/mm ²)		
	Brinell	Vickers	Knoop
Co-Cr	180-350	200-460	350-400
Type IV gold alloys	120	160-220	-
Ni-Cr	230	200-360	314
Ti	200	210	-

Other important mechanical properties of dental alloys are wear resistance, fatigue resistant, resilience, bending, breaking force, fracture force [3], [6], [7], [10], [11]. Therefore, the mechanical properties of dental materials must be known so they can understand their behavior and for superior quality work achievement. With mechanical properties, a major importance presents chemical properties. Hereby, corrosion resistance is a property on which is taken the achievement decision for dental restoration (with biocompatibility, mechanical properties and cost) from certain type of material. Because dental alloys are placed in mouth of the patients for a long term and in mouth cavity is present a favorable environment for corrosion appearance (humidity and heat) most metals present a tendency to corrode. Due to this phenomenon, a large quantity ions will be released in mouth cavity, ions that will lead to biological reactions appearance such as: gingival inflammation, allergies, inflammatory processes or poisoning [1], [12].

3. Conclusion

In present there are on world market a large variety of products made from noble alloys or non-precious, which are capable to satisfy the same requests of a dental alloy. Mechanical, physical and chemical properties of dental materials present a special importance in devices design and new materials assembly. Therefore, mechanical properties mention creates the specific framework for entire dental material study beginning, which, without these data knowledge it could just prevent or to influence in a negative way the expected results. These properties have to be known before any medical application, but these also have to be known compared with the changes that can occur in time in the human body.

Received: February 17, 2010

"Gheorghe Asachi" Technical University of Iași,
Department of Materials Engineering and Industrial Safety
e-mail: monica.lohan@yahoo.com

*Faculty of Mechanics
e-mail: ionutbistricianu@yahoo.com

REFERENCES

1. Rincic N., Celebic A., Baucic I., Stipetic J., Prohic E., Miko S., *The Release of Ions from the Base Co-Cr-Mo Casting Alloy in Vitro Into the Phosphate Buffer at pH 6.0*. Acta Stomat Croat, 13-16 (2003).
2. J. O'Brien W., *Dental Materials and Their Selection* - 3rd Ed. (2002). Quintessence Publishing Co, Inc, ISBN 0-86715-406-3, (2002)
- 3.. Craig R.G, Powers M.J., *Restorative Dental Materials*. Eleventh Edition (2002) by Mosby-Year Book
4. Hryniewicz T., Rokicki R., Rokosz K., *Co-Cr Alloy Corrosion Behaviour After Electropolishing and "Magneto-electropolishing" Treatments*. Science Direct, Materials Letters 62, 3073–3076, (2008).
5. Chiba A., Kumagai K., Nomura N., Miyakawa S., *Pin-on-disk Wear Behavior in a Like-on-Like Configuration in a Biological Environment of High Carbon Cast and low Carbon Forged Co-29Cr-6Mo Alloys*. Acta Materialia 55, 1309–1318 (2007).
6. Wang L., D'Alpino P.H.P., Lopes L.G., Pereira J.C., *Mechanical Properties of Dental Restorative Materials: Relative Contribution of Laboratory Tests*. J. Appl Oral Sci, 11(3): 162-167 (2003).
7. Stelea O., Panaite S., Morariu C., *Metalurgie stomatologică și biomateriale*. Edit. Apollonia, Iași, 2000.
8. Niinomi M., *Mechanical Biocompatibilities of Titanium Alloys for Biomedical Applications*. J. of the Mechanical Behavior of Biomedical Materials, 1, 30–42 (2008).
9. Toru Okabe, Chikahiro Ohkubo, Ikuya Watanabe, Osamu Okuno, Yukyo Takada, *The Present Status of Dental Titanium Casting*. JOM, J. of the Minerals, Metals and Materials Society. 50, 9, September 1998, 24-29.
10. Suthiwarapirak A., Suprichakorn S., Takahashi H., Arksornnukit M., *Wear Resistance of Titanium and Co-Cr Alloys Opposing Enamel*. The IADR/AADR/CADR 83rd General Session, March 9-12, 2005.
11. Zupan Rok, Legat Andra, Funduk Nenad, *Electrochemical and Mechanical Properties of Cobalt-Chromium Dental Alloy Joints*. Materials and technology 41 (2007) 6, 295–300.
12. Gottfried Schmalz, Dorthe Arenholt Bindslev, *Biocomparitbility of Dental Materials*. Publisher – Springer, 2009.

ASUPRA PROPRIETATILOR MECANICE A ALIAJELOR
DENTARE NENOBILE Co-Cr

(Rezumat)

În prezent, pe piața mondială, o mare varietate de aliaje dentare sunt disponibile, iar o selecție corectă a acestora este o sarcină dificilă. Proprietățile mecanice ale materialelor dentare reprezintă un criteriu de alegere a acestora, cu toate că aceste proprietăți nu reprezintă neapărat performanțele lor clinice. În general, aliajele

dentare sunt plasate în gura pacientului pentru o lungă perioadă de timp și acestea trebuie să reziste atât solicitărilor mecanice cât și acțiunii corozive. De aceea o mare importanță se acordă cunoașterii proprietăților mecanice și fizice ale acestora deoarece la alegerea un material pentru fabricarea unei lucrări protetice se ține cont și de aceste proprietăți, alături de bicompatibilitate și cost. Lucrarea reprezintă o sinteză a referințelor celor mai importante lucrări publicate și prezentarea unor proprietăți mecanice a unor aliajelor nenobile dentare, în comparație cu cele ale unui aliaj pe bază de aur.

BULETINUL INSTITUTULUI POLITEHNIC DIN IAȘI

Publicat de

Universitatea Tehnică „Gheorghe Asachi” din Iași

Tomul LVI (LX), Fasc. 1, 2010

Secția

ȘTIINȚA ȘI INGINERIA MATERIALELOR

THICKNESS ANNALISIS OF TUNGSTEN COATING LAYER DEPOSITED BY ELECTRODE VIBRATOR METHOD

BY

**MANUELA CRISTINA PERJU, CARMEN NEJNERU, DAN-GELU GĂLUȘCĂ,
PETRICĂ VIZUREANU and TUDOR RĂILEANU**

Abstract. The paper is to achieve some metallic materials with superior functional performances. The obtained layer by vibrator electrode coating method must have a high adherence to the surface of the part and a high chemical and thermal compatibility with the sublayer, and a high fatigue and oxidation proprieties as well. So in the paper have been studied: tungsten layer thickness coated on ferito-perlitic cast iron sublayer, layer roughness and crack analysis. Pictures were made with electronic-scanning microscope.

Key words: electric spark alloying, layer thickness, crack, roughness, electronic scanning microscope.

1. Introduction

In present, part achievement assumes new materials utilization, created by artificial methods, with high hardness, high corrosion resistance, refractory, wear resistance etc. In making new products, geometric shape is more and more complex and meets difficulties fabricating them applying classic processing technologies, implicating tools through witch effect energy is applied in the processing area by direct contact of the tool with the material.

Direct contact tool-material causes some effects, that modifies the initial proprieties of the material (double way diffusion, strain hardness, plastic and elastic distortion, wear, etc.)

Material coating is one of the most important method for improving mechanical proprieties of metallic parts. For example wear resistance of some soft metals can be substantially increased by some treatments that can raise the

level of metallic surface hardness to be comparable to that of refractory materials.

For material coating there are some methods including electric spark coating method, that recently won an increase interest as a promising technique for material surface engineering, thanks to its simplicity, efficiency and low cost of production. Electric spark coating is a surface process that is actually a micro welding with pulsating discharge.

Now electrode coating method is used for component coating in aerospace industry and nuclear components processing.

The goal of this work is studying ferrite-perlitic cast-iron surface hardening that can be used with benefic effect on water desalination pumps, working in a high wear is to lengthen their life. One of the metal coating methods is the vibrator electrode.

2. Methodology

Electric sparking manufacturing process of materials is based on electroerosion phenomenon and anode material (electrode) polar transfer to cathode (metallic part) during electrical discharge into impulses between anode and cathode, discharge that takes place in a gaseous environment. Unlike classical processing by electroerosion, in electro sparking, a pulsing recovered current with inversed polarity is used. In this case, electro sparking processing method environment is air, the electrode performing a vibrating movement.

The essence of the process lies in that, in case of electrical spark discharge, in a gaseous environment, especially a electrode material (anode) erosion is produced, and a erosion products transfer takes place on the superficial processed part (cathode). The surface manufacturing process starts with approaching the electrode to the part, and at perforation critical distance, the impulse electrical discharge is triggered, that in most cases is continuous and just finishes at electrodes contact.

Following the material transfer and thermal changes in the discharge area, in the metallic material superficial discharge process by electric spark the cathode superficial layer modifies the structure and chemical composition.

The characteristics of this layer can variate between large limits depending of electrode material, of environment composition between the electrodes, impulse discharge parameters and other layer forming conditions on the cathode.

3. Discussions and Results

The paper proposed, in this context, has the following goals:

a) Tungsten coating layer thickness analysis, obtained by two layer deposition;

- b) Inside crack analysis of the coating layer;
- c) Layer surface roughness testing;

For this experiment ferito-perlitic gray cast iron was used, in witch chemical composition is presented in Table 1, composition witch was obtained with Foundry Master Spectrometer.

Table 1
Basic Material Chemical Composition, %

C	Si	Mn	P	S	Cr	Ni	Cu	Mo
3.97	2.87	0.25	0.06	0.07	0.28	0.126	0.17	0.03

The tests were made with Elitron 22 machine and wolfram was used as addition material. Pictures that show the ferito-perlitic cast-iron microstructure (Fig.1) were made with an optical microscope.

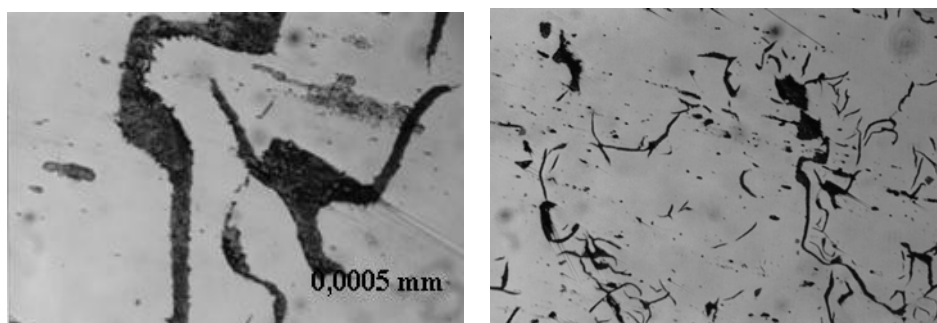


Fig. 1 – Basic material microstructure.

Using the electronic scanning microscope elements distribution were marked and we can see a good and uniform tungsten repartition both surface and in depth.

The coating layer has a uniform thickness, between 30,25÷60,41 μm . From layer thickness picture we can see tungsten layer quality. Even at double coating, the tungsten electrode creates material evulsions (gaps) and adherence areas, when unemelted materials adhere to the part surface creating micro bumps.

The double coated tungsten layer has a good coherence with ferito-perlitic matrix, but with pronounced cracks.

EDX analysis shows tungsten atoms presence in the exterior layer, with the depth lower than 30 μm , the layer showing some areas with adherences and cracks caused by the carbon lamellas from the part surface.

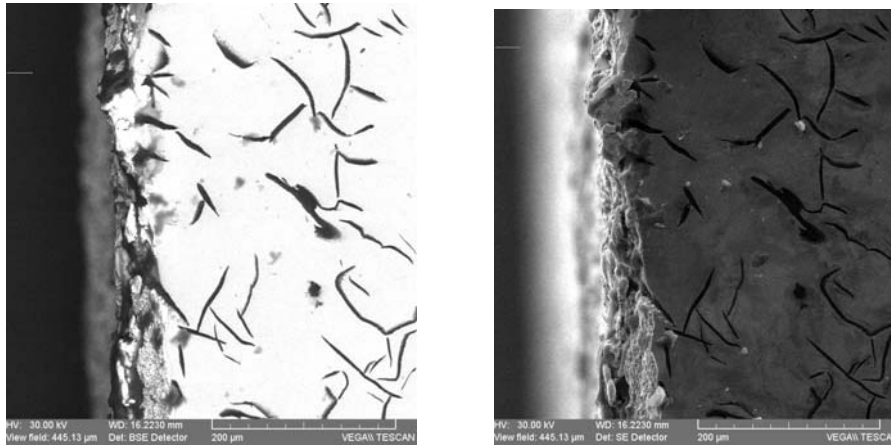


Fig. 2 –Two layers wolfram thickness coating.

Material extraction, cracks, layer unlevelness, and oxides presences represents coating characteristics with wolfram electrode.

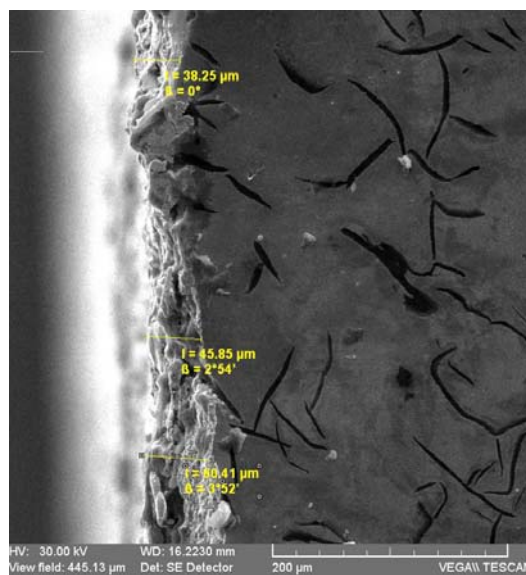


Fig. 3 – Layer thickness index.

Crack analysis is presented in the picture 4.

Improperly named coating because wolfram accidentally is involved in exterior layer hardening. This is achieved by exterior layer melting and fast solidifying witch leads to a cementite area forming (white cast-iron structure).

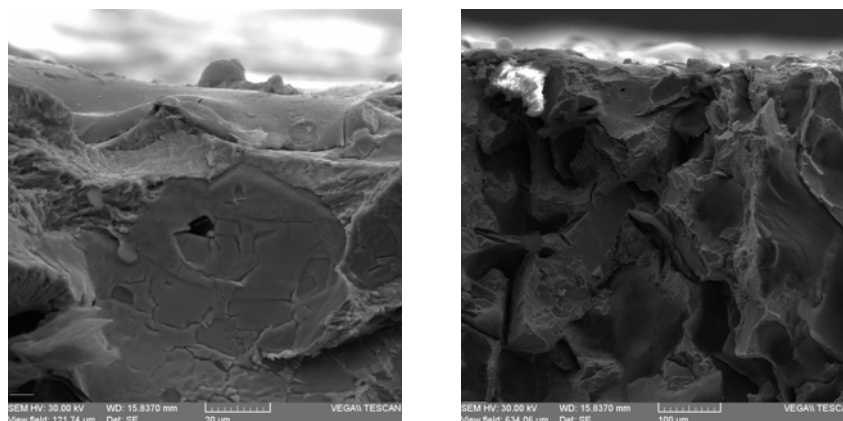


Fig. 4 - Double layer tungsten coating crack areas.

The measurements are done with a Surtronic 3+ roughness meter, and results interpretation was made with Talyprof program. This program is processing the experimental data, achieving indications from medium roughness and also measured profile data.

Table 2
Roughness Proportions

Coating layer	R_a [μm]
Basic material	0.400
W two layers	7.31

A complete roughness measurements file for wolfram double coating is presented in picture 5. Tungsten electrode for double layer coating, achieves a high roughness, with 7.31 μm . Tungsten coating electrode has high roughness, thing that can be explained by supplementary uprooting achieved by wolfram electrode that is difficult to work with, obtaining a more oxide surface and strong material uprooting.

4. Conclusion

1) Ferito-perlitic cast-iron hardening, with tungsten electrode, using electrode vibrator method, is done, mainly, because of a hard white cast-iron layer is formed. This layer is specific to superficial quenching.

2) Hardened layer thickness, obtained by tungsten coating, two layers, has a thickness between 38 μm and 60 μm .

3) Inside the crack we see that the hardened layer has a good coherence with the basic matrix. This leads to exfoliation absence. Part roughness is very big, because of material extractions caused by tungsten coating.

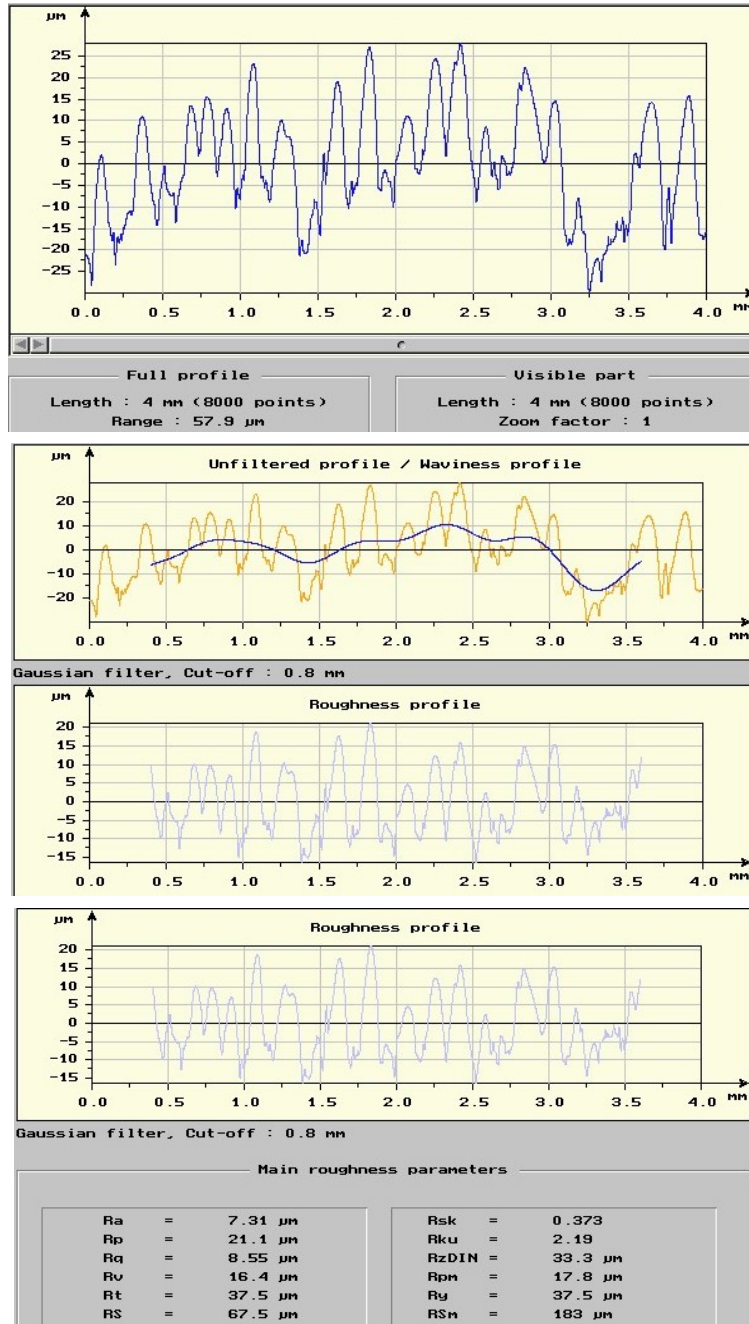


Fig. 5 – Roughness measurements for wolfram double coating.

Received: February 18, 2008

“Gheorghe Asachi” Technical University of Iași,
e-mail: (cryss_ela@yahoo.com)

REFERENCES

1. Alexandru A., *Contributii privind alierea si depunerea superficiala prin scanteiere electrica si influenta tratamentelor termice asupra caracteristicilor straturilor obtinute ale materialelor metalice*. Ph. D. Diss., Iași, 2002
2. Perju M.C., Gălușcă D.G., Nejneru C., Sandu A.V., Carabet R.G., *Determinarea caracteristicilor mecanice ale straturilor prin depunere, pe suport de fonta, cu electrozi de TiC si W, prin metoda electrodului vibrator*. Simpozionul national al tinerilor cercetatori in domeniul ingineriei materialelor, Bucuresti, 2008.
3. Perju M., Nejneru C., Răileanu T., Axinte M., Hopulele I., *Researches Concerning the Hardening of the Grey Cast iron Through the Vibrating Electrode Method Using a WC Electrode and in Combination with TiC and Ti Electrode*. The Annals of "Dunarea de Jos" Univ. of Galati, **IX**, 1, Metallurgy and Materials Science, 2008.
4. Vermesan G., Vermesan E., Jichisan-Matiesan D., Cretu A., Negrea G., Vermesan H., Vlad M., *Introducere în ingineria suprafețelor*. Edit. Dacia, 1999.

ANALIZA GROSIMII STRATULUI DE WOLFRAM DEPUS PRIN METODA ELECTRODULUI VIBRATOR

(Rezumat)

Lucrarea are în vedere realizarea unor materiale metalice cu performanțe funcționale superioare. Stratul obținut prin metoda electrodului vibrator trebuie să aibă o foarte bună aderență la suprafața piesei și o mare compatibilitate chimică și termică cu substratul, precum și calități ridicate de rezistență la uzare și oxidare. Astfel, în lucrare au fost studiate: grosimea stratului depus cu electrod de wolfram pe substrat de fontă ferito-perlitică, analiza în casură și rugozitatea stratului. Fotografiele au fost obținute cu ajutorul microscopului cu scanare electronică.

BULETINUL INSTITUTULUI POLITEHNIC DIN IAȘI

Publicat de

Universitatea Tehnică „Gheorghe Asachi” din Iași

Tomul LVI (LX), Fasc. 1, 2010

Secția

ȘTIINȚA ȘI INGINERIA MATERIALELOR

RESEARCHES CONCERNING THE COOLING CHARACTERISTICS OF THE POWDER BACKING IN FLUIDIZED BED TIP SAND, SALT AND SHAVINGS CAST IRON BARBOTAGED WITH AIR

BY

**IRINA SURDU*, CARMEN NEJNERU*, ROXANA CARABET*,
DAN GELU GĂLUȘCĂ* and MARCEL AGOP****

Abstract. The paper presents the researches on the cooling thermal transfer in fluidized beds.

There were used for the experiments sand, salt and shavings cast iron particles. The cooling curves were drawn with a silver control cylinder within a cromel-alumel thermocouple connected to an y-t recording apparatus. By studying the variation graphics of the cooling curves it can be noticed that sand has the biggest cooling velocity and salt has the smallest. The others are between the two curves with closer medium values.

Key words: fluidized bed, cooling velocity, cooling curve, heat transfer, sand particle.

1. Introduction

The fluidized bed is a heterogeneous, non-adiabatic system where the solid particles are executing a continuous motion on the enclosure, under the influence of a turbulent beat of pulses of a fluid stream.

The fluid strains among the particle layer without moving them at small speed. As long as the loss of pressure is smaller than the weight of the layer, reported to the fluidization surface, the layer remains fixed.

At a certain speed the individual particles get a liberty degree which allows an easy vibration of the particles round about the primary position. In this condition the particles mass behaves like a viscous liquid, the solid and the fluidization agent forming one phase (the dense phase).

The agent velocity which is completing this condition is called the minimum fluidization velocity (v_{im}) when appears the homogenous fluidization. Homogenous fluidization is characterized by uniform distribution of the particles and an uniform expansion of the layer, the distance between the particles increasing together with agent velocity.

Increasing continuously the speed of the fluid ($v > v_{im}$) turns out that the layer explodes a lot and the movement of the particles became violent and chaotic.

A part of the fluid goes through the layer like some irregular bubbles which are breaking at the fluidized medium surface, throwing up a jet of particles, the whole layer looking like boiling water. This is the non homogenous fluidization which is interested in applications with a view to heating in thermo-chemical and heat treatment.

During fluidization can appear secondary phenomena which produce the perturbation of the fluidized bed, specific to the non-homogenous fluidization such as: insistence and canalization.

The nature, size and form of the solid particles belonging to the fluidized bed influence directly the structure and the characteristics of yield of fluidized bed.

The size of the particles is one of the most important parameters of the fluidization, both hydrodynamic and heat and mass change. For the achievement of an optimum fluidization it is necessary that the field scattering of the particles size must be as limited as it can.

If the fluidized bed is composed of particles whose size has a field scattering wide, the fluidization velocity grows so that it can lead to the appearance of the small particles entrainment phenomena.

The size of the particles influences directly the velocity of the fluidization (specially the minimum fluidization speed) which grows proportionally with d_p^2 , and also influences the pressure loss and specific weight of the layer.

It has been experimentally determined that optimum density of the particles material is between 1280 – 1600 kg/m³. Dense materials produce low coefficients of heat transfer and need a bigger velocity of fluidization gas.

In fluidization are used materials such as: sand, corundum, graphite, aluminum oxide and other particles which are physical and chemical stable at the work temperature. The volume weight of the particles determines the specific weight of the fluidized bed and influences the minimum fluidization velocity and also the loss pressure in the layer.

2. Objectives

The fluidized beds can be used in heat and thermo-chemical treatments as active mediums, as heating mediums, soaking steps, and also as cooling mediums.

The cooling velocity is an important parameter of the heat and thermo-chemical treatments.

The paperwork is presenting an experimental study concerning the cooling capacity of the fluidized bed using different solid backing and as fluidization agent: air.

Advantages comparing to salt baths:

- a) it is favorable for an uniform cooling but slow, being used lesser in hardening and more in annealing.
- b) it is non-toxic comparing to salt baths.
- c) it is easy to handle and to get, and there are needed simple installations easy to be upkeep.
- d) it do not consume and damage like salt baths (it must always be added substances in order to be built-up the percentage).
- e) it is cheaper than the salt baths, and easier to be maintained constant as properties.

As a disadvantage is the fact that they cannot be used for pieces bigger than 100 mm, the fluidization could be badly bred, the specific convection of the fluidized bed being clogged.

Conclusion:

- the most important advantage is that in certain circumstances they can replace the salt baths.

It was experimentally analyzed the factors which influence thermic transfer in fluidized bed.

3. Results

In order to determine the cooling medium like fluidized bed, it was used a control cylinder from silver within a chromel-alumel thermocouple which permits temperature measurement with a recording apparatus y-t. The control cylinder is heated up to the desired temperature (800°C) and cooled down in the fluidized bed.

The silver test bar has the following sizes and characteristics:

$$\varnothing = 13 \text{ [mm]}, h = 28 \text{ [mm]}, S = 1408 \text{ [mm}^2\text{]}, m = 39.9 \text{ [g]}, \rho_{Ag} = 10.5 \text{ g/cm}^3$$

$$\lambda_{Ag} = 418.5 \text{ W/m}\cdot\text{K}$$

The equipment used in experimental determination of the cooling curves is formed from:

- air fluidization system;
- heating system of the silver test bar (circular pipestill with electrical resistance);
- measurement system represented by an y-t recording apparatus (with modification apparatus of the shifting rate of the recording apparatus);
- Transformer of the filling variation of the ventilator for modification

the air velocity.

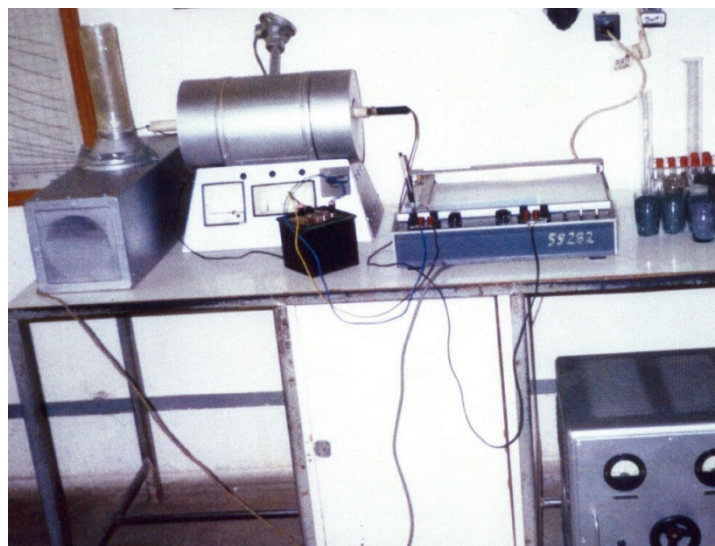


Fig. 1 – Equipment for the determination of fluidized beds cooling characteristics.

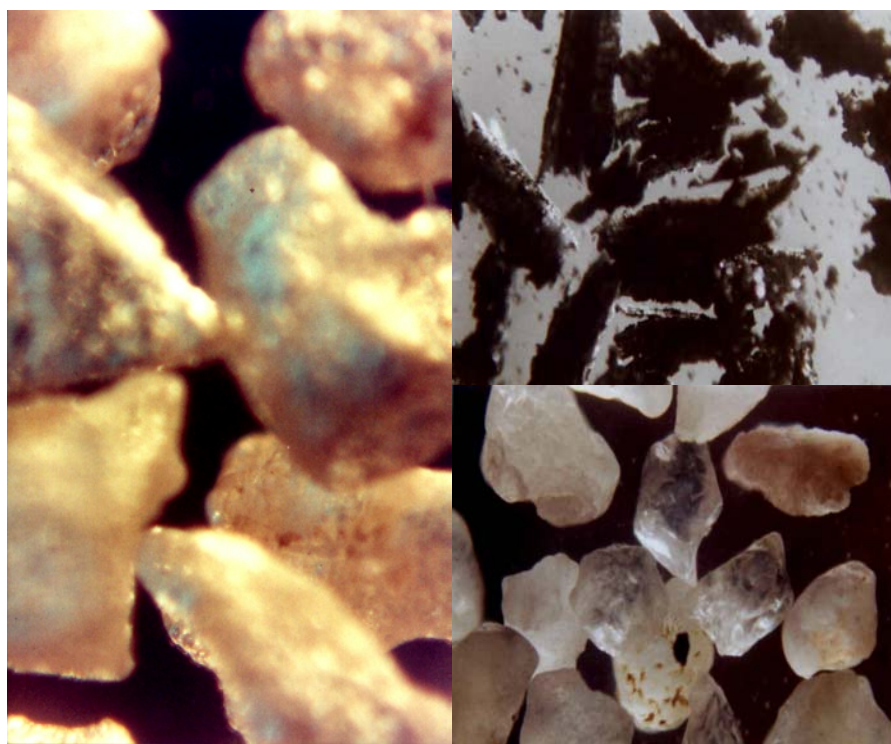


Fig. 2 – *a* – salt particles, *b* – shavings cast iron, *c* – sand particles 1400 - 3000 μm .

The dusty environments mentioned before were fluidized with air.

The silver test bar was conducted in a circular pipestill until 800°C and then was introduced in the fluidized bed, the cooling curve being recorded by the y-t recording apparatus.

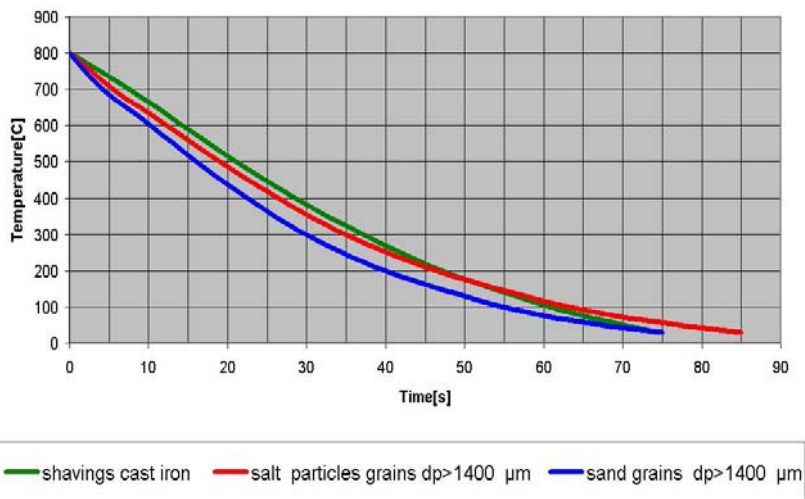
For each cooling environment was calculated.

All the studied environments are for annealing (they cannot be used for hardening because of the small cooling velocities)

The Cooling Curves for Salt Particles Grains $d_p > 1400 \mu\text{m}$, Shavings Cast Iron and Sand Grains $d_p > 1400 \mu\text{m}$

$T[^\circ\text{C}]$	shavings cast iron	salt particles grains $d_p > 1400 \mu\text{m}$	sand grains $d_p > 1400 \mu\text{m}$
800	0	0	0
700	7,5	5,5	4,2
600	14,2	12,25	10,2
500	21	19	16
400	28,7	26,5	22,6
300	37,2	35	30
200	47,2	46,5	40
100	61	63,25	55
50	70	77	67,2
30	74,5	85	75

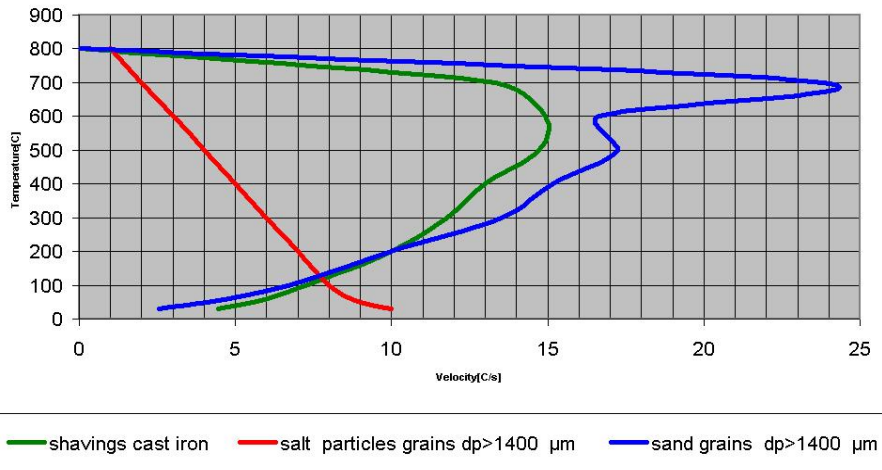
The cooling curves for salt particles grains $d_p > 1400 \mu\text{m}$, shavings cast iron and sand grains $d_p > 1400 \mu\text{m}$



*Velocities Variation Cooling for Salt Particles Grains $D_p > 1400 \mu\text{m}$,
Shavings Cast Iron And Sand Grains $D_p > 1400 \mu\text{m}$*

$T [^{\circ}\text{C}]$	shavings cast iron	salt particles grains $d_p > 1400 \mu\text{m}$	sand grains $d_p > 1400 \mu\text{m}$
800	0	0	0
700	13,33	18,18	23,81
600	14,93	14,81	16,67
500	14,71	14,81	17,24
400	12,99	13,33	15,15
300	11,76	11,76	13,51
200	10	8,7	10
100	7,25	5,97	6,67
50	5,56	3,64	4,10
30	4,44	2,5	2,56

Velocities variation cooling for salt particles grains $d_p > 1400 \mu\text{m}$, shavings cast iron and sand grains $d_p > 1400 \mu\text{m}$



4. Conclusions

1. It can be noticed from graphics that sand, shavings cast iron a salt particles size influence the cooling velocity in fluidized bed.

2. As a first step, the salt, being a good insulator, absorbs the heat from the test bar and yields it when the cooling velocity gets slower.

3. The form and the irregularity of the sand sands and shavings cast iron has an important influence; the form of the sand grains are rounded and semi-elongation with amount of crown. shavings cast iron has a taper and elongated

4. The velocity fluctuations between 700-400 C appear because of the form and irregularity of the sand and shavings cast iron.

- due to the size of the particle (fluidization is very well made on larger size of the particle) it can be noticed an approaching of the cooling curves;

- it can also be noticed that sand has the biggest cooling velocity and salt has the smallest cooling velocity due to particulate forms. speed corresponding particles closer to the spherical shape.

Received: January 20, 2010

“Gheorghe Asachi” Technical University of Iași

* Faculty of Materials Science and Engineering

e-mail: dangalusca@yahoo.com

** Department of Physics

e-mail: m.agop@yahoo.com

REFERENCES

1. Samoila I.C., Ionescu M.S., Druga C., *Tehnologii si utilaje moderne de incalzire in metalurgie*. Edit. TehnicĂ, București, 1986.
2. Grace J.R., Chaouki J., Pugsley T., Fluidized Bed Reactor *Encyclopedia of Chemical Processing*, Published on 30 November 2005

CERCETĂRI PRIVIND CARACTERISTICILE DE RĂCIRE ÎN PAT FLUIDIZAT A MEDIILOR PULVERULENTE TIP NISIP, SARE ȘI ȘPAN DE FONTĂ BARBOTATE CU AER

(Rezumat)

Lucrarea prezintă cercetările experimentale asupra transferului termic la răcire în medii pulverulente (nisip de turnătorie, sare și span de fonta) barbotate cu aer.

Pentru experimente s-a folosit nisip și sare cu mărimea granulelor cuprinsă între $d_p \in (1400 \div 3000) \mu\text{m}$, unde d_p este diametrul mediu al particulei

Curbele de răcire au fost tratate cu ajutorul unei epruvete de argint cu termocuplu înglobat și conectat la un incriptor y-t.

Studiind graficele de variație ale curbelor de răcire se observă că viteza cea mai mare de răcire o are nisipul și cea mai mică sarea. Celelalte fiind cuprinse între cele două curbe cu valori intermediare foarte apropiate.

ON THE THERMAL TRANSFER IN NANOSTRUCTURES(III). CONVECTION TYPE BEHAVIOR

BY

IOANNIS ZERICHOTIS*, ANCA ALUCULESEI*, RAZVAN LITOIU*, DAN
GELU GALUSCA* and MARICEL AGOP**

Abstract. Using the fractal theory, the convective type behavior of the heat transfer in nanostructures is analyzed. In such context, the momentum law conservation, the mass law conservation and the equation of heat transfer are obtained. The numerical solutions for these equations law imply a Lorenz type ‘‘medianism’’.

Key words: nanostructures, convective behaviour, heat transfer

1. Introduction

Recent papers [1], [2] shows that the fractal structure of space –time implies the presence of the fractal operator

$$(1) \quad \frac{\hat{d}}{dt} = \frac{\partial}{\partial t} + \vec{v} \cdot \nabla \pm \frac{\lambda^2}{2\tau} \left(\frac{dt}{\tau} \right)^{\left(\frac{2}{D_f} \right) - 1} \Delta$$

Using this operator in the present paper same transport equations are obtained.

2. The Transport Equations

The inertial principle in its strong covariance from (Nottale’s principle[3]) is reduced to an equation of the Navier-Stokes type

$$(2) \quad \frac{\hat{d}\vec{v}}{dt} = \frac{\partial\vec{v}}{\partial t} + \hat{v} \cdot \nabla\vec{v} = \frac{\partial\vec{v}}{\partial t} + \vec{v} \cdot \nabla\vec{v} - i \frac{\lambda^2}{2\tau} \left(\frac{dt}{\tau} \right)^{\left(\frac{2}{D_F} \right) - 1} \Delta\vec{v} = 0$$

With a imaginary viscosity coefficient ν

$$(3) \quad \nu = i \frac{\lambda^2}{2\tau} \left(\frac{dt}{\tau} \right)^{\left(\frac{2}{D_F} \right) - 1}$$

The measure λ is the leight scale, dt is the temporal resolution and τ the temporal scale.

This means that local complex acceleration field $\partial v/\partial t$ the convective term, $v \cdot \nabla v$, and the dissipative one, ∇v , reciprocally compensate in any point of the fractal curve. Moreocover, the behaviour of the fractal fluid is visco-elastic type.

Such results are in agreement with the opinions given in [3], [4]: the fractal fluid can be described by Kelvin-Voight or Maxwell rheological model with imaginary structure coefficient ν .

Two types of motion are distinguished:

i) Rotational motions

Replacing the complex speed field $v=V-iu$ in geodesies equation (2) and separating the real and the imaginary parts we obtain:

$$(4a, b) \quad \begin{aligned} \frac{\partial\vec{V}}{\partial t} + \vec{v} \cdot \nabla\vec{V} - \vec{U} \cdot \nabla\vec{U} - \frac{\lambda^2}{2\tau} \left(\frac{dt}{\tau} \right)^{\left(\frac{2}{D_F} \right) - 1} \Delta\vec{U} &= 0 \\ \frac{\partial\vec{U}}{\partial t} + \vec{U} \cdot \nabla\vec{V} - \vec{V} \cdot \nabla\vec{U} \pm \frac{\lambda^2}{2\tau} \left(\frac{dt}{\tau} \right)^{\left(\frac{2}{D_F} \right) - 1} \Delta\vec{V} &= 0 \end{aligned}$$

Using the operatorial relations:

$$(5 a,c) \quad \begin{aligned} \nabla(\vec{V} \cdot \vec{U}) &= (\vec{V} \cdot \nabla)\vec{U} + (\vec{U} \cdot \nabla)\vec{V} + \vec{V} \times (\nabla \times \vec{U}) + \vec{U} \times (\nabla \times \vec{V}) \\ \nabla\vec{V}^2 &= 2(\vec{V} \cdot \nabla)\vec{V} + 2\vec{V} \times (\nabla \times \vec{V}) \\ \nabla\vec{U}^2 &= 2(\vec{U} \cdot \nabla)\vec{U} + 2\vec{U} \times (\nabla \times \vec{U}) \end{aligned}$$

Eqs. (4 a,b) become:

$$(6a, b) \quad \begin{aligned} \frac{\partial \bar{U}}{\partial t} + \nabla(\bar{V} \cdot \bar{U}) - \bar{V} \times (\nabla \times \bar{U}) - \bar{U} \times (\nabla \times \bar{V}) + \frac{\lambda^2}{2\tau} \left(\frac{dt}{\tau} \right)^{\left(\frac{2}{D_f}\right)^{-1}} \Delta \bar{V} &= 0 \\ \frac{\partial \bar{V}}{\partial t} + \nabla \left(\frac{\bar{V}^2}{2} - \frac{\bar{U}^2}{2} \right) - \bar{V} \times (\nabla \times \bar{V}) + \bar{U} \times (\nabla \times \bar{U}) - \frac{\lambda^2}{2\tau} \left(\frac{dt}{\tau} \right)^{\left(\frac{2}{D_f}\right)^{-1}} \Delta \bar{U} &= 0 \end{aligned}$$

and moreover, introducing "the vortices"

$$(7 a,b) \quad \bar{\Omega}_v = \frac{1}{2}(\nabla \times \bar{V}), \quad \bar{\Omega}_U = \frac{1}{2}(\nabla \times \bar{U},)$$

$$(8 a,b) \quad \begin{aligned} \frac{\partial \bar{V}}{\partial t} + \nabla \left(\frac{\bar{V}^2}{2} - \frac{\bar{U}^2}{2} \right) - 2\bar{V} \times \bar{\Omega}_v + 2\bar{U} \times \bar{\Omega}_U - \frac{\lambda^2}{2\tau} \left(\frac{dt}{\tau} \right)^{\left(\frac{2}{D_f}\right)^{-1}} \Delta \bar{U} &= 0 \\ \frac{\partial \bar{U}}{\partial t} + \nabla(\bar{V} \cdot \bar{U}) - 2\bar{V} \times \bar{\Omega}_U - 2\bar{U} \times \bar{\Omega}_v + \frac{\lambda^2}{2\tau} \left(\frac{dt}{\tau} \right)^{\left(\frac{2}{D_f}\right)^{-1}} \Delta \bar{V} &= 0 \end{aligned}$$

Relations (8a,b) characterize the transport of the specific momentum both at the differentiable scale(8a) and the fractal scale (8b). It is conditioned by the inertial effects,

$$\left(\nabla \bar{V}^2, \nabla \bar{U}^2 \right), \quad \left(\nabla(\bar{V} \cdot \bar{U}) \right) \quad \text{rotational effects}$$

$$\left(\bar{V} \times \bar{\Omega}_v, \quad \bar{U} \times \bar{\Omega}_U \right), \quad \left(\bar{V} \times \bar{\Omega}_U, \quad \bar{U} \times \bar{\Omega}_v \right) \text{ and dissipative effects } ((\Delta V, \Delta U));$$

Irrotational motions.

In this case

$$(9) \quad \nabla \times \bar{v} = 0$$

so that the speed field can be expressed through the gradient of a scalar function Φ ,

$$(10) \quad \bar{v} = \nabla \varphi$$

named the scalar potential of the complex speed field,

$$\varphi = \text{Re } \varphi + i \text{Im } \varphi$$

Substituting Eq. (10) in Eq. (2) and using the operatorial relationship

$$(11a,b) \quad \frac{\partial}{\partial t} \nabla = \nabla \frac{\partial}{\partial t}$$

It results

$$(11c) \quad \nabla \cdot \left[\frac{\partial \varphi}{\partial t} + \frac{1}{2} (\nabla \varphi)^2 - i \frac{\lambda^2}{2\tau} \left(\frac{dt}{\tau} \right)^{\left(\frac{2}{D_F} \right)^{-1}} \Delta \varphi \right] = 0$$

and by integration, a Bernoulli type equation

$$(12) \quad \frac{\Delta \psi}{\psi} = \Delta \ln \psi + (\nabla \ln \psi)^2$$

with $F(t)$ a function which depends only on time. Particularly, for Φ of the form

$$(13) \quad \varphi = -\frac{\lambda^2}{2\tau} \left(\frac{dt}{\tau} \right)^{\left(\frac{2}{D_F} \right)^{-1}} \ln \psi$$

where Ψ is a new complex scalar function, Eq. (12) with the operatorial identity

$$(14) \quad \frac{\Delta \psi}{\psi} = \Delta \ln \psi + (\nabla \ln \psi)^2$$

takes the form

$$(15) \quad \frac{\lambda^4}{4\tau^2} \left(\frac{dt}{\tau} \right)^{\left(\frac{4}{D_F} \right)^{-2}} \Delta \psi + i \frac{\lambda^2}{2\tau} \left(\frac{dt}{\tau} \right)^{\left(\frac{2}{D_F} \right)^{-1}} \frac{\partial \psi}{\partial t} + \frac{F(t)}{2} \psi = 0$$

From here, "Schrodinger" type geodesies result for $F(t) = 0$, *i.e.*

$$(16) \quad \frac{\lambda^4}{4\tau^2} \left(\frac{dt}{\tau} \right)^{\left(\frac{4}{D_F} \right)^{-2}} \Delta \psi + i \frac{\lambda^2}{2\tau} \left(\frac{dt}{\tau} \right)^{\left(\frac{2}{D_F} \right)^{-1}} \frac{\partial \psi}{\partial t} = 0$$

Particularly, for the movement on fractal curves of the Peano's type, *i. e.* in the fractal dimension $D_F = 2$, and Compton's length and temporal scales,

$$(17a,b) \quad \lambda = \frac{\hbar}{2m_0c}, \quad \tau = \frac{\hbar}{m_0c^2},$$

Eq. (16) takes the Schrodinger standard form

$$(18) \quad \frac{\hbar^2}{2m} \Delta \psi + i\hbar \frac{\partial \psi}{\partial t} = 0$$

where \hbar is reduced planck's constant.

Also, a fractal hydrodynamic model can be developed. Thus, by replacing the complex speed field (10) in eq. (2), and separating the real and imaginary parts we obtain

$$(19a, b) \quad \begin{aligned} \frac{\partial \bar{U}}{\partial t} + \nabla \cdot (\bar{V} \cdot \bar{U}) + \frac{\lambda^2}{2\tau} \left(\frac{dt}{\tau} \right)^{\left(\frac{2}{D_F}\right)-1} \nabla \bar{V} &= 0 \\ m_0 \frac{\partial \bar{V}}{\partial t} + m_0 \bar{V} \cdot \nabla \bar{V} &= -\nabla(Q) \end{aligned}$$

where Q is the fractal potential,

$$(20) \quad Q = -\frac{m_0 \bar{U}^2}{2} - m_0 \frac{\lambda^2}{2\tau} \left(\frac{dt}{\tau} \right)^{\left(\frac{2}{D_F}\right)-1} \nabla \cdot \bar{U}$$

The explicit form of the complex speed field is given by means the expression

$$(21) \quad \psi = \sqrt{\rho} e^{iS}$$

with ρ the amplitude and S the phase. Then Eq. (10) with

$$(22) \quad \varphi = -i \frac{\lambda^2}{2\tau} \left(\frac{dt}{\tau} \right)^{\left(\frac{2}{D_F}\right)-1} \ln(\sqrt{\rho} e^{iS})$$

involves the complex velocity field components

$$(23a, b) \quad \vec{V} = \frac{\lambda^2}{\tau} \left(\frac{dt}{\tau} \right)^{\left(\frac{2}{D_F} \right)^{-1}} \nabla S, \quad \vec{U} = \frac{\lambda^2}{2\tau} \left(\frac{dt}{\tau} \right)^{\left(\frac{2}{D_F} \right)^{-1}} \nabla \ln \rho$$

while the fractal potential (20), is given by the simple expression

$$(24) \quad \nabla \left(\frac{\partial \ln \rho}{\partial t} + \mathbf{V} \cdot \nabla \ln \rho + \nabla \cdot \mathbf{V} \right) = 0$$

With equations (23 a,b), the equation (19b) takes the form:

$$(25) \quad \nabla \left(\frac{\partial \ln \rho}{\partial t} + \vec{V} \cdot \nabla \ln \rho + \nabla \cdot \vec{V} \right) = 0$$

or, by integration with

$$(26) \quad \begin{matrix} \rho \neq 0 \\ \frac{\rho \neq 0 \partial \rho}{\partial t} + \nabla \cdot (\rho \vec{V}) = T(t) \end{matrix}$$

with $T(t)$, a function which depends only on time.

Equation (19b) corresponds to the momentum conservation law, while Eq. (26), with $T(t) = 0$, to the probability density conservation law. So equations:

$$(27a, b) \quad \begin{matrix} m_0 \left(\frac{\partial \vec{V}}{\partial t} + \vec{V} \cdot \nabla \vec{V} \right) = -\nabla(Q) \\ \frac{\partial \rho}{\partial t} + \nabla \cdot (\rho \vec{V}) = 0 \end{matrix}$$

with Q given by (24), form the fractal hydrodynamic equations in the fractal dimension D_F . The fractal potential (24) is induced by the non-differentiable space-time.

The equations (27a,b) and the heat transfer equation can be used in the transport phenomena in nanostructures. In this context, giving a particular term of the equations (27a,b), Lorenz type mechanism for the transport phenomena can be established.

3. Conclusions

The main conclusions of the present paper are the followings:

- 1) using the fractal theory, the momentum law conservation, and the mass law conservation are obtained;
- 2) this equations and mat transfer equations can be used in the numerical simulation of the transport phenomena in nanostructures;
- 3) for a particular form of this system a Lorenz type "mechanis" appear.

Received: February 17, 2010

"Gheorghe Asachi" Technical University of Iași,
* Faculty of Materials Science and Engineering
e-mail: dangalusca@yahoo.com
** Department of Physics
e-mail: m.agop@yahoo.com

REFERENCES

1. Aluculesei A., Litoiu R., Zerichiotis I., Baciu C., Agop M., *On the Thermal Transfer in Nanostructures(I). Mathematical Model*. Bul. Inst. Polit., Iași, LVI (LX), 1, s. de Știința Materialelor (2010 in press).
2. Litoiu R., Zerichiotis I., Aluculesei A., Galusca D.G., Agop M., *On the thermal transfer in nanostructures(II). Conductive type behavior*. Bul. Inst. Polit., Iași, LVI (LX), 1, s. de Știința Materialelor (2010 in press).
3. Imry L., *Introduction tr Mesoscopic Physics*. Oxford Univerity Press, Oxford, 2002.
4. Nottale L., *Fractal Space-time, and Microphysics: Towards a theory of scale Relativity*, World Scientific. Singapore, 1993.

TRANSFERUL TERMIC IN NANOSTRUCTURI (III). COMPORTAMENTUL DE TIP CONVECTIV

(Rezumat)

Utilizând teoria fractalică se analizează comportamentul de tip convectiv al transferului de căldură în nanostructuri. Într-un asemenea context se reține legea de conservare a impulsului masei și ecuația transferului de căldură. Soluțiile numerice pentru aceste ecuații pot implementa un mecanism de tip Lorenz.